

Ali Mahar, M., Pavlis, T.L., Bowman, J.R., Conrad, W.K., and Goodell, P.C., 2018, Early Cretaceous ridge subduction beneath southern Alaska: Insights from zircon U-Pb geochronology and hafnium and oxygen isotopic compositions of the Western Chugach tonalite-trondhjemite suite: GSA Bulletin, <https://doi.org/10.1130/B31918.1>.

Data Repository

Supplementary File S1 – p. 2–13

Supplementary File S2 – p. 14–15

Supplementary File S3 – p. 16–158

Supplementary File S4 – p. 159

Supplementary Table T1. Whole rock geochemical, Sr-Nd and oxygen isotopic composition of rocks in the study area.

Supplementary Table T2. SIMS oxygen isotope analyses.

Supplementary Table T3. U-Pb geochronologic analyses.

Supplementary Table T4. Hf isotopic data.

Supplementary Table T5. U-Pb, Hf And O isotopic data.

DATA SUPPLEMENT- S1

1: Petrographic descriptions of representative samples from the wolverine creek plutons

1) *Border Zone Cumulate Hornblende-Biotite Gabbro*

Pavlis et al. (1988) described volumetrically minor gabbro found at or near the margins of the Wolverine Creek plutonic body. Coarse-grained hornblende-biotite gabbro is observed near a contact with country-rock amphibolite schists and a photograph illustrating this gabbro in place is given in Pavlis et al. (1988, p. 1186). This coarse-grained gabbro (82-Mo-34a, Fig. 1a; Table 1 and 2) is cross-cut by veinlets of quartz-diorite. The coarse-grained hornblende-biotite gabbro sample 82-Mo-34a (1) is considered to be a cumulate rock, i.e. an accumulation of early crystallizing mineral phases from tonalite. Cumulate gabbro is also found near the upper margin the Wolverine Creek pluton (85-PaW-102; Fig. 1b; Table 1), near an outcrop where plutonic quartz diorite (85-Paw-105; Fig. 1c; Table 1) was observed contacting overlying country rock.

1.1) Modal Description

Hornblende-biotite gabbro contains 48-54 vol.% euhedral hornblende, 28-42 vol.% plagioclase, 2-8 vol.% early crystallized biotite and 2-9 vol. % quartz. The whole-rock chemistry is basaltic (gabbroic), with 52 wt. % SiO₂, and 55 % normative anorthite. Calculated whole-rock modes blending microprobe analyses of minerals (Table 1) indicate average relatively sodic composition of plagioclase (An₃₈₋₃₉) which would otherwise be characteristic of rocks classified as andesitic under the IUGS scheme. Nevertheless, these overall low-silica, hornblende-dominated compositions are designated basaltic (gabbroic).

1.2) *Detailed Mineral Description*

Hornblende in the gabbros is notable for its large size, up to 0.5 by 1.5 cm. in dimension, and is euhedrally terminated. The gabbros have a “pegmatite appearance”, that is coarsely-crystalline appearance in hand samples, suggesting presence of a vapor/fluid phase to allow euhedral and large growth during crystallization of hornblende and plagioclase. The gabbro sample 85-PaW-102c (Table 1) contains 0.1-0.2 by 0.5-1 cm, elongate hornblende with radiating clusters of interpenetrating hornblende protruding into plagioclase-rich areas that give an acicular, as well as “pegmatite appearance”.

Typically equant, subhedral to euhedral plates of plagioclase in the gabbros reach 6 mm in size. Plagioclase crystals are saussuritized in core areas, with saussuritized alteration bands that are likely due to preferential alteration in original areas more of anorthitic, early crystallized plagioclase, which was presumably susceptible to secondary saussuritization. Quartz occurs as interstitial plates and is also poikilitically enclosed in hornblende margins. Plagioclase enclosed within hornblende displays distinctive 0.1 to 1 mm vermicular intergrowths, also suggesting crystallization in the presence of fluid or vapor.

Red-brown chloritized biotite crystallized early, evidenced by up to 0.2 by 1 mm subhedral to euhedral crystal forms, now containing or completely replaced by secondary prehnite. Biotite enclosed in amphibole is generally aligned with amphibole cleavages, but some blocky crystals sharply terminate interior cleavage structures, indicating that growth of amphibole occurred around pre-existing biotite.

Accessory minerals are abundant in the coarse-grained gabbros. Primary sphene is prominent as large, 1 mm by 3 mm sphenoidal crystals whose margins are mutually poikilitic with optically continuous grain edges of amphibole and quartz. Other accessory minerals are:

primary 0.1-0.2 mm apatite, 0.05-0.1 mm zircon, and 0.1-0.3 mm euhedral opaques (likely formerly titanomagnetite). One sample has sphene enclosing apatite.

1.3) Secondary Metamorphism

Judging from replacement habits, secondary prehnite and rutile are breakdown products of biotite, saussuritized plagioclase and oxidized primary opaque (titanomagnetite?) minerals. The secondary assemblages contain sericite, chlorite, prehnite, calcite, laumontite, together with recrystallized actinolitic amphibole, and appear to be accompanied by crystal textures indicating deformation. Concentric zoning and patchy extinction in hornblende indicates compositional variation for which microprobe analyses show wide ranges in Al content, from tschermakitic to actinolitic hornblende. Because microprobe analyses of hornblendes grains in both gabbro samples 82-Mo-34a and 85-PaW-102 (Figs. 1a and 1b; Table 1 and 2) (described above) have identical compositions (i.e, maximum Mg#’s, Cr and Al contents) these are considered attributable to igneous crystallization, while the lower-Al actinolitic amphiboles are considered likely due to secondary recrystallization in the greenschist or amphibolite metamorphic facies.

2) *Hornblende-Biotite Quartz Diorite*

2.1) *Summary Classification and Rock Description*

Quartz-diorites (Streckeisen et al., 1973) have whole-rock SiO₂ of 58-65 wt.%, 38-49 wt.% normative anorthite, and 7-37 vol.% hornblende, 6-8 vol.% biotite and 5-15 vol.% quartz (see Table 2 for tabulated and calculated modes).

More felsic quartz-diorites and hornblende-rich tonalities samples include 85-PaW-105c and 82-Mo-40 (Fig. 1c; Table 1 and 2). As less mafic quartz diorites grade into intermediate tonalites, modal hornblende decreases, eventually falling below biotite, plagioclase reaches 60-65 vol.%, and quartz exceeds 15-20 vol.%

3) Tonalite

3.1) Summary Classification and Description

Tonalites (i.e., modal quartz:plagioclase ratio >0.2 (Streckeisen, 1973)) have 60-70 wt.% SiO₂, 33-41 wt.% normative anorthite, 7-9 vol.% biotite with 15 vol.% to near 0% hornblende, and also minor magmatic muscovite.

Rock-slabs and thin-section photographs show that orientations of the marginal mafic minerals range from random to preferred, the latter becoming a foliated fabric of biotite and hornblende around quartz and plagioclase. Pavlis et al. (1988) provide additional petrographic descriptions and photomicrographs, describing primary igneous foliation in relation to subsequent deformation textures (recrystallized quartz, kinked biotite) in the tonalites.

The majority of the large pluton extending up the south fork of Wolverine Creek (Fig. 1 in the paper) in Wolverine Creek is felsic tonalite (Pavlis et al, 1988), falling in a spectrum between samples 85-PaW-7a and 85-PaW-40 (Fig. 3a in the paper; Table 1 and 2). These contain 67-70 wt.% SiO₂, and are described here as leucocratic biotite tonalities that contain subordinate to minor hornblende. Modal data for typical, but unanalyzed, samples are given in Table 2.

3.2) Mineral Description

Subhedral, bent, wispy crystals of biotite (both fresh and chloritized with prehnite) and elongate, up to 3 mm, euhedral hornblende crystals are typically concentrated at the margins of 3-5 mm equant subhedral-euhedral plagioclase crystals. Similar-size areas of anhedral quartz enclose smaller inclusions of biotite and euhedral hornblende.

Magmatic epidote is present in trace amounts in intermediate tonalite (e.g. sample 85-PaW-7a), but felsic varieties (e.g., 85-PaW-40; Table 1) have 2-4 vol.% euhedral, twinned crystals reaching 1 mm in size. Apatite increases in modal abundance (Table 2), continuing a 0.5

mm blocky habit found in the most mafic quartz diorites, and in felsic tonalites dusky magmatic overgrowth zones are visible in apatite. Zircon becomes much more prevalent in tonalites as compared to quartz-diorites with euhedral grains reaching 0.1 mm enclosed in all phases, producing pleochroic haloes in biotite.

The most felsic tonalite sample examined from the Wolverine Creek plutons (sample 85-PaW-40) contains an assemblage with magmatic epidote, late-stage magmatic muscovite and resorbed hornblende (Fig. 3a in the paper). Texturally it is similar to biotite-hornblende-epidote tonalites described above, except without any hornblende at plagioclase grain margins, and with 0.1-0.2 mm euhedral muscovite enclosed within and sharply terminating cleavages in biotite. The muscovite grain size is perhaps ambiguous evidence for a primary origin, but it is compositionally similar to unequivocal large crystals with magmatic appearance in a mineralogically identical sample from the Carpenter Creek plutons (described below). Hornblende is completely enclosed within plagioclase and quartz as small 0.1-0.5 mm grains, often with rounded margins suggesting resorption.

Igneous textural relationships in the suite of tonalite samples thus indicate an early crystallization period with aluminous and tschermakitic hornblende, anorthitic plagioclase, biotite and quartz followed by continued crystallization of biotite, quartz, more sodic plagioclase and epidote +/- muscovite, while in reaction with hornblende.

4) *Trondhjemite Dikes*

In the Wolverine Creek pluton(s), trondhjemite, (i.e., normative anorthite:albite ratio <0.3) containing variable proportions of biotite and muscovite are only present in the form of dikes. Sample 85-PaW-71 (Fig. 1d; Table 1) is from a 25 m² body cross-cutting tonalite exposed at the southern margin of the large Wolverine Creek pluton. It is notably finer-grained

than nearby tonalite, but clearly igneous in texture, with a hypidiomorphic granular matrix of saussuritized 1-2 mm plagioclase set within anhedral interstitial quartz. Large subhedral to euhedral 0.5 by 1.5 mm muscovite crystallized early, as it is sometimes completely enclosed in plagioclase. Biotite, completely converted to green chlorite, can occur within plagioclase and intergrown with early muscovite; however, it is typically elongate, 0.2 by 1 mm, with a bent and wispy habit conforming to plagioclase and quartz margins. Rare zircon is an accessory mineral, and apatite and opaques appear to be absent.

Many dikes observed in the field are presumably trondhjemites, judging by high plagioclase and quartz contents and low percentages of ferromagnesian minerals. Biotite, often completely altered to green chlorite is ubiquitous with lesser muscovite.

5) Almandine Garnet-Biotite-Muscovite Trondhjemite Dikes

Biotite-muscovite trondhjemite containing 1-7 vol.% almandine garnet is also observed cross-cutting tonalite in the plutons (see Fig. 3b in the paper). Two samples (85-PaW-38, 82-Mo-8; Table 1 and 2) examined here are from outcroppings of a single large body, and a third was found as a moraine cobble high in the cirque heading the south fork of Wolverine Creek, suggesting unobserved exposures of this rock type. The almandine garnet trondhjemites appear to be chemically and mineralogically unrelated to the biotite-muscovite trondhjemite dikes described in the above section.

Plagioclase and quartz are relatively coarse in size, 2-4 mm, and hypidiomorphic granular in texture. Biotite, chloritized red-brown and interleaved with prehnite, is distributed at plagioclase margins and within interstitial quartz. Primary muscovite occurs as small 0.1-0.3 mm euhedral grains enclosed in biotite. Opaques (oxidized ilmenite?), zircon, sphene and apatite

are primary accessory phases, and epidote appears secondary, rather than magmatic. Almandine garnet displays variable textures and abundance (from 0 to 10 grains in a single thin-section. Where garnet occurs within quartz, anhedral 2-3 mm garnet is poikilitically intergrown and often resorbed, suggesting reaction. Where garnet contacts plagioclase, it is sharply euhedral. The absence of any metasedimentary character, together with primary igneous features such as of 0.5 mm blocky subhedral apatite, preclude this garnet from being xenocrystic.

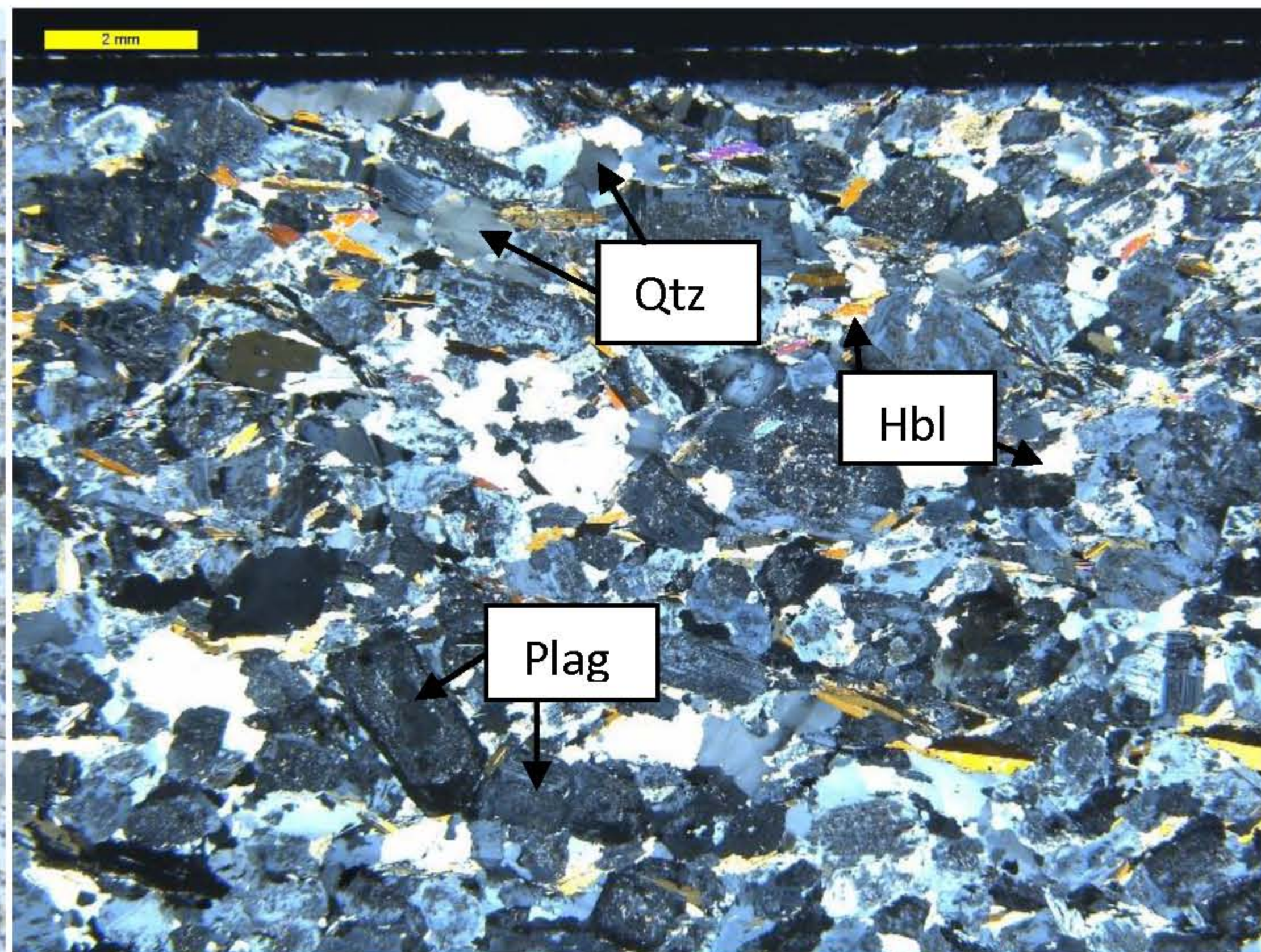
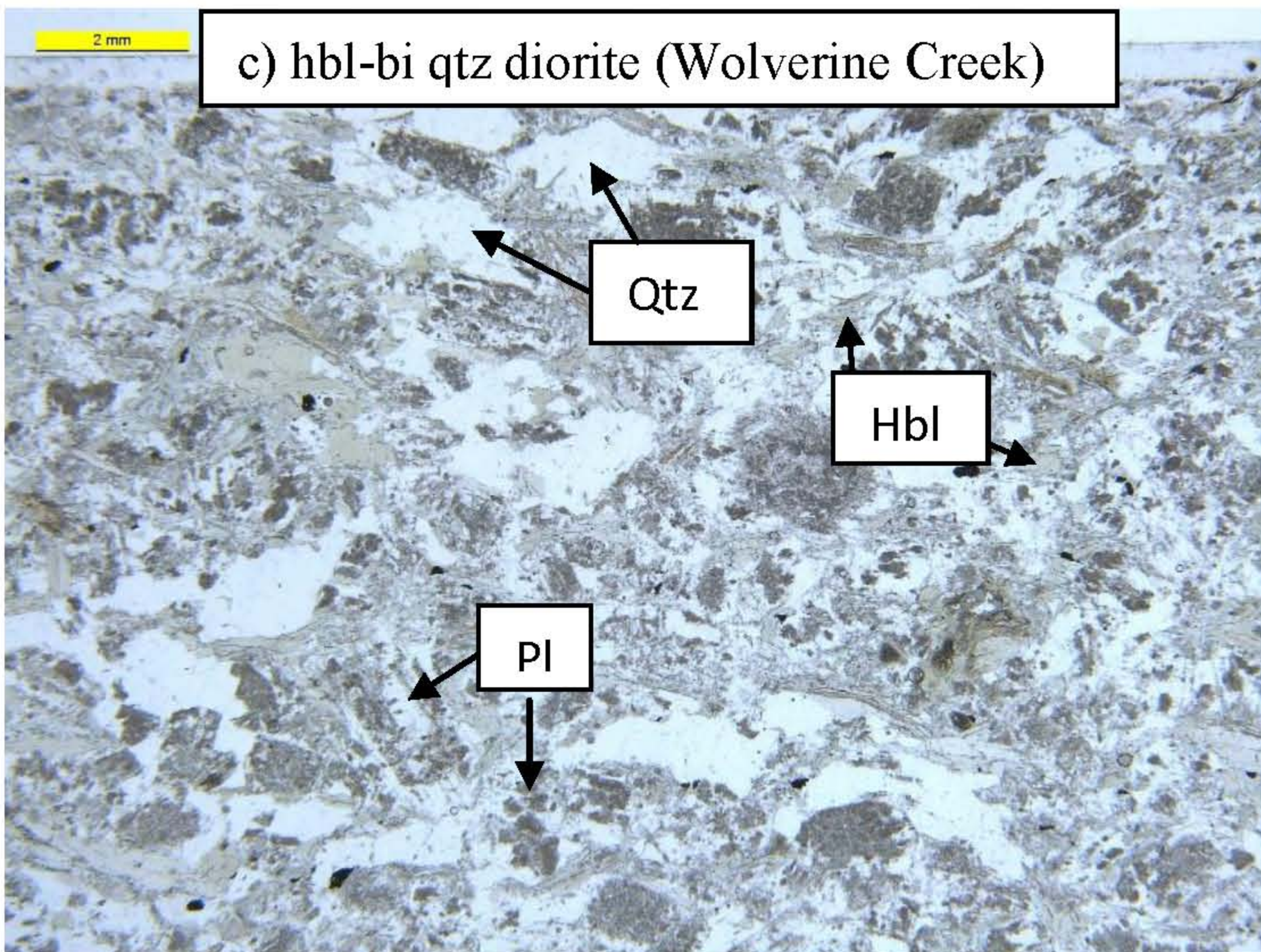
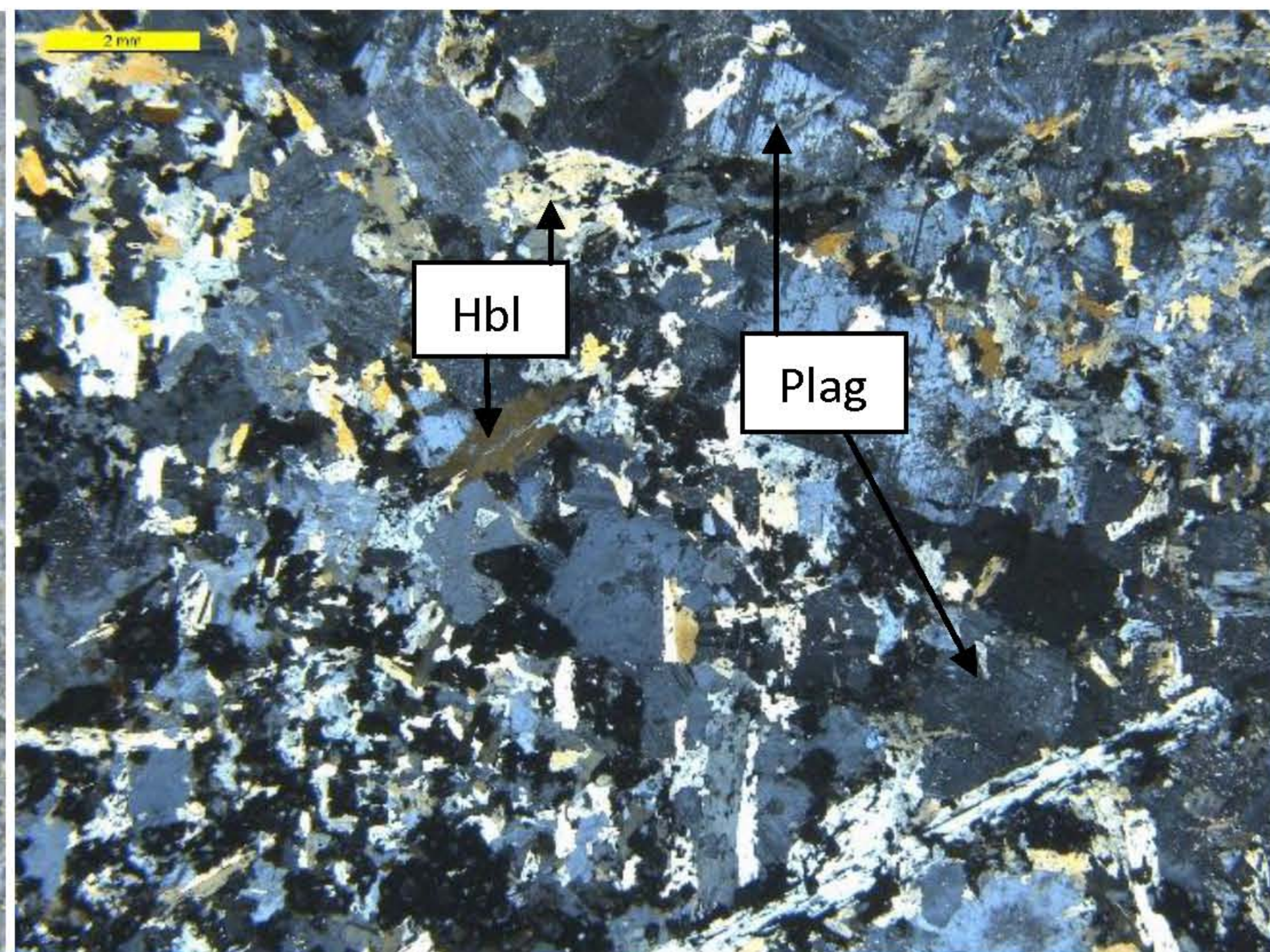
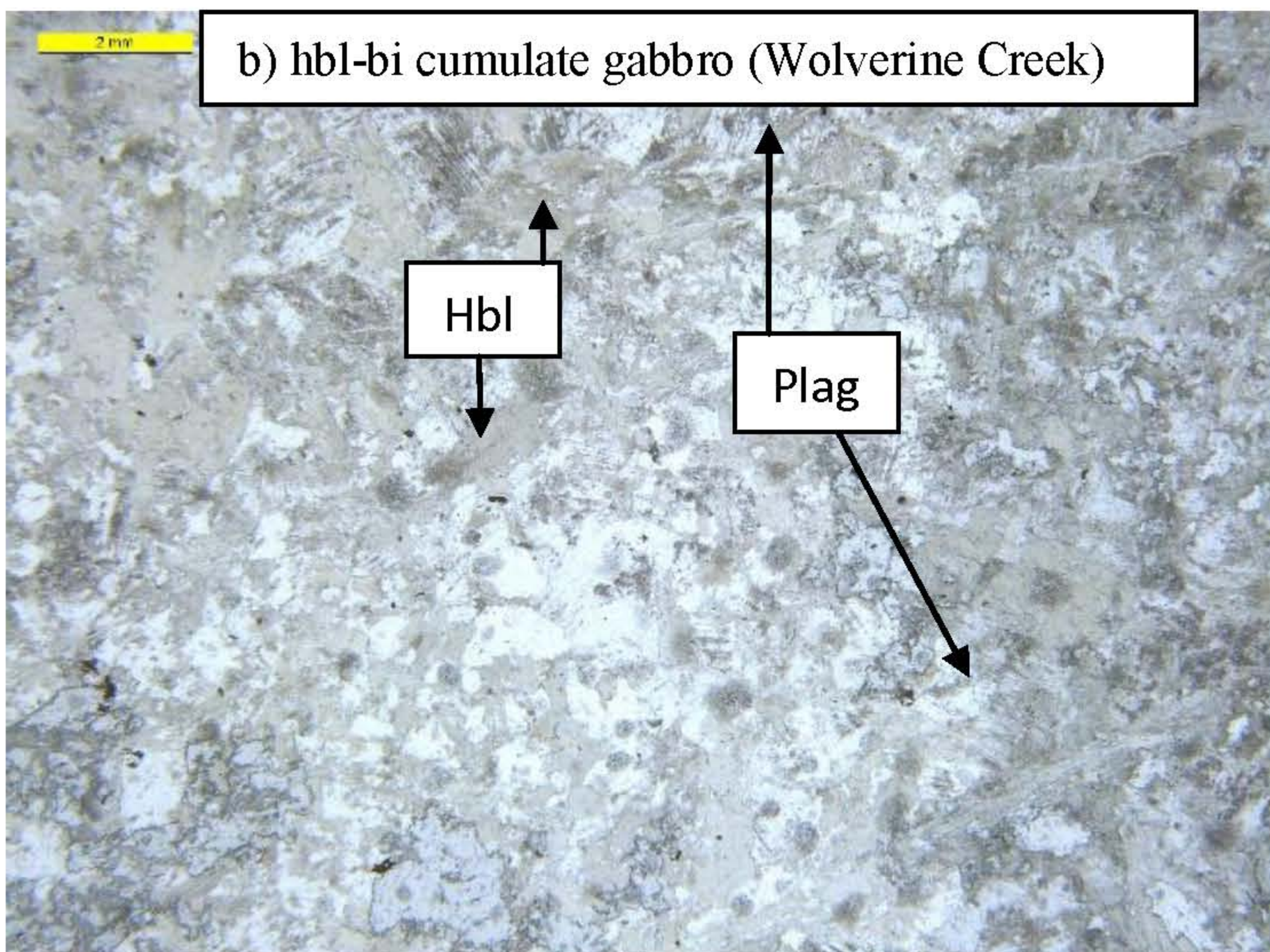
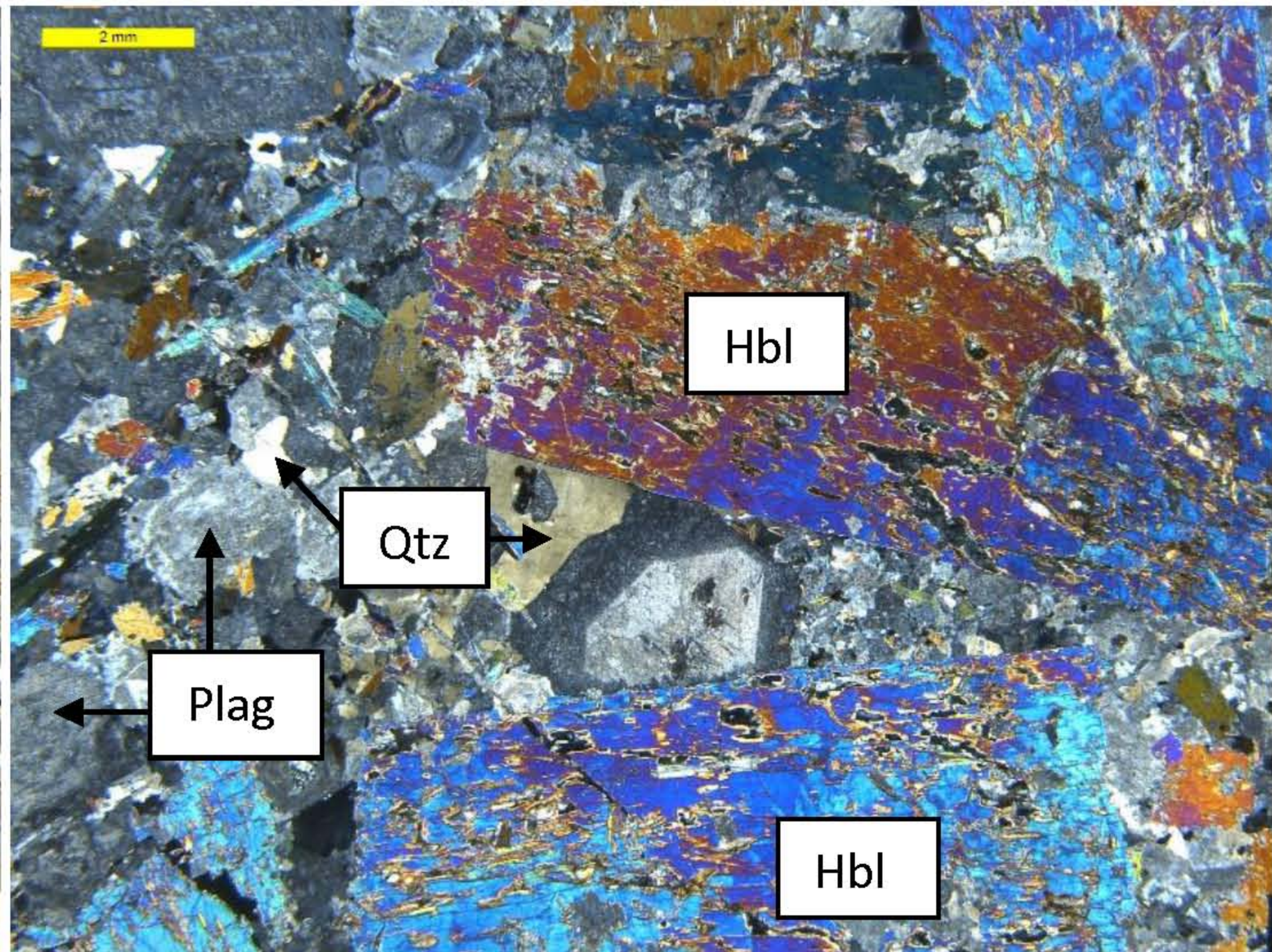
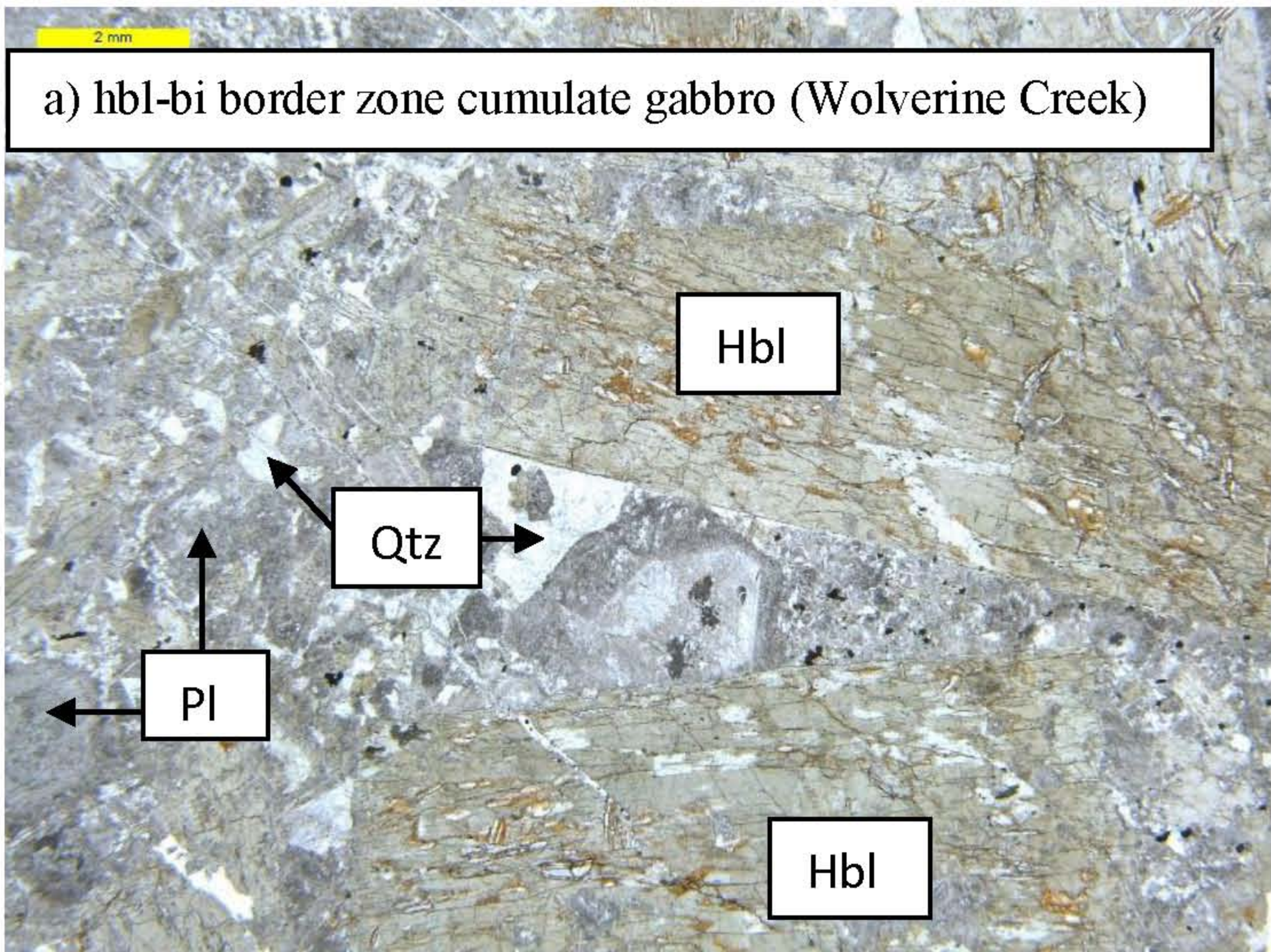
Carpenter Creek Plutons

The diverse lithologies observed in the Wolverine Creek plutons have not been found in the Carpenter Creek area. Border zone gabbros were not observed, and only a limited number of hornblende-bearing quartz diorite and tonalite lithologies were available for study. These samples (86-PaC-109, 86-PaC-102, C-80-38; Fig. 1e and f; Table 1 and 2) are texturally and mineralogically similar to those in Wolverine Creek. Modal data (Table 2) show the quartz diorite sample from Carpenter Creek to have the highest ratio of plagioclase to quartz in any sample, suggesting there may be some plagioclase accumulation.

1) Biotite-muscovite Tonalite/Trondhjemite

Felsic tonalite lithologies are observed in Carpenter Creek. It is notable because it is similar to the most felsic tonalite in Wolverine Creek and contains a mineralogically transitional assemblage of primary muscovite and resorbed hornblende (see Fig. 3c in the paper). Sample C-80-38 contains blocky, subhedral-euhedral plagioclase and interstitial quartz plates with marginal biotite, texturally typical of tonalites described previously. Large, wispy biotite up to 0.9 by 3.5 mm contains interpenetrating 1 mm tabular muscovite and 0.5 mm subhedral-euhedral epidote.

Growth of biotite around muscovite is clearly indicated. Hornblende is only found within the 1-2 mm interstitial quartz. It ranges from 0.1-0.2 mm pleochroic green prismatic grains to 0.05 mm resorbed-appearing blebs. One instance is a 0.2 mm fluid- or melt-inclusion with intergrown hornblende and biotite.



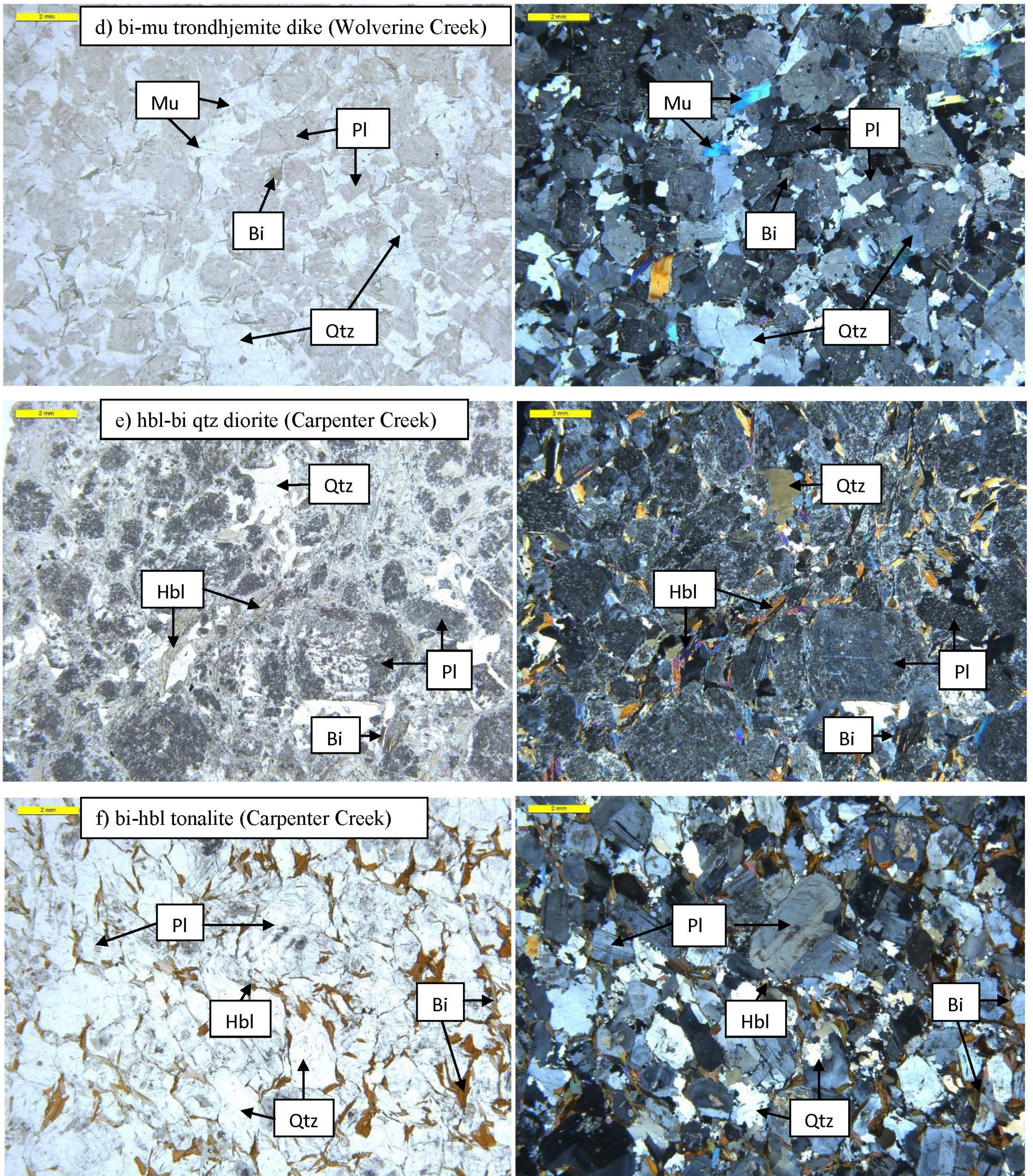


Figure 1: a, b) hornblende biotite Cumulate gabbro, c) hbl biotite quartz diorite, d) biotite muscovite trondhjemite dike, e) hbl biotite quartz diorite and f) hbl-bi tonalite.

Table 1: Calculated Vol.% Modes

Sample	Rock Type	Mg#	An#	ASI	SUM	Gt	Mu	Qtz	Plag	An%	Epi	Bi	Mg#	Hbl	Mg#	Al(*)	Apt	Mt	Chl	Q/P	Sum
Wolverine Creek Body																					
85 PaW 38	Alm gt-bi-mu trond. dike (gt-accu)	0.24	0.14	1.23	0.07	6.1	0.4	32.6	55.4	13		5.4	44				0.14			0.37	100.00
82 Pa UW 7a	Alm gt-bi*-mu trond. cobble	0.38	0.25	1.07	0.20	2.7	0.0	22.6	67.1	23		7.3	43				0.30			0.25	100.00
82 Mo 8	Alm gt-bi*-mu trond. dike	0.39	0.17	1.12	0.00	0.9	1.0	30.5	60.5	16		7.0	44				0.13			0.34	100.00
85 Paw 71	Bi*-mu trond. dike	0.40	0.19	1.14	0.16		4.0	38.3	52.3	16		5.2	55				0.22			0.42	100.00
82 Mo 18	Bi-hbl* tonalite	0.53	0.38	1.03	0.06			18.8	65.2	35	0.0	9.3	58	6.4	55	12.5*	0.02	0.33		0.22	100.00
85 Paw 40	Bi-mu tonalite (hbl resb)	0.54	0.34	1.03	0.01		0.0	31.5	59.5	31	1.2	7.7	59	0.0	50		0.15			0.35	100.00
85 Paw 7a	Bi-hbl tonalite	0.62	0.36	1.00	0.00			24.0	64.1	33		7.5	61	4.3	67	7.6	0.15	0.04		0.27	100.00
85 Paw 27	Hbl-bi* tonalite	0.64	0.46	0.90	0.03			15.2	59.0	37		6.1	61	19.6	64	10.5	0.14	0.00		0.20	100.00
82 Mo 24	Hbl*-bi* tonalite	0.66	0.38	0.99	0.05			16.5	65.2	32		6.9	66	11.3	66	11.5*	0.04	0.10		0.20	100.00
85 Paw 105c	Hbl-bi* qtz-diorite	0.69	0.45	0.94	0.13			14.9	64.2	37		6.1	64	14.5	72	8.1	0.13	0.20		0.19	100.03
85 Paw 75	Hbl -bi* qtz-diorite (w chl)	0.75	0.49	0.90	0.05			9.6	55.4	38		5.8	72	22.5	78	7.7	0.11	0.08	6.5	0.15	100.01
85 Paw 75	Hbl* -bi* qtz-diorite	0.75	0.49	0.90	0.72			6.8	57.3	32		6.8	72	28.8	76	10.0*	0.00	0.21		0.11	99.95
82 Mo 34a(2)	Hbl*-bi* brdrz cumulate gabbro	0.71	0.65	0.71	0.06			8.9	28.4	38		7.6	72	53.7	77	12.2*	0.08	1.43		0.24	100.01
85 Paw 102	Hbl*-bi* cumulate gabbro	0.73	0.55	0.78	0.07			1.2	52.4	39		6.9	72	39.3	73	10.9*	0.10	0.03		0.02	100.00
Carpenter Creek Body																					
86 Pac 115c	Mu-sp gt trond. dike	0.39	0.07	1.17	0.01	0.6	7.6	35.4	44.4	8		0.0					0.00	0.00	11.9	0.44	100.00
86 Ruc 100	Bi-mu tonalite/trond.	0.52	0.34	1.06	0.00		1.0	31.0	58.1	32	0.7	9.1	55				0.13	0.03		0.35	100.00
C 80 38	Bi-mu tonalite (hbl resb)	0.54	0.29	1.09	0.00		4.1	30.8	58.4	26	1.0	5.5	63				0.15	0.05		0.35	100.00
86 Pac 102c	Bi-hbl tonalite	0.59	0.3	1.06	0.01			34.9	49.6	28		13.6	59	1.6	66	6.2	0.21	0.06		0.41	100.00
86 Pac 109a	Hbl*-bi* qtz-diorite	0.69	0.44	0.96	0.11			7.2	68.3	35		8.1	64	16.3	71	10.3*	0.15	0.07		0.09	100.00

Notes: Least-squares calculations using FORTRAN program PETMIX (Aust. Natl. Univ. modification of Wright and Doherty, 1973). Weighting factors were used.

Unless otherwise noted, inputs are whole-rock and average or calculated mineral compositions.

Mineral abbreviations: garnet (Gt), muscovite (Mu), epidote (Epi), biotite (Bi), hornblende (Hbl), chlorite (Chl), K-feldspar (Ksp), Ti-magnetite (Mt), apatite (Apt), quartz (Qtz), plagioclase (Plag).

Other abbreviations: Alm = almandine, Sp = spessartine, hbl resb. = armoured hbl in plag and qtz only, gt accum. = excess gt.

SUM = sum of squares for residuals of Si, Ti, Al, Fe, Mn, Mg, Ca, Na, K, P.

Wt.% modes calculated in PETMIX were converted to Vol.% using molar volume data in Robie et al. (1978) and Ferry (1979).

Whole-rock molar parameters: Mg# = moles MgO/(MgO + FeO), An# = moles CaO/(CaO + Na2O), ASI = moles Al2O3/(CaO + Na2O + K2O)

brdrz = border zone of pluton, trond. = trondhjemite. Hbl* = linear mixing with hbl more Al-rich than average microprobe analysis.

Bi* = calculated stoichiometric biotite. (w chl) = chl replacing hbl in PaW-75.

Mineral parameters: An%, Mg# = An content and Mg-Fe solid-solution compositions. Al = wt.% Al2O3 in average or calculated (*) hbl, anhydrous.

Q/P = %Qtz/(%Plag + %Qtz); 0.2 divides qtz-diorite from tonalite (Streckeisen et al, 1973).

References

Ferry, J.M, 1979. Reaction mechanisms, physical conditions, and mass transfer during hydrothermal alteration of mica and feldspar in granitic rocks from south-central Maine, USA. Contrib. Mineral. Petrol. 68, 125-139.

Robie, R.A., Hemingway, B.S. and Fisher, J.R., 1978. Thermodynamic properties of minerals and related substances and 298.15K and 1 bar and at higher temperatures. U.S. Geological Survey Bulletin 1452.

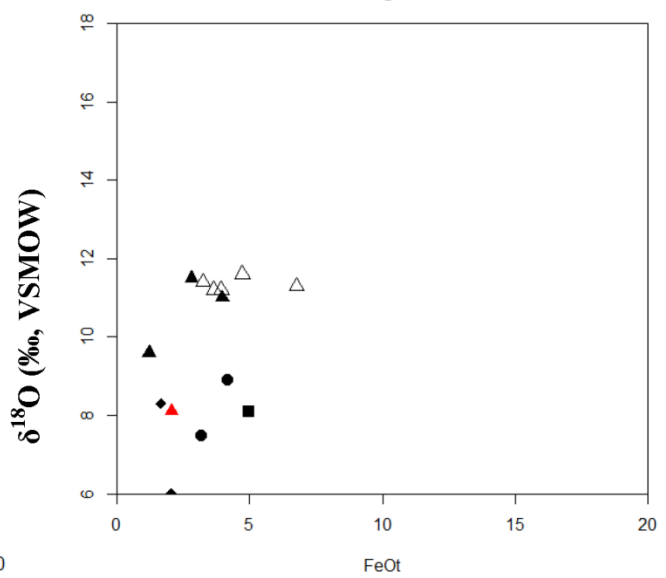
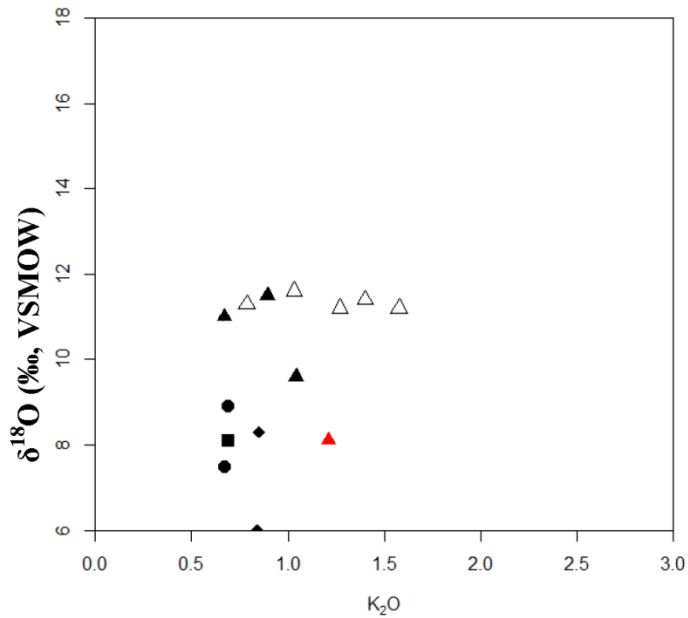
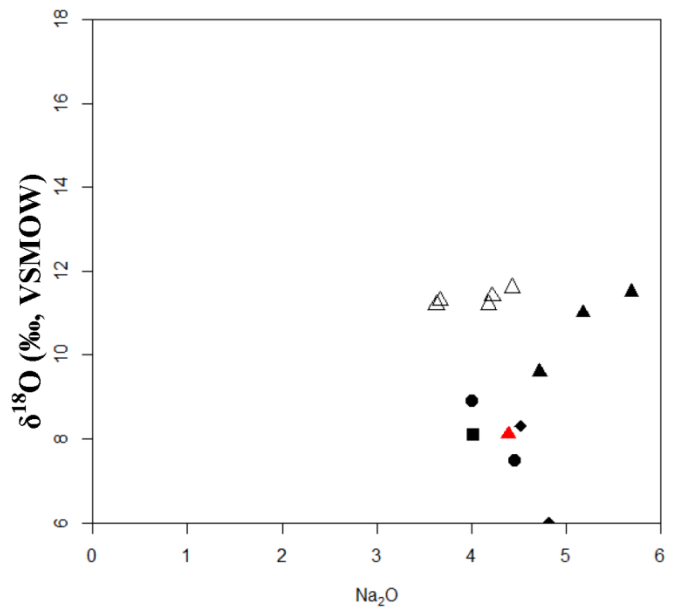
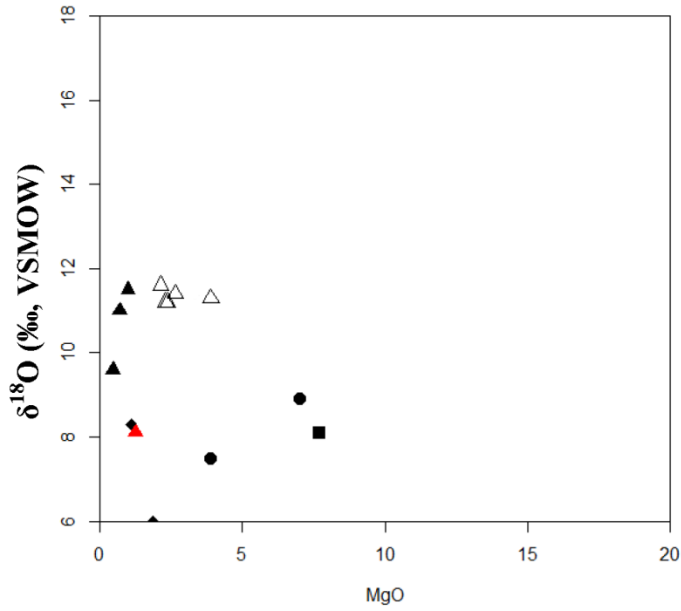
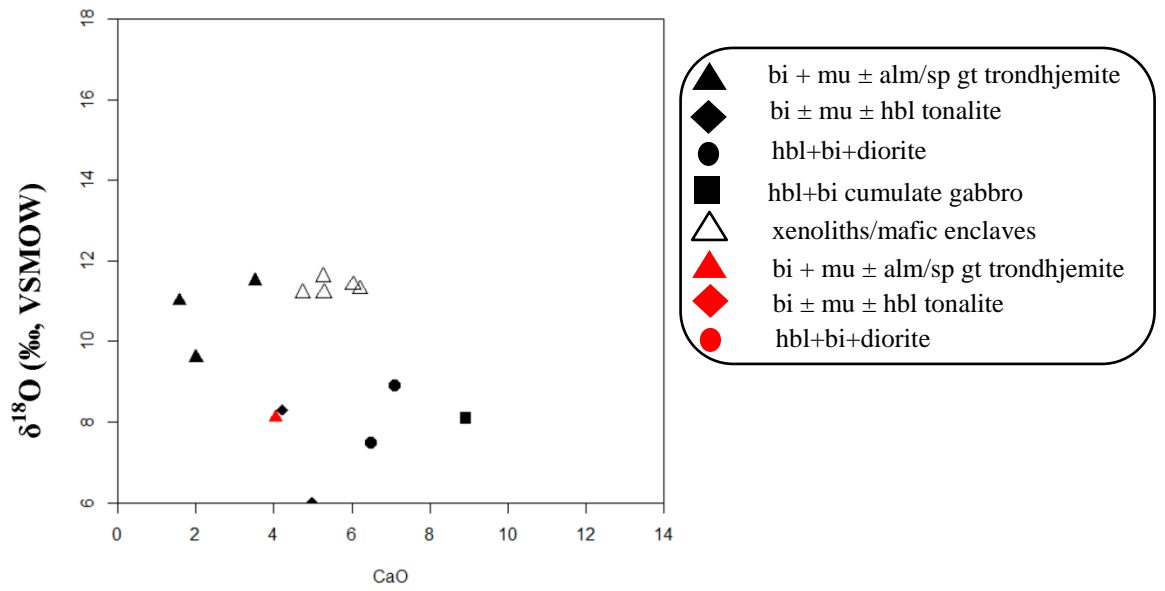
Wright, T.L. and Doherty, P.C., 1970. A linear programming and least squares computer method for solving petrologic mixing problems. Bull. Geol. Soc. Amer. 81, 1995-2008.

Table 2: Tabulated Vol.% Modes

Sample	Rock Type	Body	Gt	Mu	Qtz	Plag	Ser	Epi	Bi	Pre	Hbl	Lm	Apt	Op	Chl	Zir	Cc	Q/P	Total
82-Mo-8	Alm gt-bi*-mu trond. dike	WC	0.2	0.0	26.4	59.9	0.9	0.3	3.7	1.7			0.20	0.00	6.7	0.00	0.0	0.31	100.0
82-PaUW-7a	Alm gt-bi*-mu trond. cobble	WC	3.4	1.3	27.9	54.1	2.6	0.4	1.1	3.1			0.10	0.00	6.0	0.00	0.0	0.34	100.0
82-PaUW-7b	Bi-mu? tonalite/trond.	WC		0.7	36.1	50.6	2.4	0.8	5.7	1.7			0.30	0.00	1.7	0.00	0.0	0.42	100.0
82-Mo-55	Bi-mu tonalite/trond.			2.9	32.3	56.2	0.3	3.6	0.8	3.9			0.00	0.00	0.0	0.00	0.0	0.36	100.0
82-Mo-16a	Bi-mu? tonalite/trond.			0.2	24.4	50.4	0.4	4.2	0.0	1.7		13.4	0.10	0.00	5.2	0.00	0.0	0.33	100.0
82-Mo-33	Bi-mu? tonalite/trond.			0.6	29.1	64.3	0.9	0.1	2.9	0.3			0.10	0.00	0.7	0.00	1.0	0.31	100.0
82-Pa-S13	Bi-hbl tonalite				24.7	59.5	0.5	1.1	2.1	1.8	5.2		0.20	0.20	4.6	0.10	0.0	0.29	100.0
C-80-42	Bi-mu tonalite (hbl resb)			1.5	23.9	60.9	0.0	0.4	8.7	2.7	0.9		0.10	0.00	0.9	0.00	0.0	0.28	100.0
82-Mo-18	Bi-hbl* tonalite	WC			19.9	58.7	1.3	1.8	6.5	2.7	7.6		0.20	0.10	1.5	0.00	0.0	0.25	100.3
C-80-14	Hbl-bi tonalite				17.5	56.6	0.3	0.1	8.4	4.5	10.6		0.10	0.20	1.6	0.10	0.0	0.24	100.0
82-Mo-24	Hbl-bi* tonalite	WC			18.3	59.7	0.0		3.5	1.6	14.9		0.29	0.10	1.5	0.10	0.0	0.23	100.0
C-80-13	Bi-mu tonalite			3.3	18.2	65.6	0.3	3.2	6.0	0.7			0.00	0.00	2.4	0.00	0.3	0.22	100.0
82-Mo-40	Bi*-hbl Qtz-diorite	WC		0.1	14.0	64.2	1.1	0.5	4.9	3.2	7.3		0.80	0.70	3.2	0.00	0.0	0.18	100.0
85-PaW-75	Hbl-bi* Qtz-diorite (also 0.1% sphene)	WC			5.5	48.2	0.0		6.1	0.8	37.3		0.30	0.10	1.6	0.00	0.0	0.10	99.9
86-PaC-109a	Hbl-bi* Qtz-diorite	CC			6.4	66.4	0.0		1.3	2.2	21.2		0.29	0.39	1.7	0.10	0.0	0.09	100.0
82-Mo-34a	Hbl-bi* brdrz cumulate gabbro	WC			2.1	30.6	0.0		7.1	2.7	53.5		0.19	0.77	2.9	0.19	0.0	0.06	100.0
85-PaW-30a	Hbl-bi*-cpx? cumulate gabbro (also 0.28% sphene, 0.09% rutile)	WC			1.3	42.2			2.5	4.1	48.2		0.00	0.19	0.9	0.10	0.2	0.03	99.6

Notes: WC = Wolverine Creek Body, CC = Carpenter Creek Body
 Bi* = biotite is chloritized. Cpx? = prehnite possibly replacing Cpx. Op = opaques, Zir = zircon.
 Mu?, Epi? = total also includes sparse muscovite, epidote of possible secondary origin.
Secondary minerals: Ser = seracite, Pre = prehnite, Lm = laumontite, Cc = calcite
 Other abbreviations as in Table 1.

Supplementary file S2



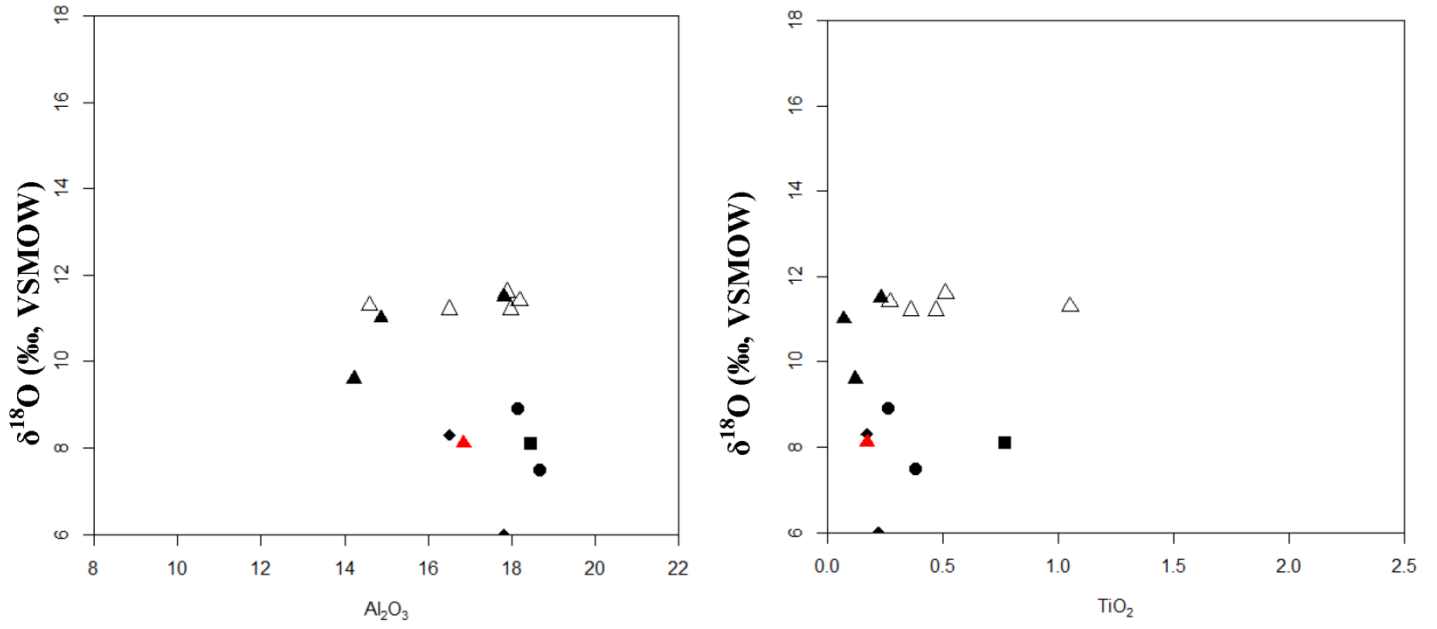
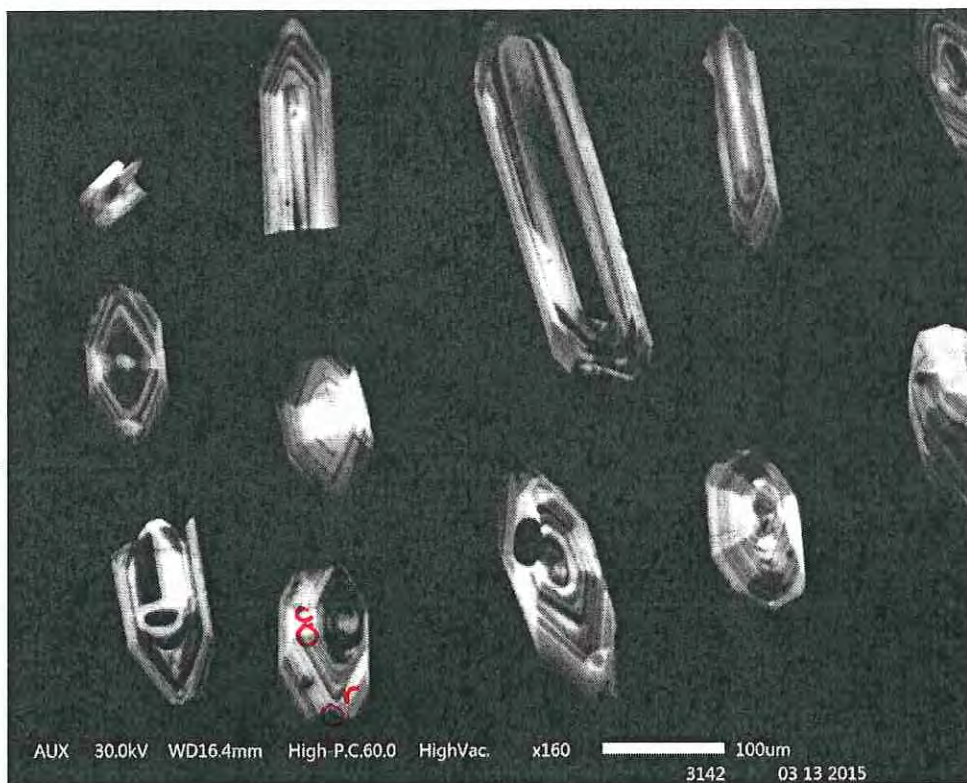


Figure: Plots showing the relationship between whole-rock $\delta^{18}\text{O}$ and major oxides. Red symbols are from Carpenter Creek while the black are from Wolverine Creek.

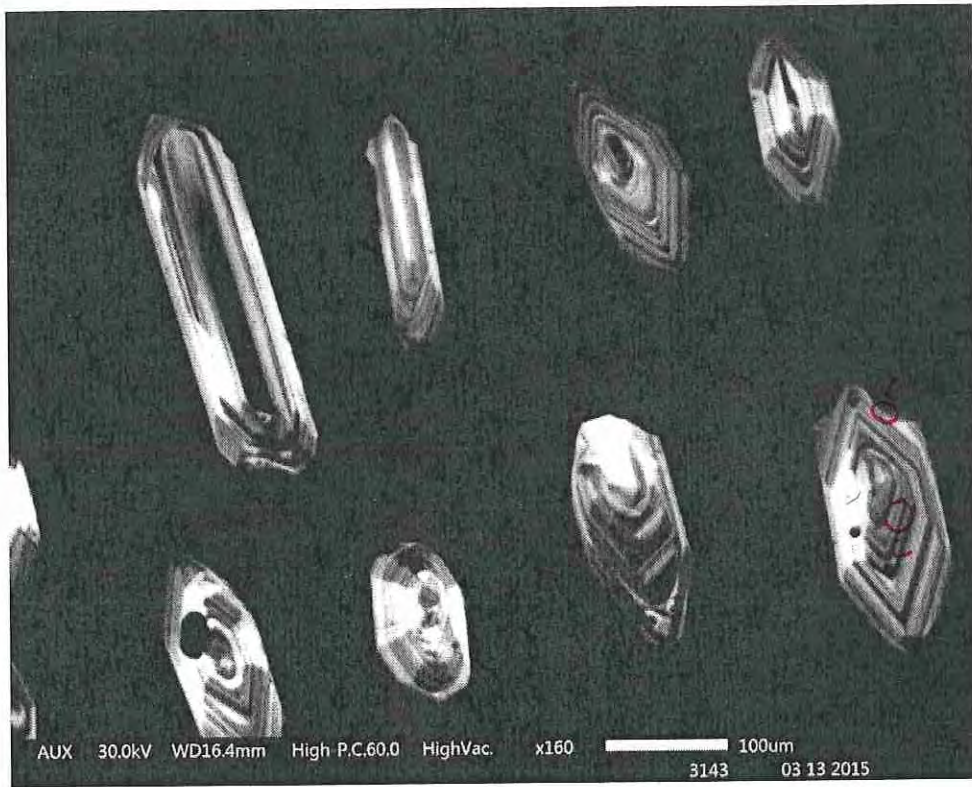
Starting sample C80-13

Mount 1, CL-1



grain 10: has dark tip at bottom

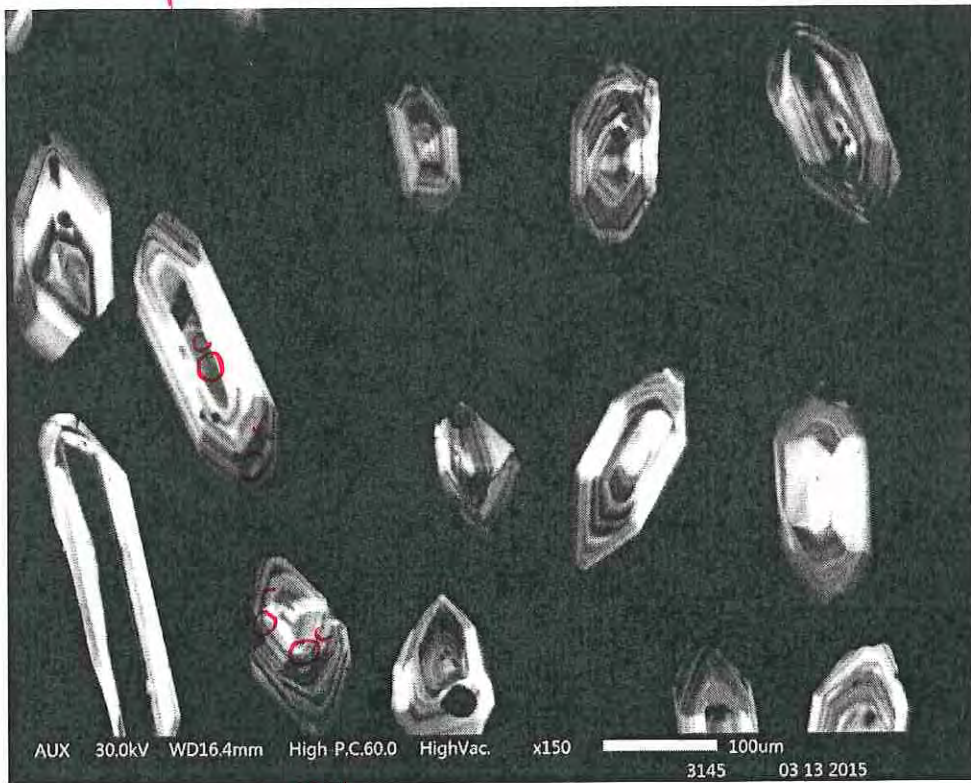
Mount 1, CL-2



grain 14:
has dark
tip at upper
right

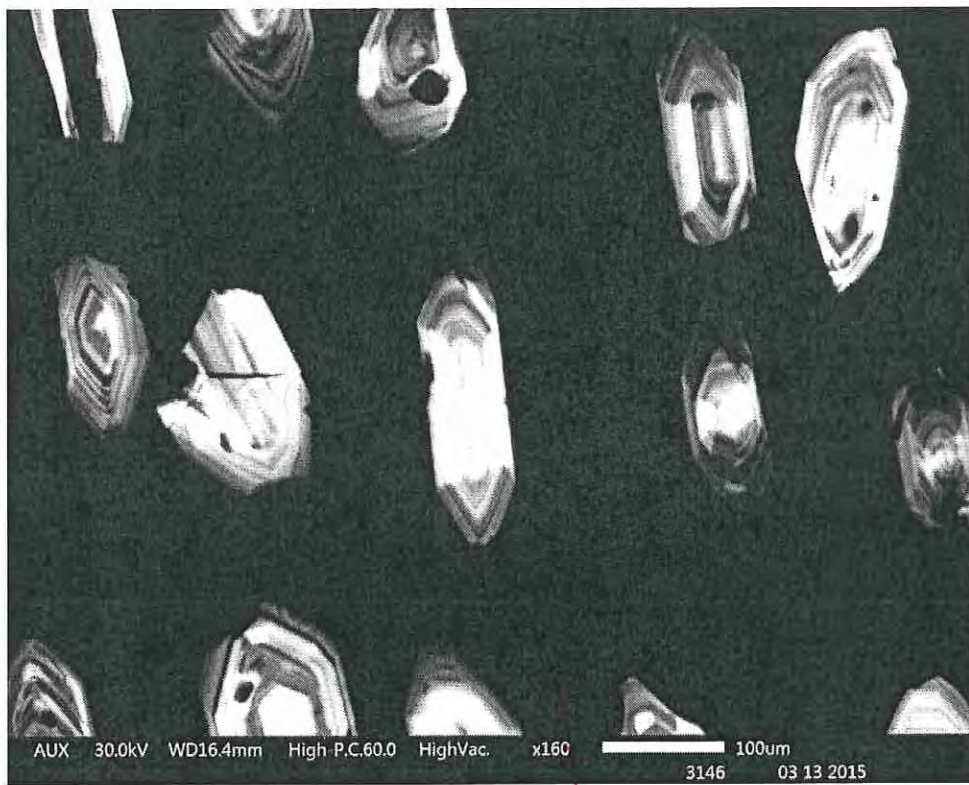
Mount 1, CL-4

17
↑



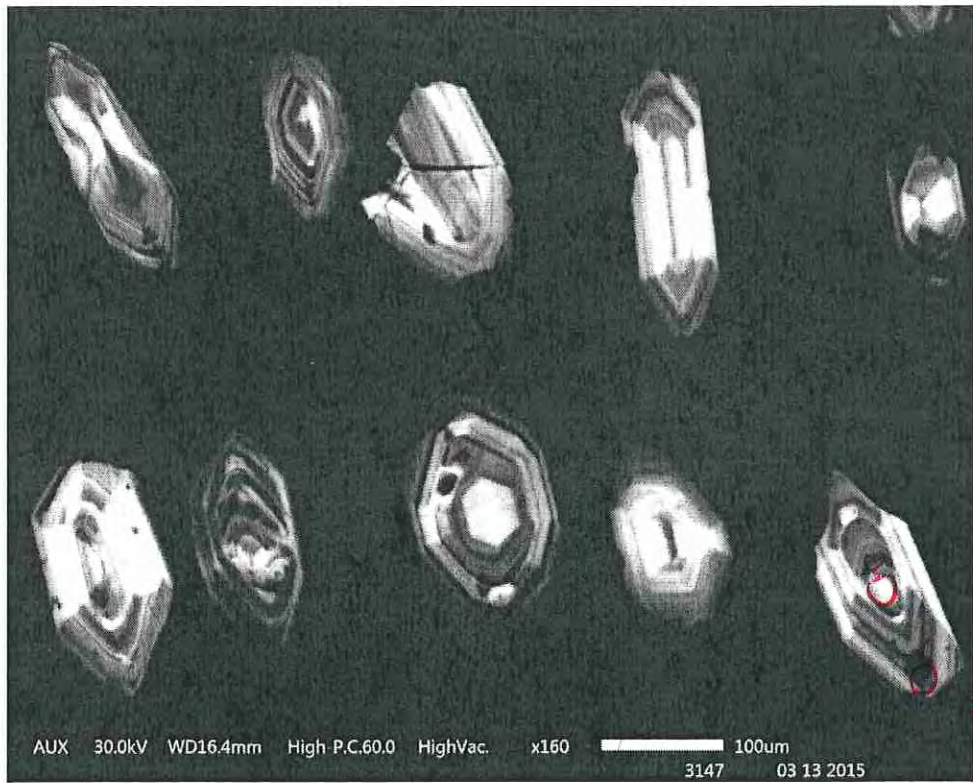
★
↓
23

Mount 1, CL-5



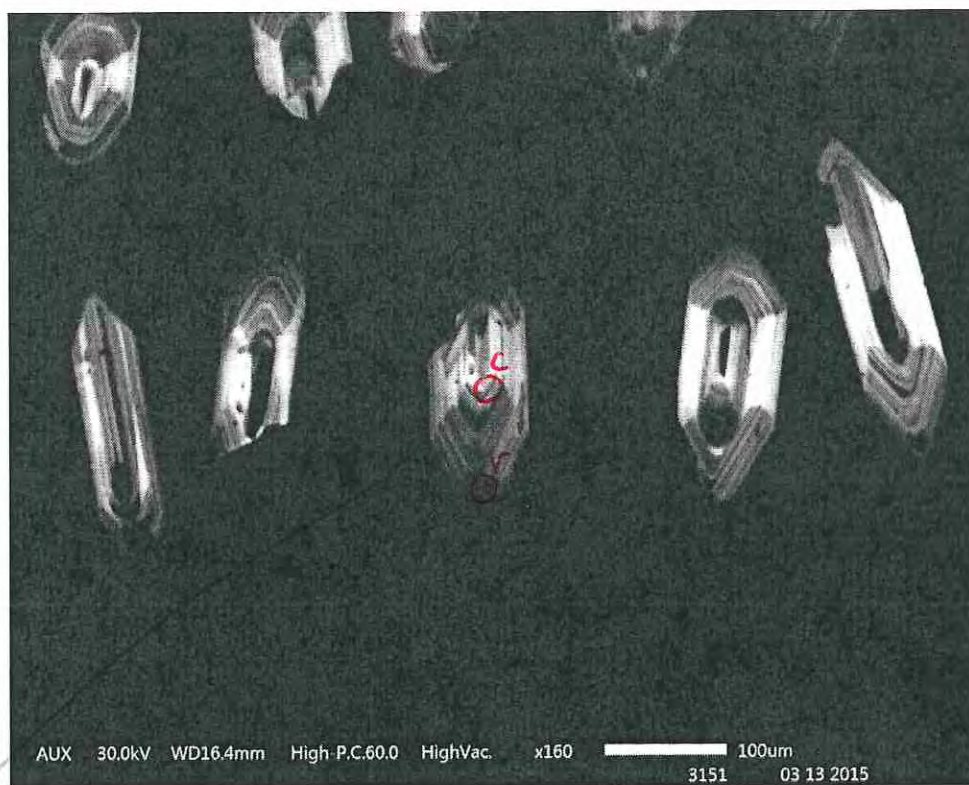
33

Mount 1, CL-6



→ 40

Mount 1, CL-10



grain 56 hrs
lower dark tip

A handwritten scribble or signature consisting of several overlapping, wavy lines.

Mount 1, CL-13

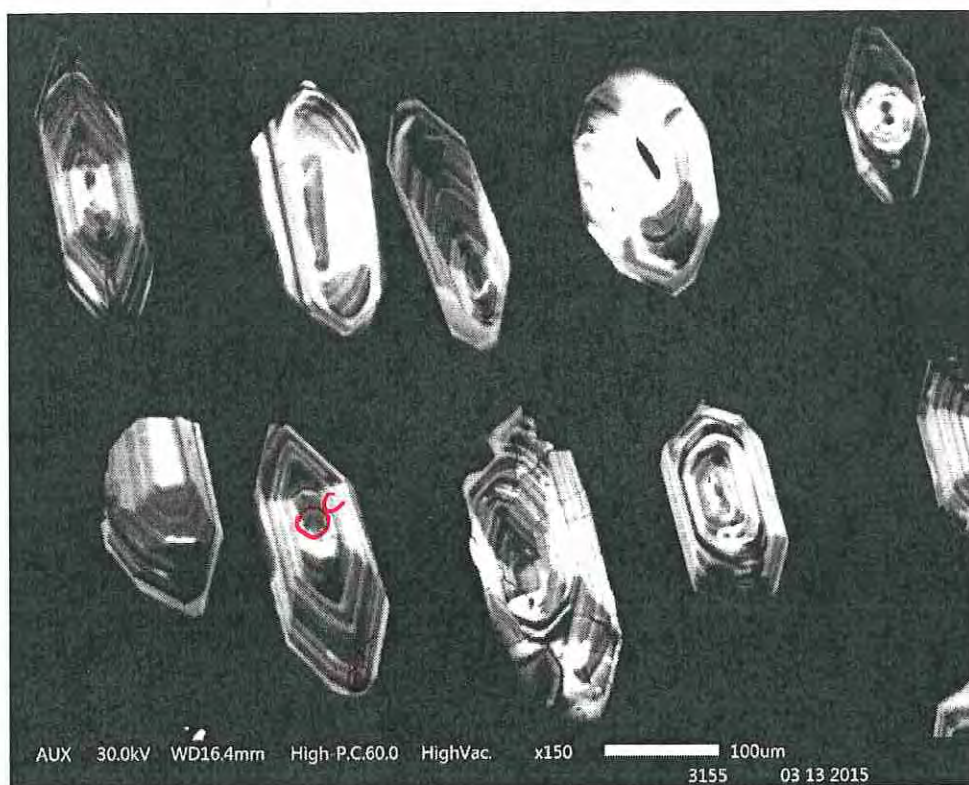
62



grain 65
has dark CL
domain on
bottom tip

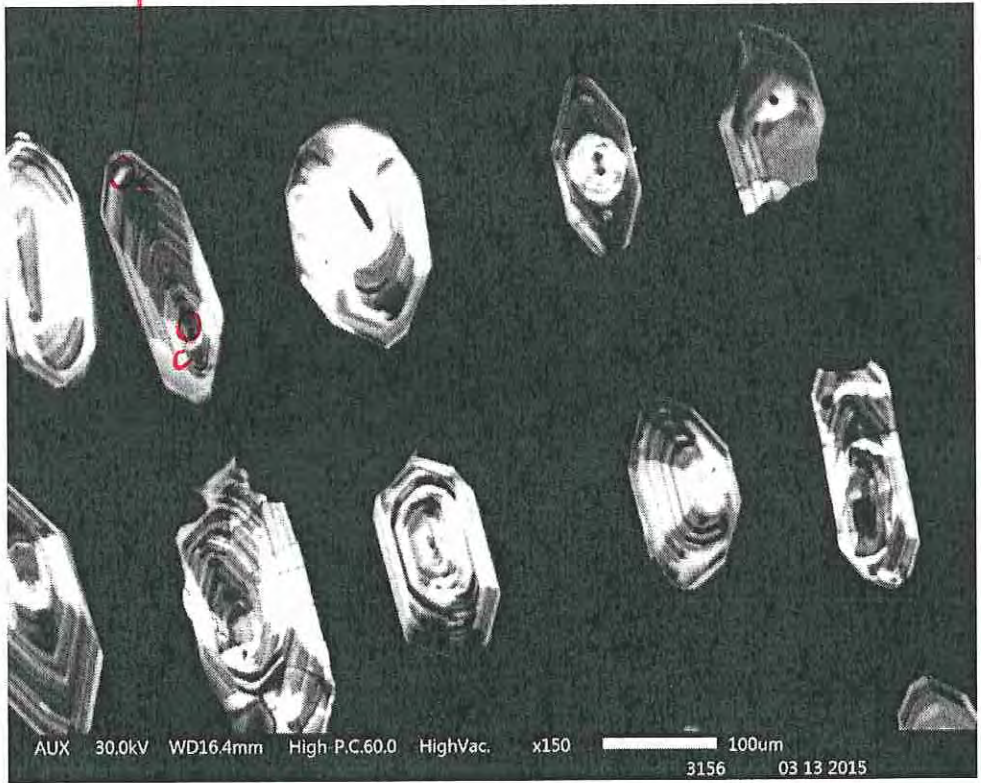
grain 71
has dark CL
domain on
bottom left
tip

Mount 1, CL-14



Mount 1, CL-15

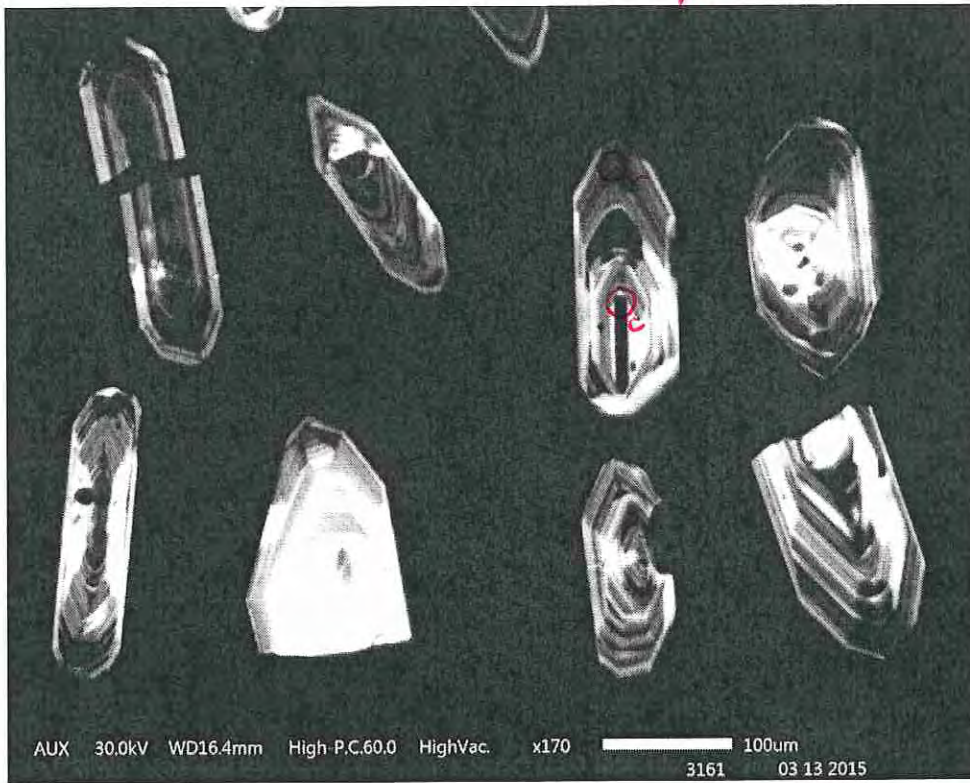
74



80

Mount 1, CL-20

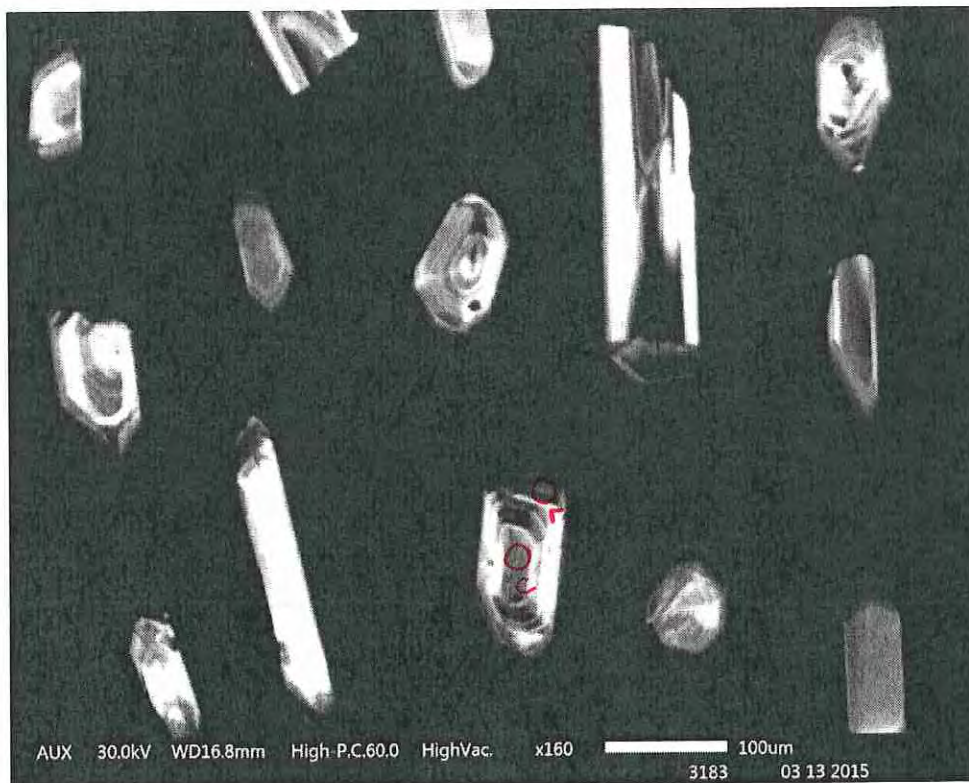
~~107/109~~
↑



Mount 1, CL-22

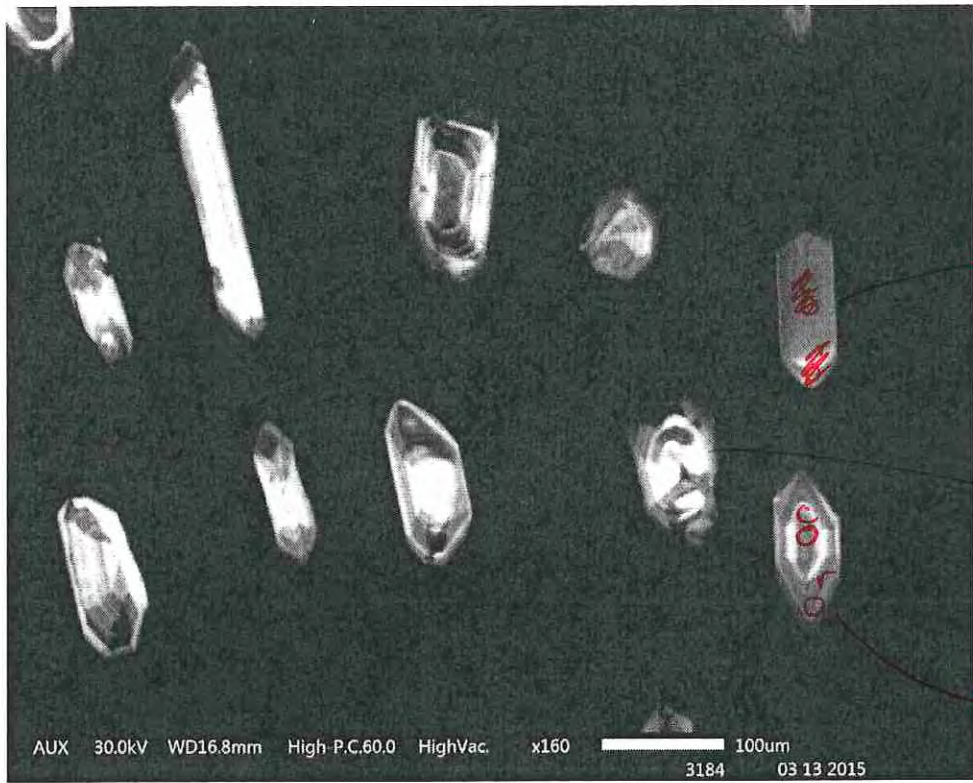


Mount 2, CL-2



grain 16 has
dark CL rim
at top of grain

Mount 2, CL-3

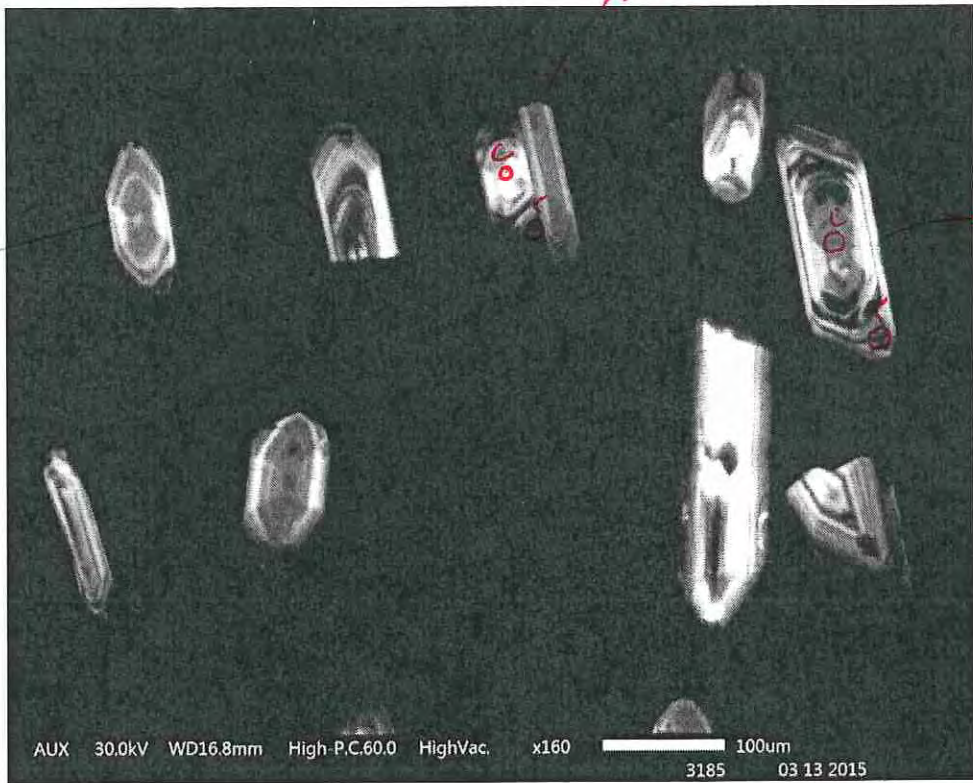


grain 22
has a look
CL upper tip

g23

Mount 2, CL-4

→ 26

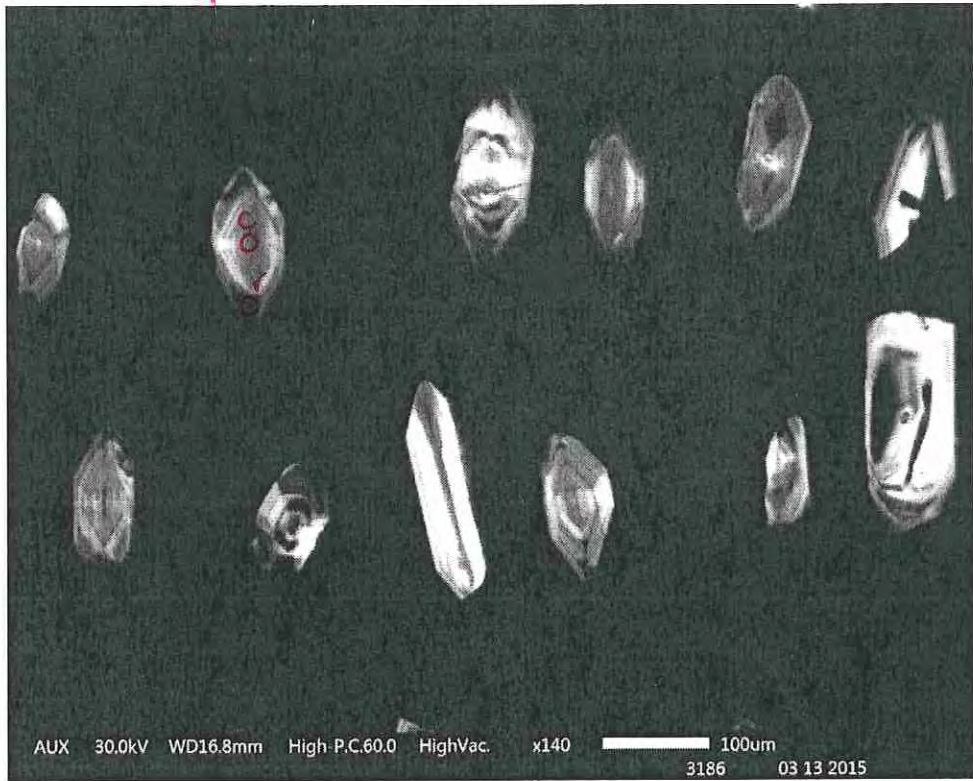


GRAIN 24
has dark CL
domains on lower
tip

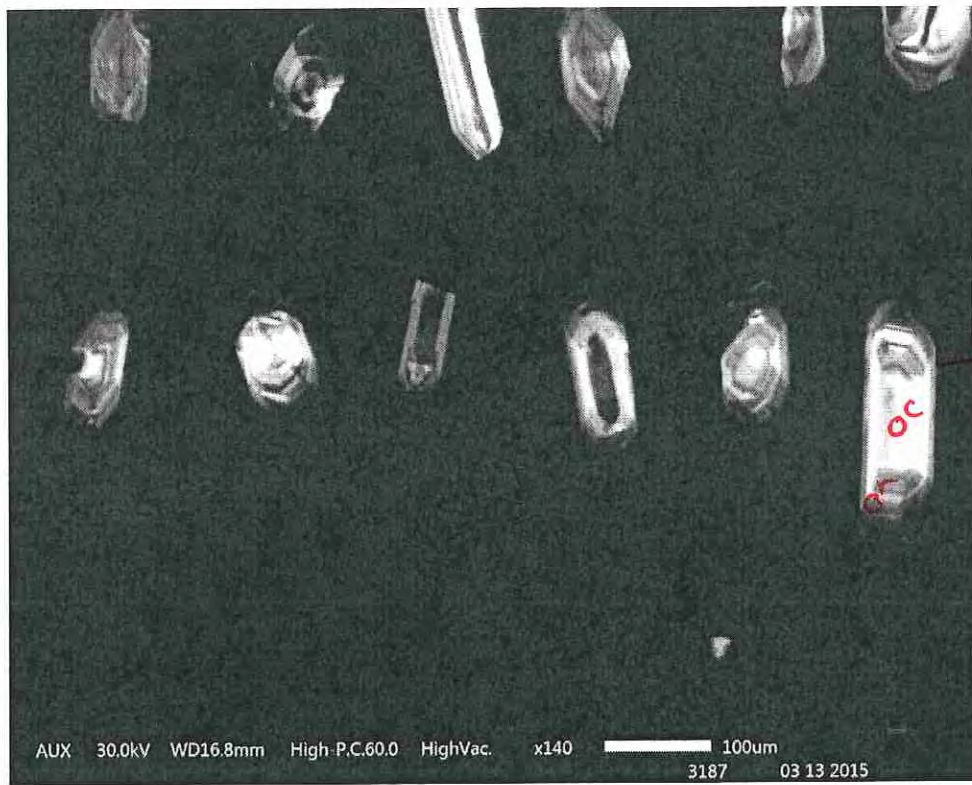
→ 28

Mount 2, CL-5

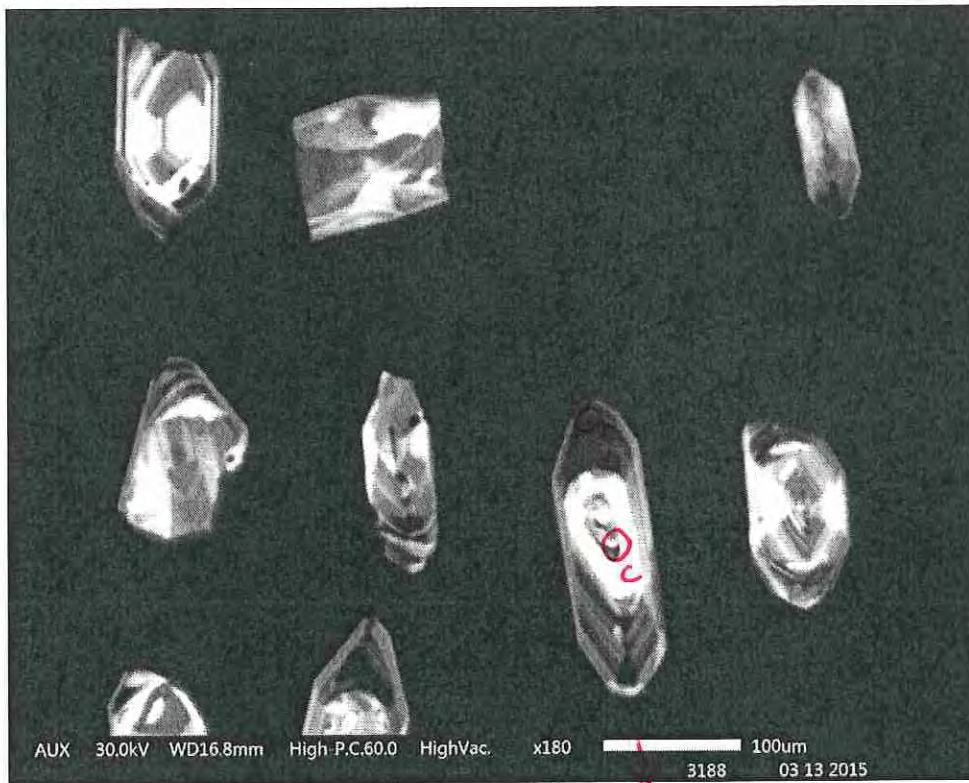
35
↑



Mount 2, CL-6



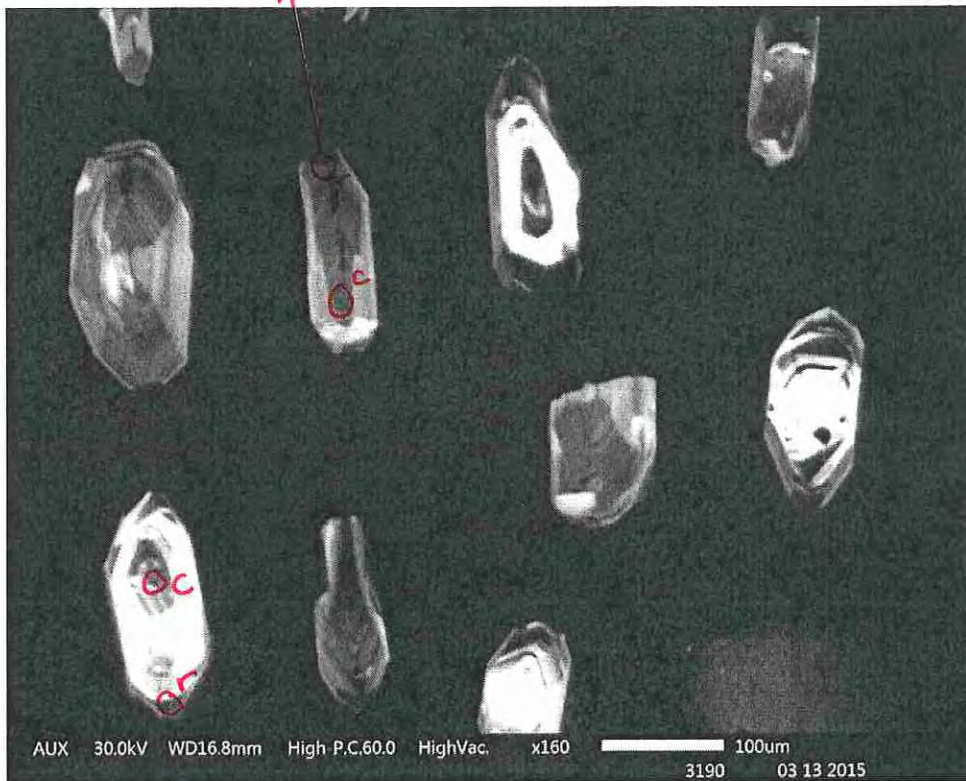
Mount 2, CL-7



58

Mount 2, CL-9

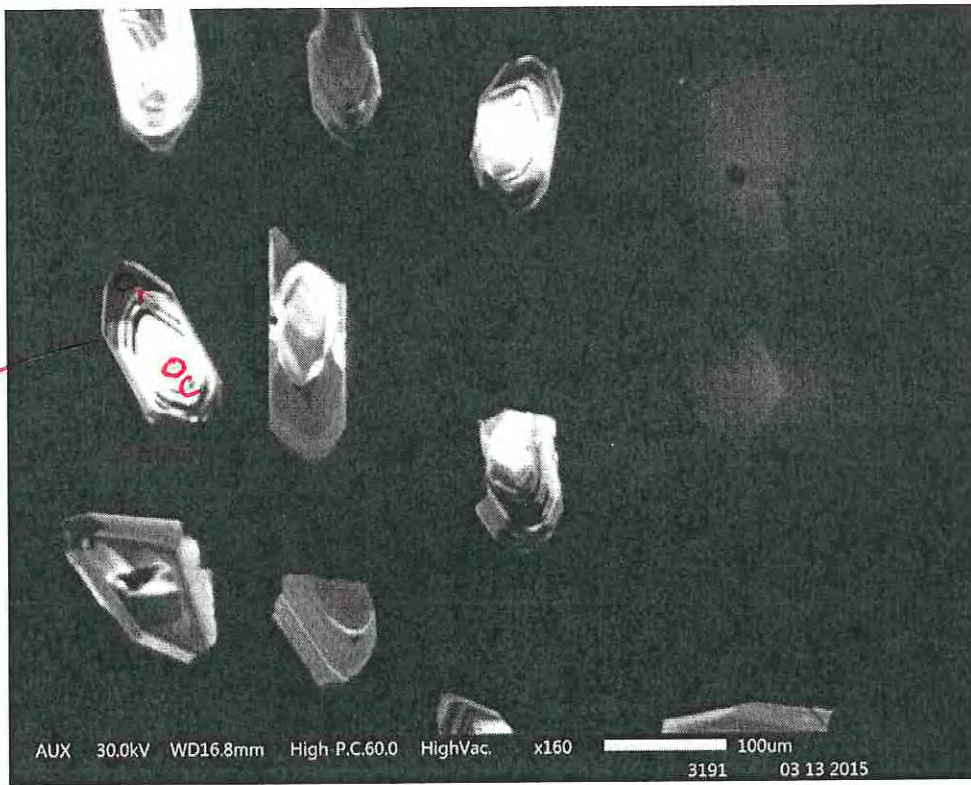
67



70

Mount 2, CL-10

74 ←





BED-C 20.0kV WD10.3mm Std.-P.C.60.0 HighVac. x600  20um

04 06 2017

EGI



AUX 20.0kV WD17.5mm Std.-P.C.60.0 HighVac. x650

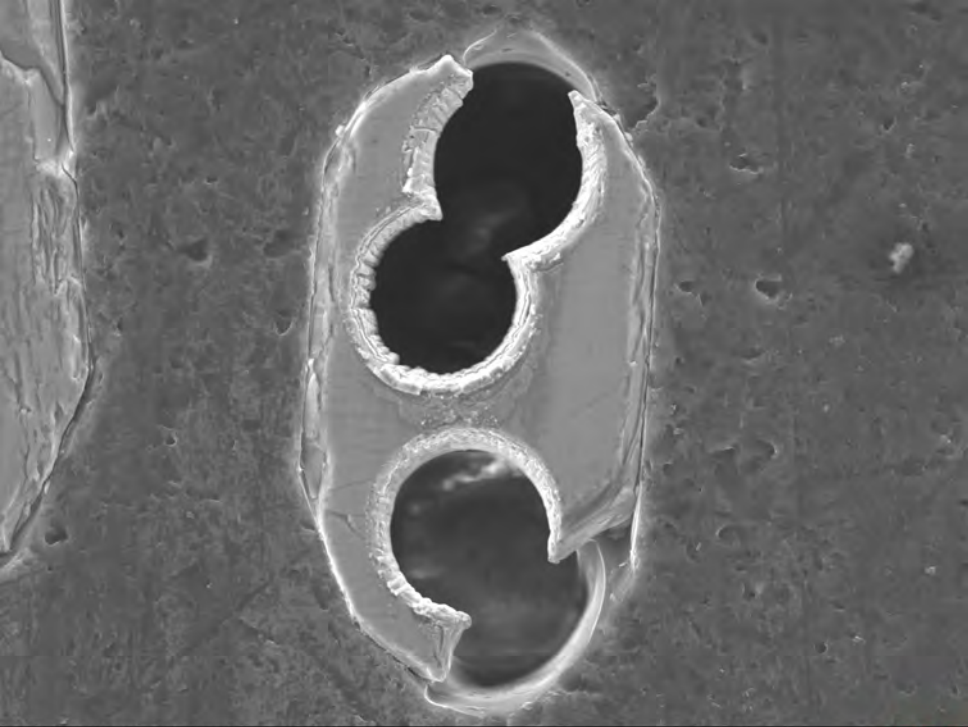


20um

04 06 2017

EGI

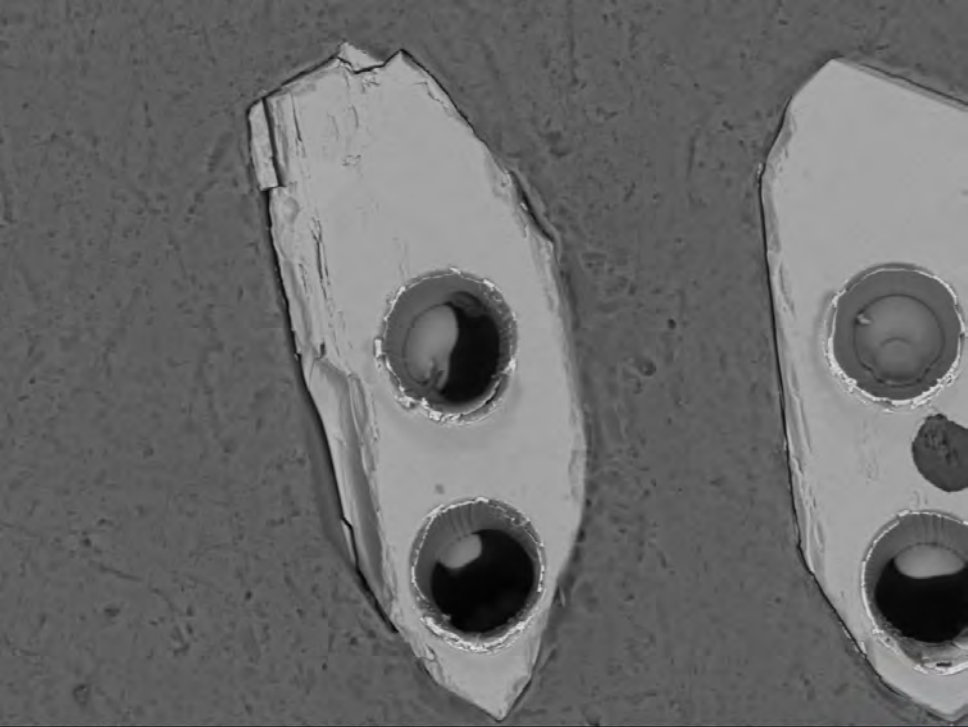




SED 20.0kV WD10.3mm Std.-P.C.60.0 HighVac. x600  20um

04 06 2017

EGI

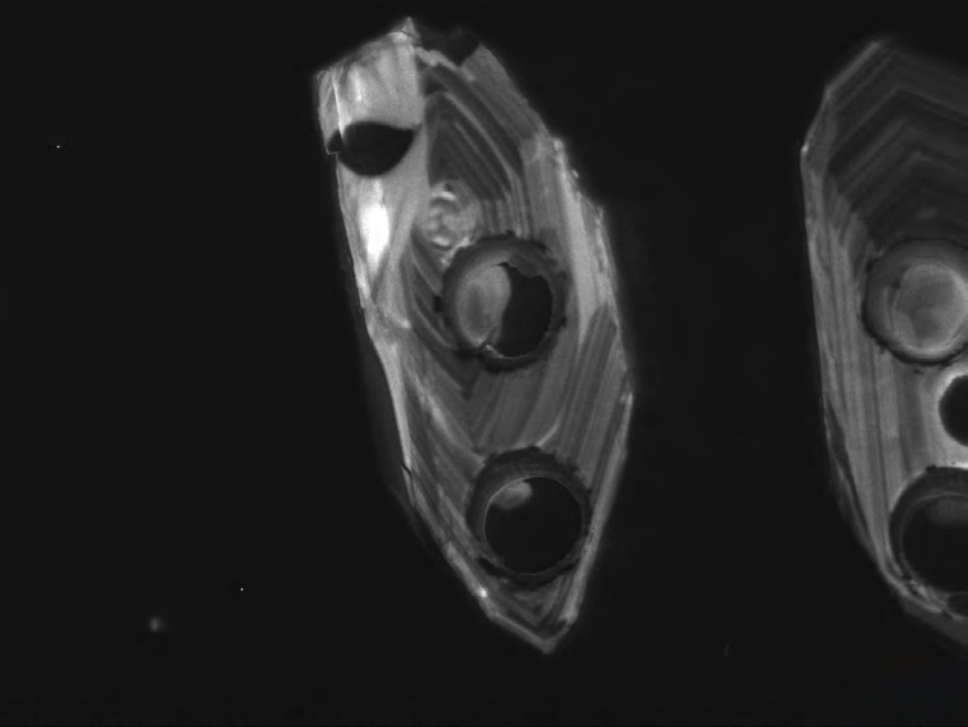


BED-C 20.0kV WD10.3mm Std.-P.C.60.0 HighVac. x430



50um
04 06 2017

EGI



AUX

20.0kV

WD17.5mm

Std.-P.C.60.0

HighVac.

x400



50um

04 06 2017

EGI

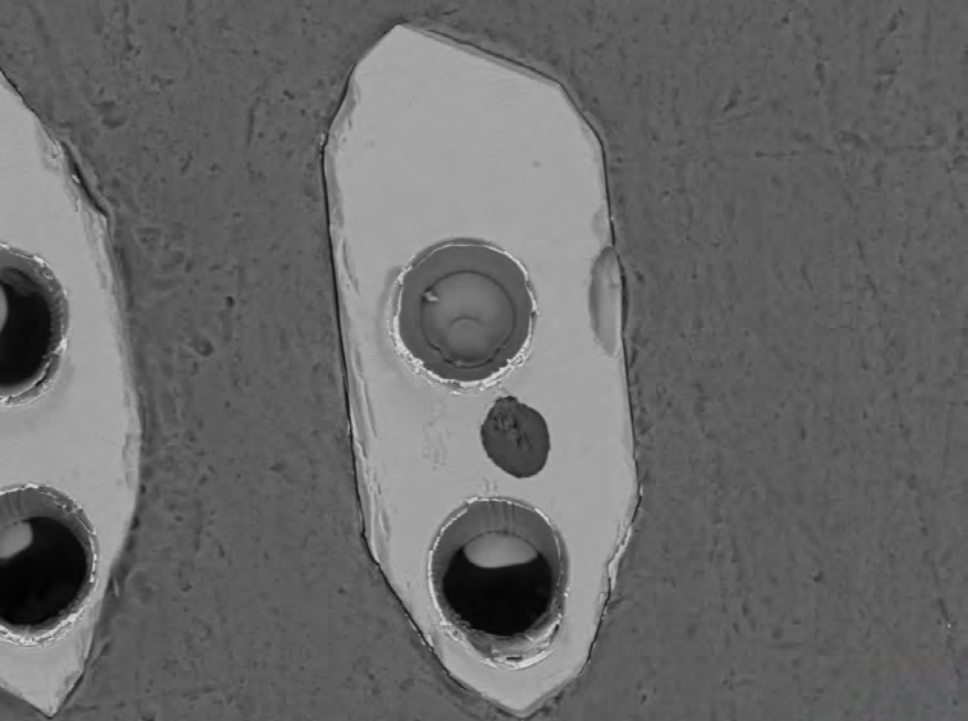


SED 20.0kV WD10.3mm Std.-P.C.60.0 HighVac. x430



50um
04 06 2017

EGI

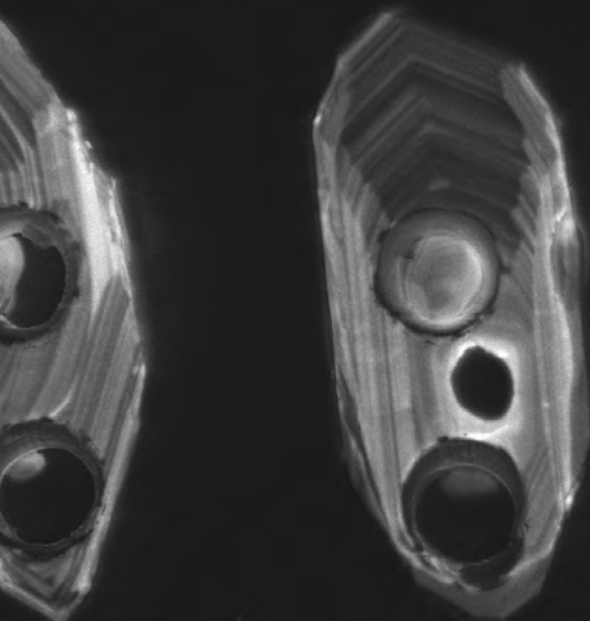


BED-C 20.0kV WD10.3mm Std.-P.C.60.0 HighVac. x450



50um
04 06 2017





AUX 20.0kV WD17.5mm Std.-P.C.60.0 HighVac. x400



50um
04 06 2017



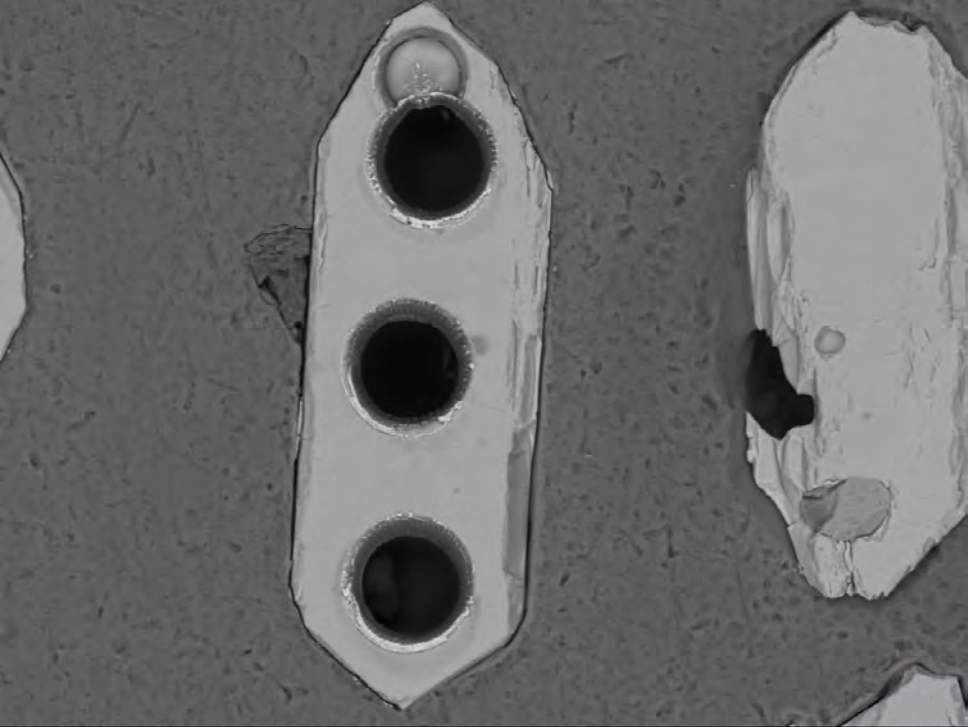


SED 20.0kV WD10.3mm Std.-P.C.60.0 HighVac. x450



50um
04 06 2017

EGI



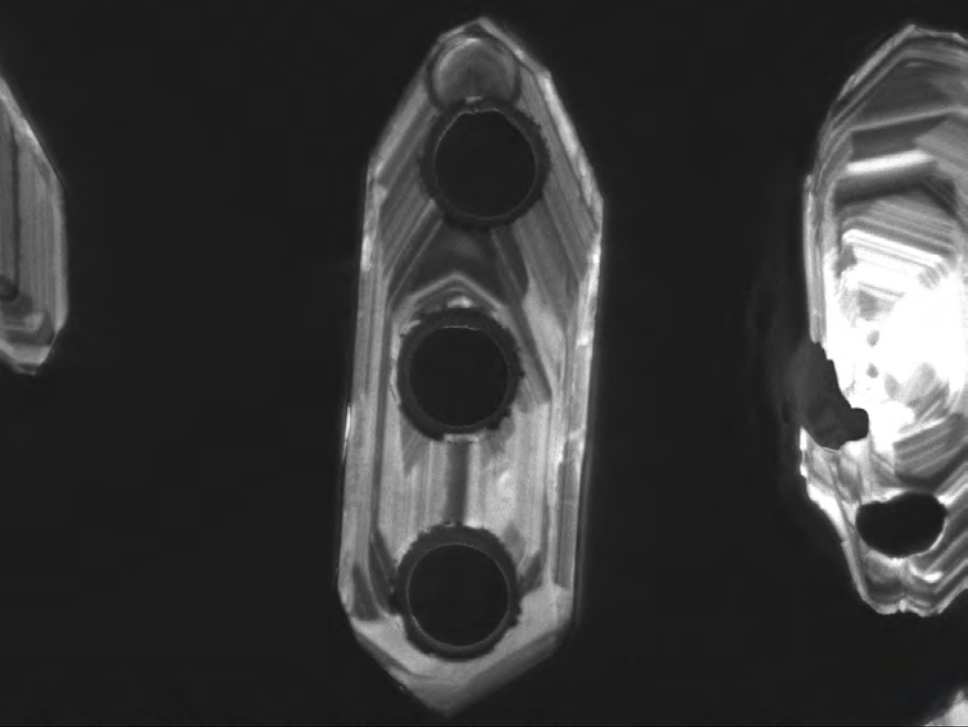
BED-C 20.0kV WD10.3mm Std.-P.C.60.0 HighVac. x400



50um

04 06 2017

EGI



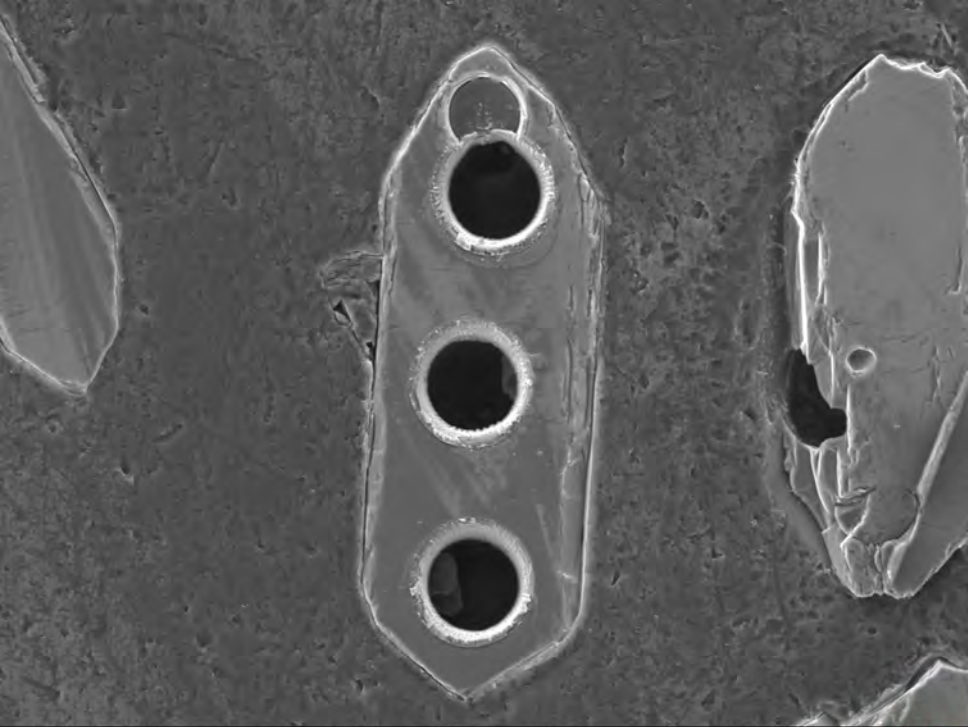
AUX 20.0kV WD17.5mm Std.-P.C.60.0 HighVac. x400



50um

04 06 2017

EGI



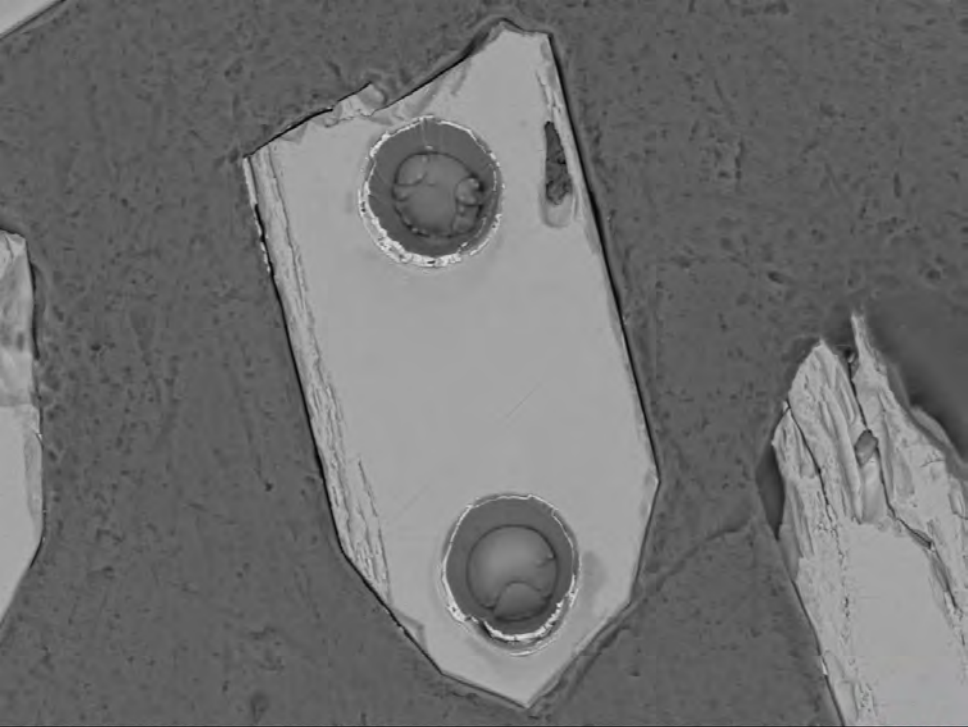
SED 20.0kV WD10.3mm Std.-P.C.60.0 HighVac. x370



50um

04 06 2017

EGI

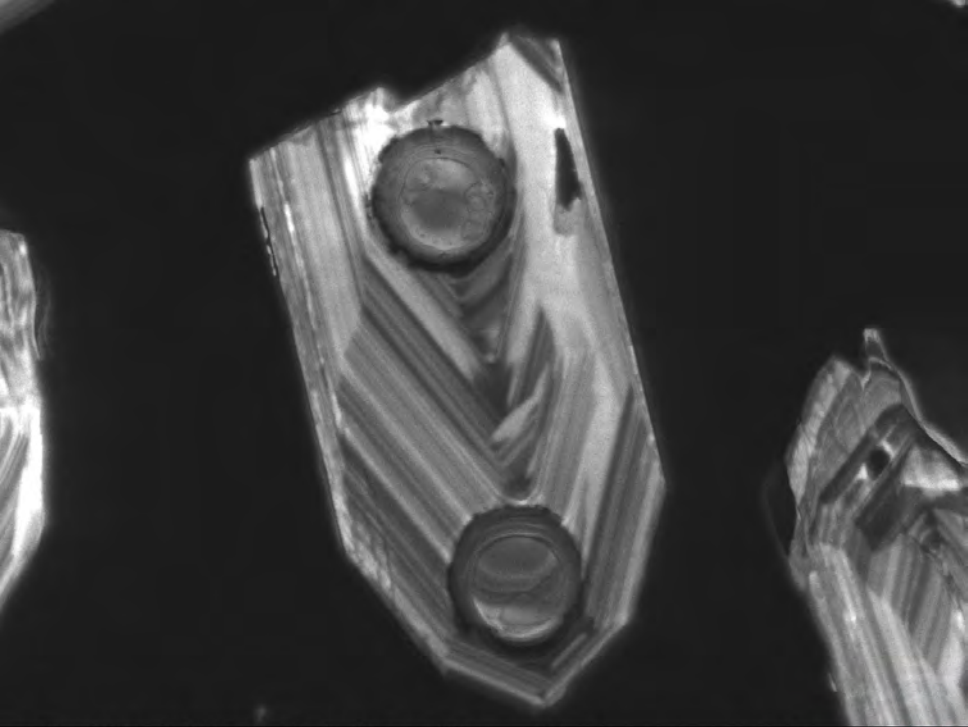


BED-C 20.0kV WD10.3mm Std.-P.C.60.0 HighVac. x430



50um
04 06 2017

EGI



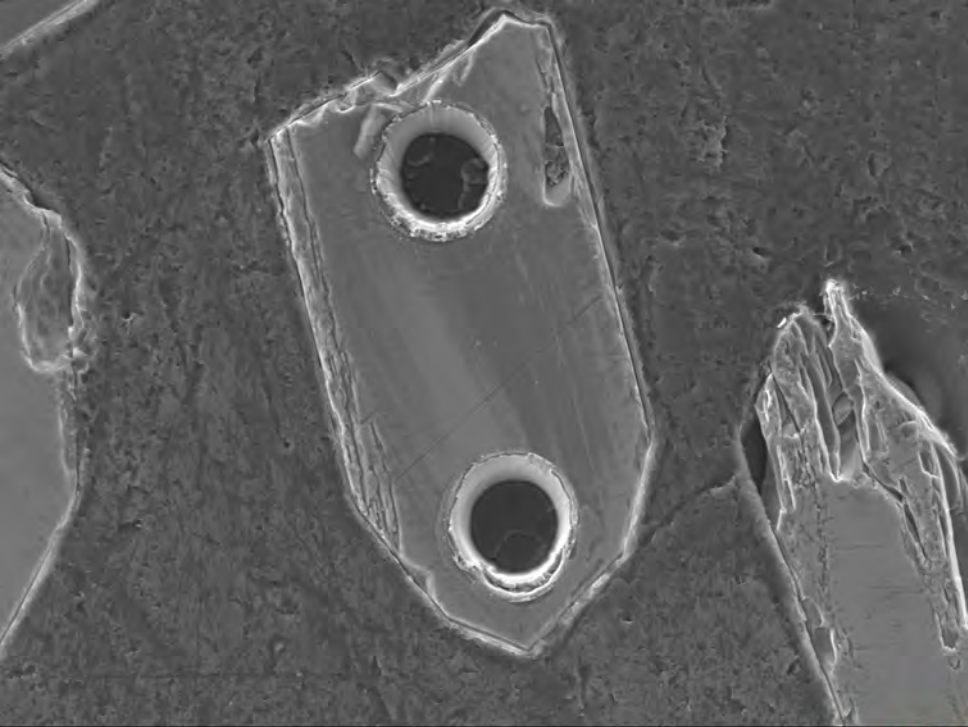
AUX 20.0kV WD17.5mm Std.-P.C.60.0 HighVac.

x430



50um
04 06 2017

EGI



SED 20.0kV WD10.3mm Std.-P.C.60.0 HighVac. x400



50um

04 06 2017

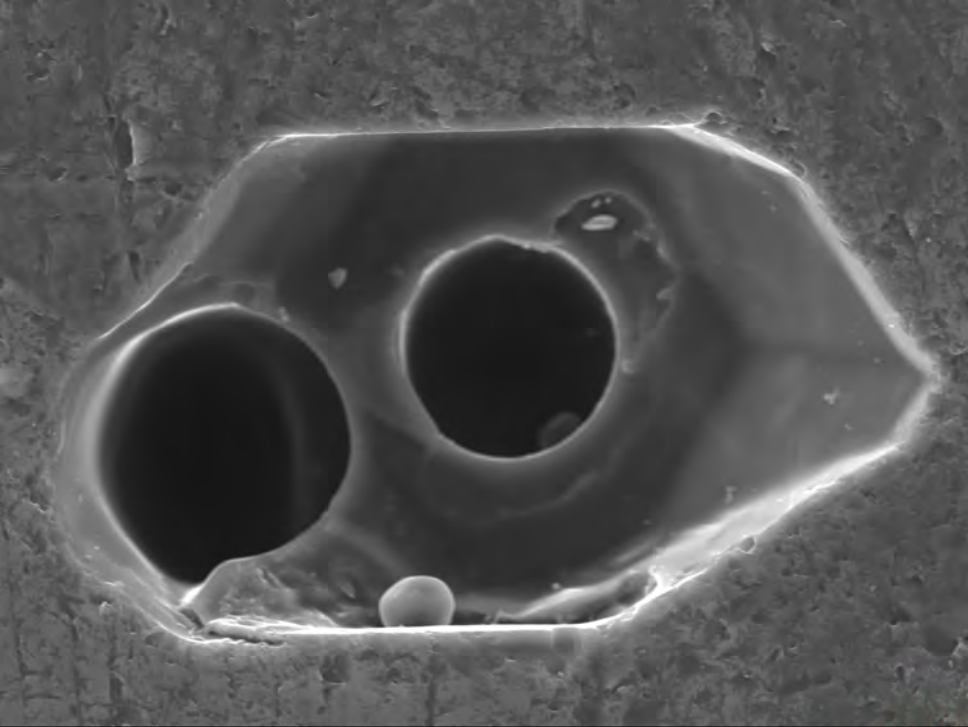
EGI



BED-C 20.0kV WD10.3mm Std.-P.C.60.0 HighVac. x600  20um

04 06 2017

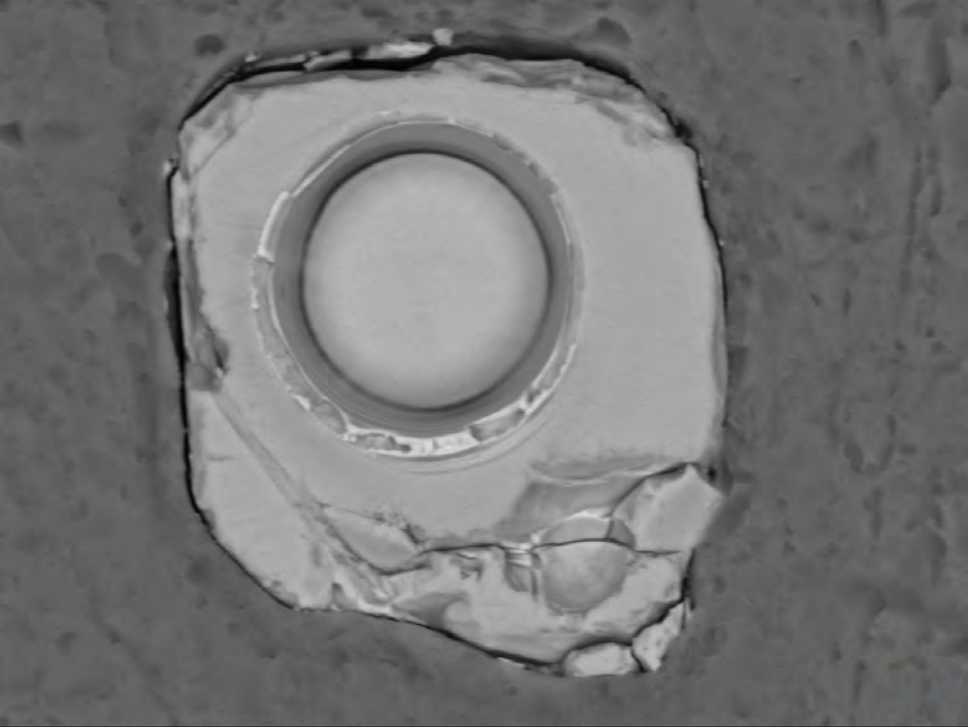
EGI



SED 20.0kV WD10.3mm Std.-P.C.60.0 HighVac. x750  20um

04 06 2017

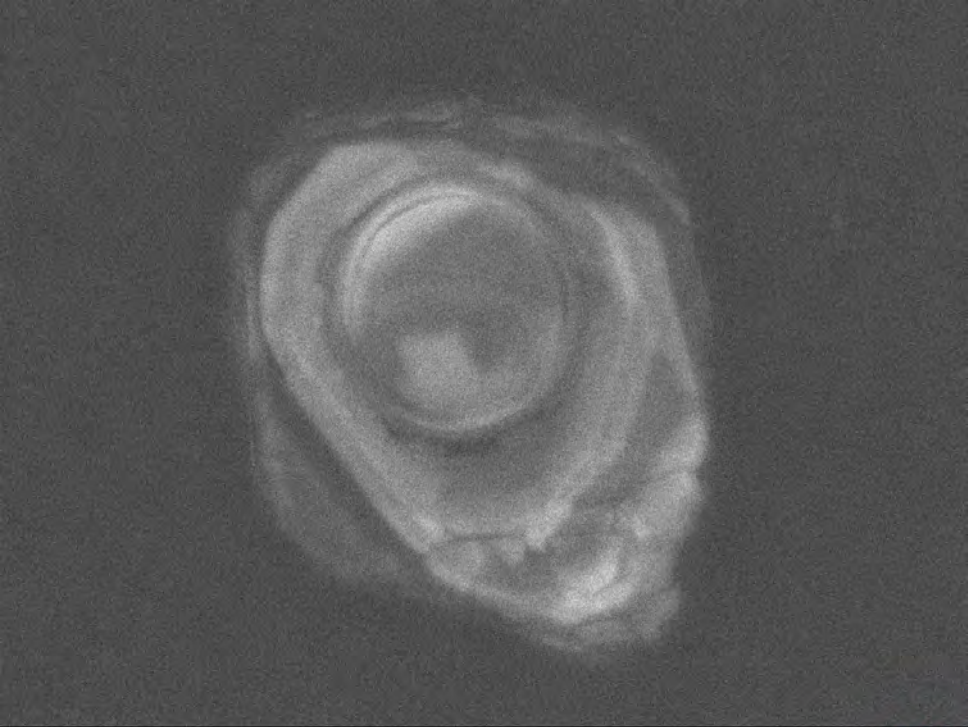
EGI



BED-C 20.0kV WD10.3mm Std.-P.C.60.0 HighVac. x1,300  10um

04 06 2017

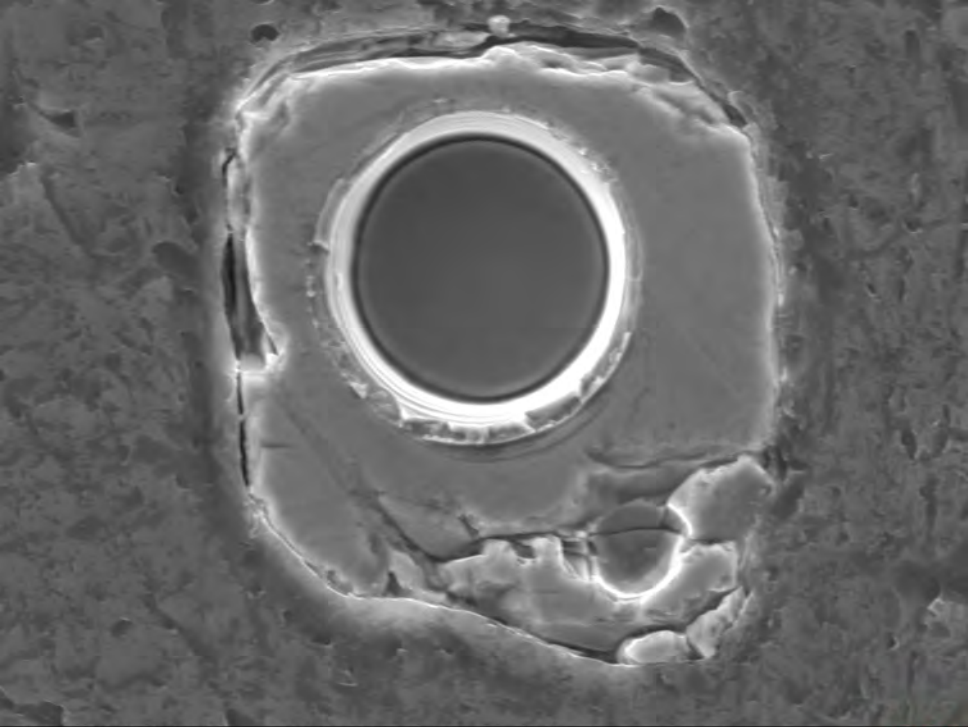
EGI



AUX 20.0kV WD17.5mm Std.-P.C.60.0 HighVac. x1,100  10um

04 06 2017

EGI



SED 20.0kV WD10.3mm Std.-P.C.60.0 HighVac. x1,300  10um

04 06 2017

EGI



BED-C 20.0kV WD10.3mm Std.-P.C.60.0 HighVac. x370



50um

04 06 2017

EGI



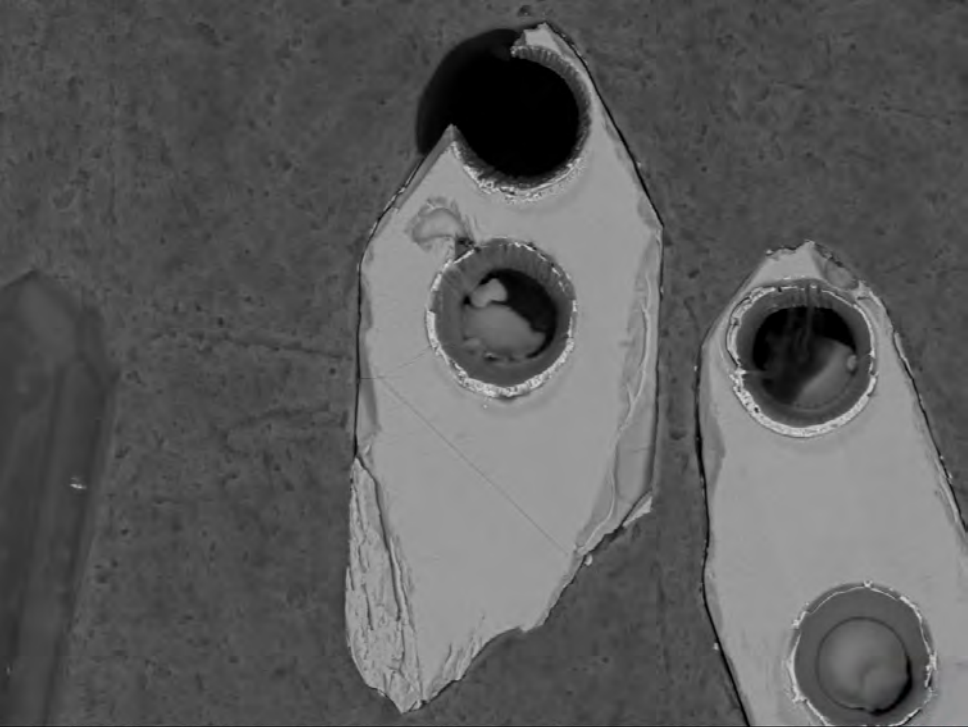
SED 20.0kV WD10.3mm Std.-P.C.60.0 HighVac. x400



50um

04 06 2017

EGI

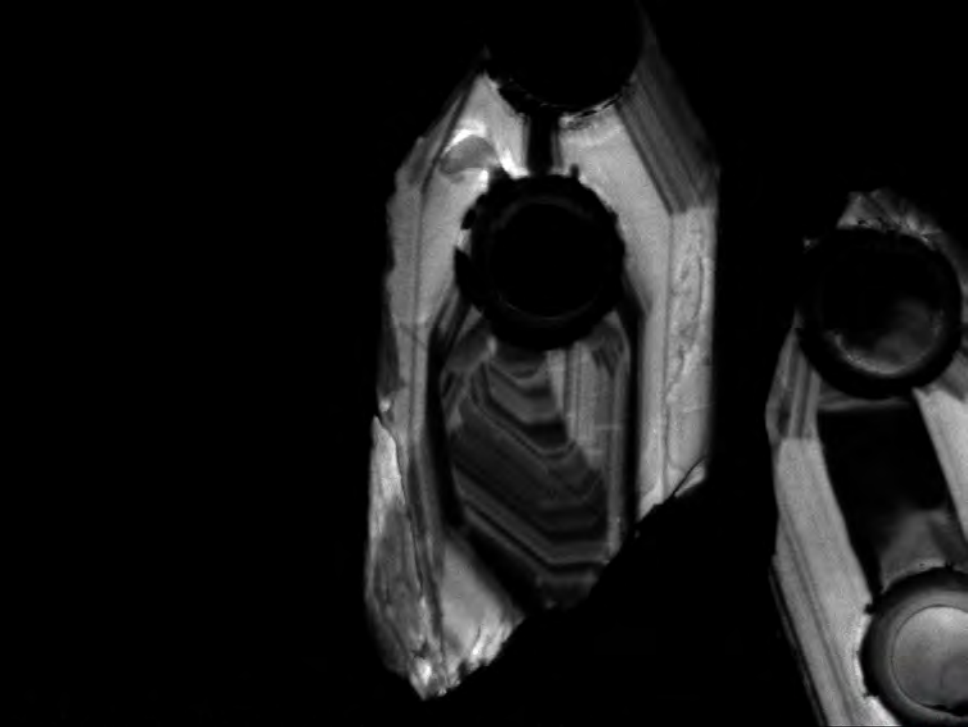


BED-C 20.0kV WD10.3mm Std.-P.C.60.0 HighVac. x450



50um
04 06 2017

EGI



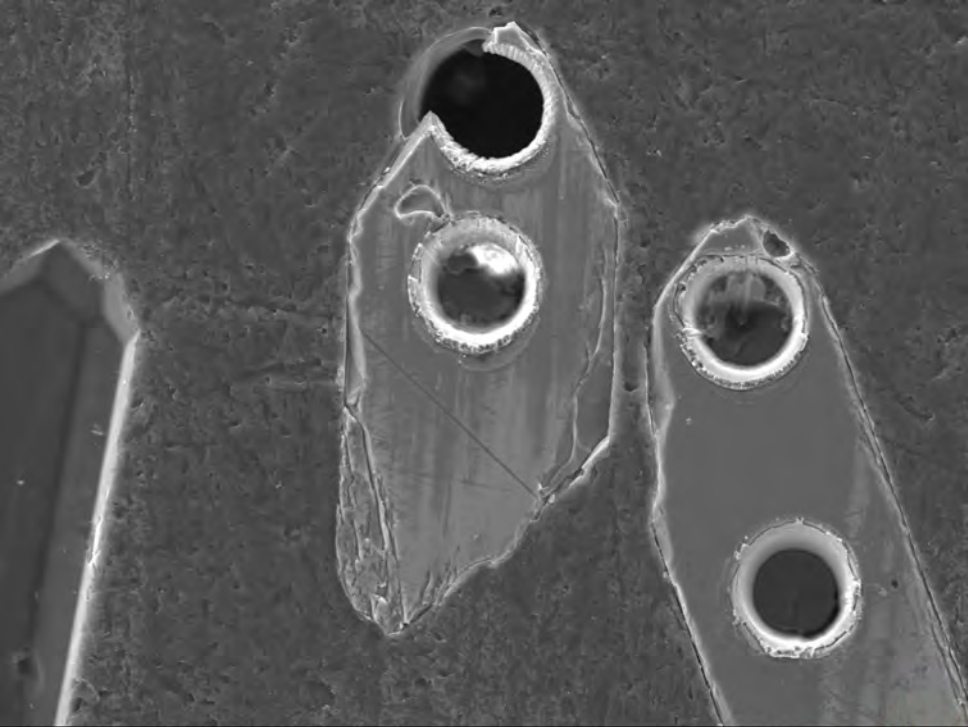
AUX 20.0kV WD17.5mm Std.-P.C.60.0 HighVac. x500



50um

04 06 2017

EGI



SED 20.0kV WD10.3mm Std.-P.C.60.0 HighVac. x400



50um

04 06 2017

EGI



BED-C 20.0kV WD10.3mm Std.-P.C.60.0 HighVac.

x370



50um

04 06 2017

EGI



AUX 20.0kV WD17.5mm Std.-P.C.60.0 HighVac. x350



50um

04 06 2017

EGI



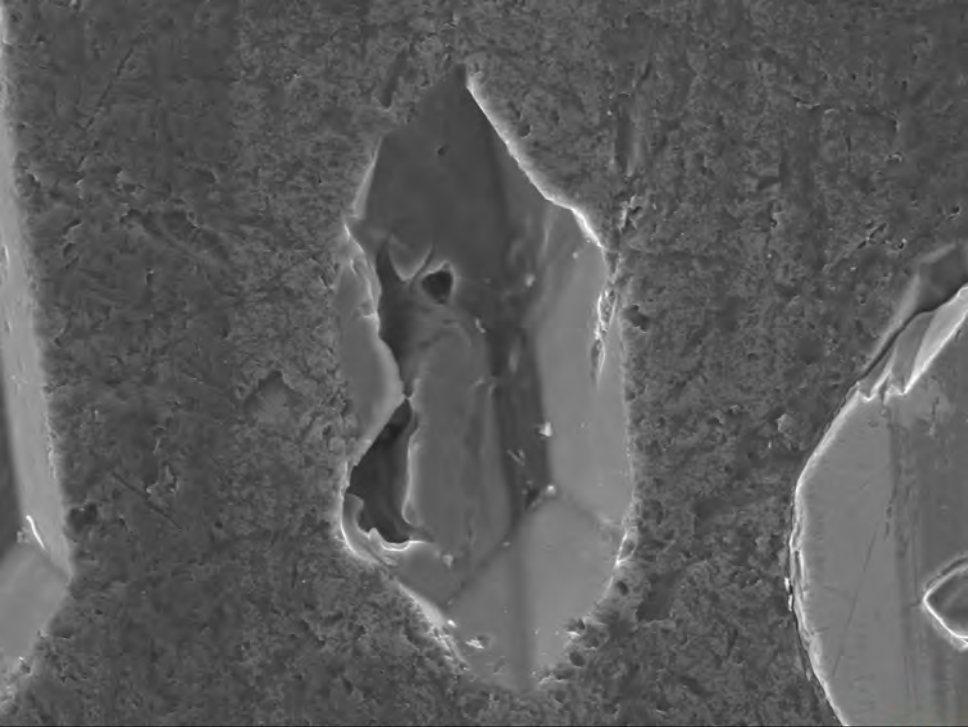
SED 20.0kV WD10.3mm Std.-P.C.60.0 HighVac. x350



50um

04 06 2017

EGI

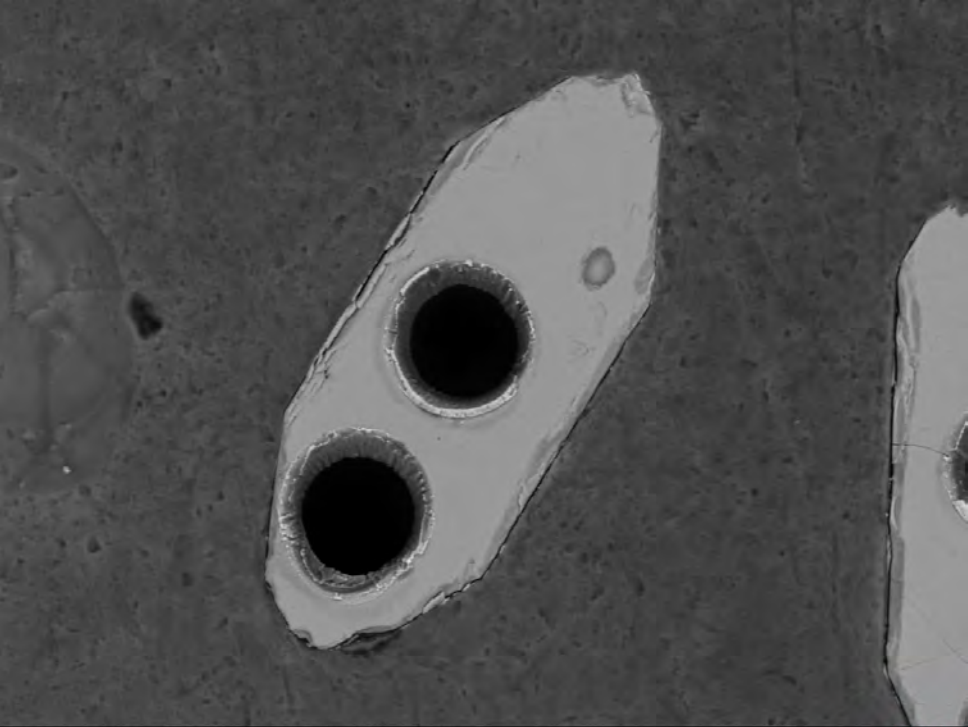


SED 20.0kV WD10.3mm Std.-P.C.60.0 HighVac. x500

50um

04 06 2017

EGI

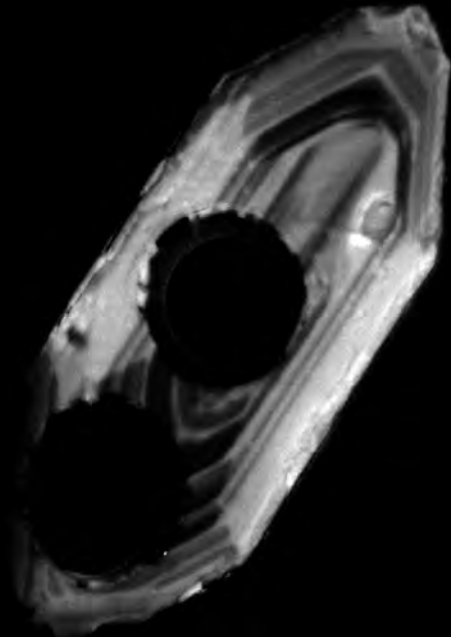


BED-C 20.0kV WD10.3mm Std.-P.C.60.0 HighVac. x450

50um

04 06 2017

EGI



AUX 20.0kV WD17.5mm Std.-P.C.60.0 HighVac. x500



50um

04 06 2017

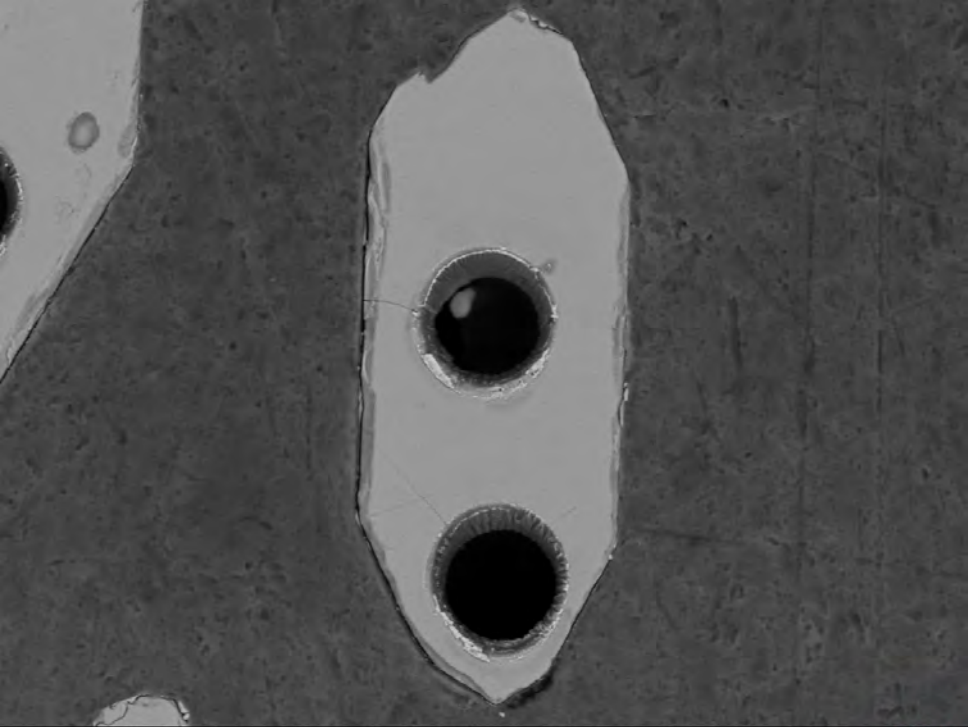




SED 20.0kV WD10.3mm Std.-P.C.60.0 HighVac. x550  20um

04 06 2017

EGI

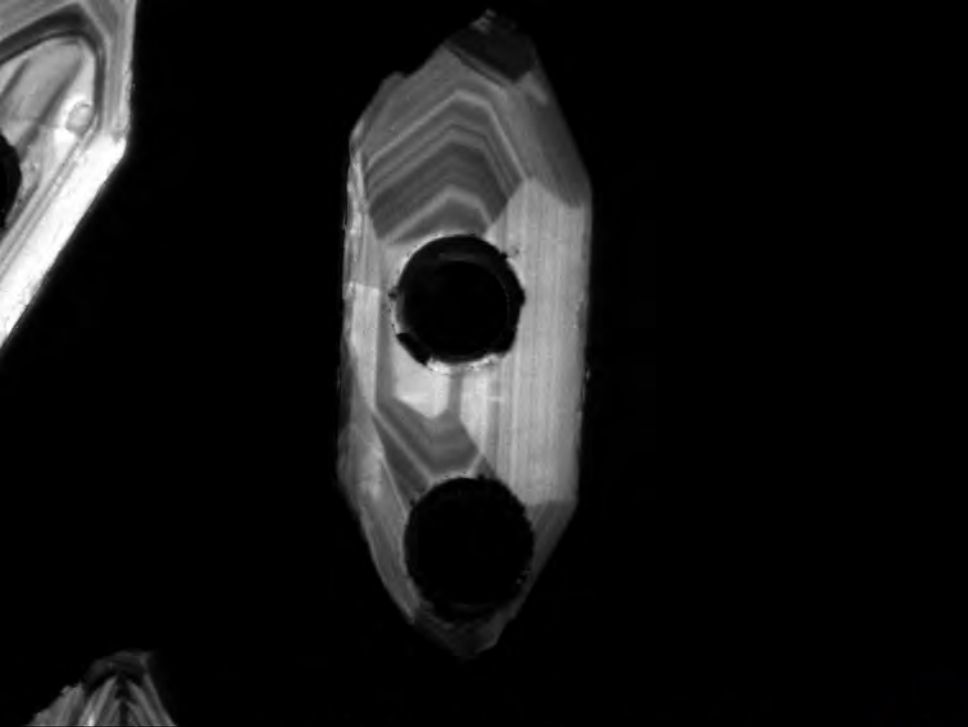


BED-C 20.0kV WD10.3mm Std.-P.C.60.0 HighVac. x430



50um
04 06 2017

EGI



AUX 20.0kV WD17.5mm

Std.-P.C.60.0

HighVac.

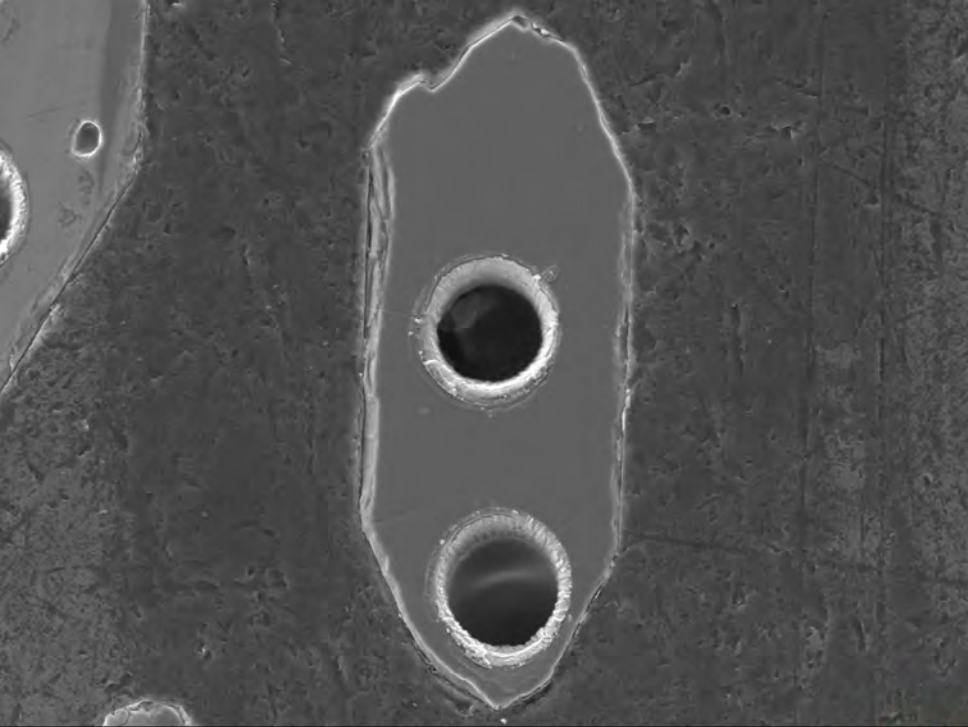
x400



50um

04 06 2017

EGI

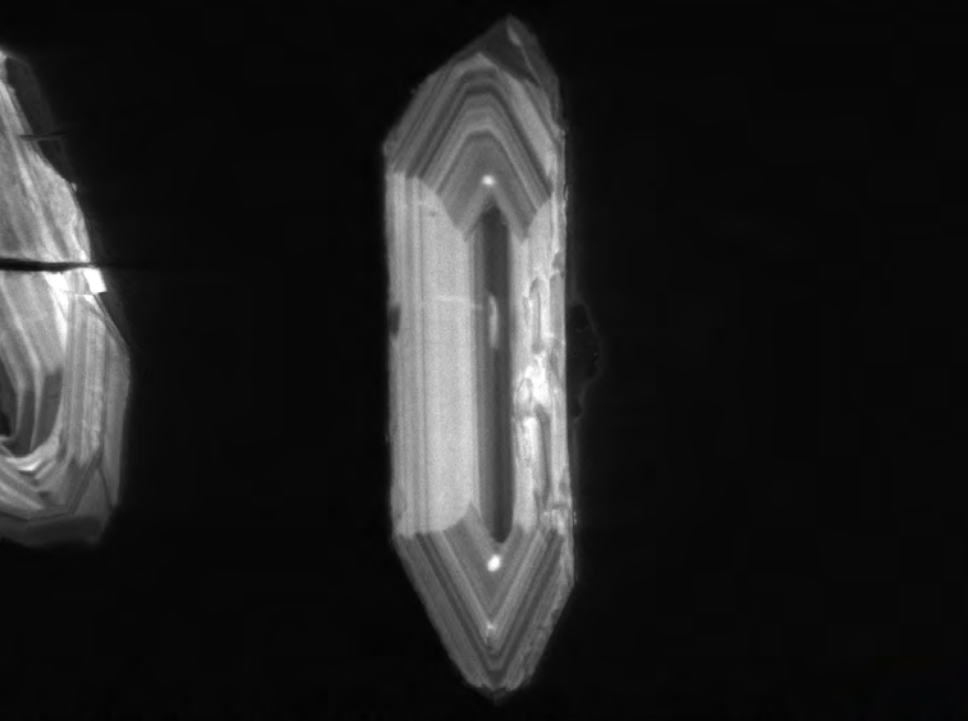


SED 20.0kV WD10.3mm Std.-P.C.60.0 HighVac. x430



50um
04 06 2017

EGI



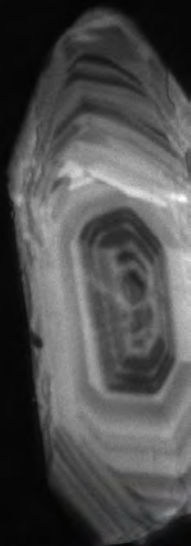
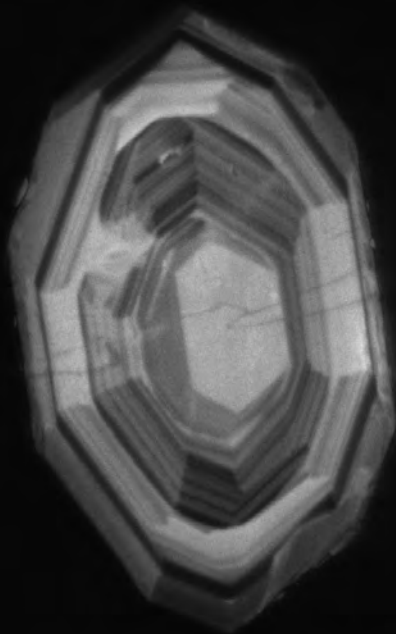
AUX 20.0kV WD17.5mm Std.-P.C.60.0 HighVac. x370



50um

04 06 2017

EGI



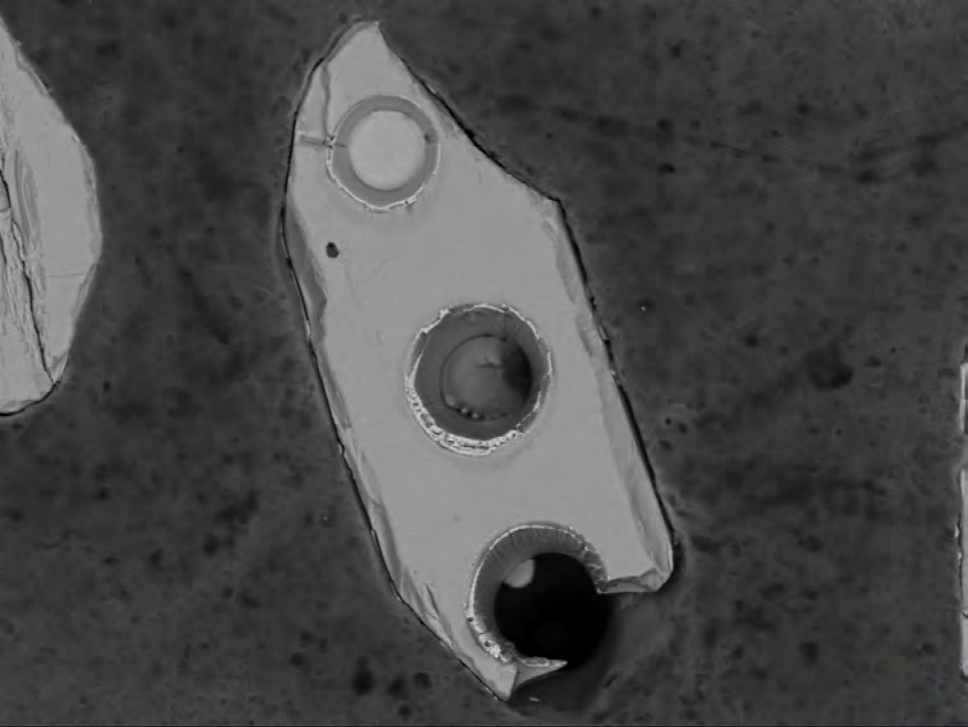
AUX 20.0kV WD17.5mm Std.-P.C.60.0 HighVac. x400



50um

04 06 2017

EGI



BED-C 20.0kV WD10.3mm Std.-P.C.60.0 HighVac. x430



50um
04 06 2017

EGI



AUX 20.0kV WD17.5mm Std.-P.C.60.0 HighVac. x430



50um
04 06 2017

EGI

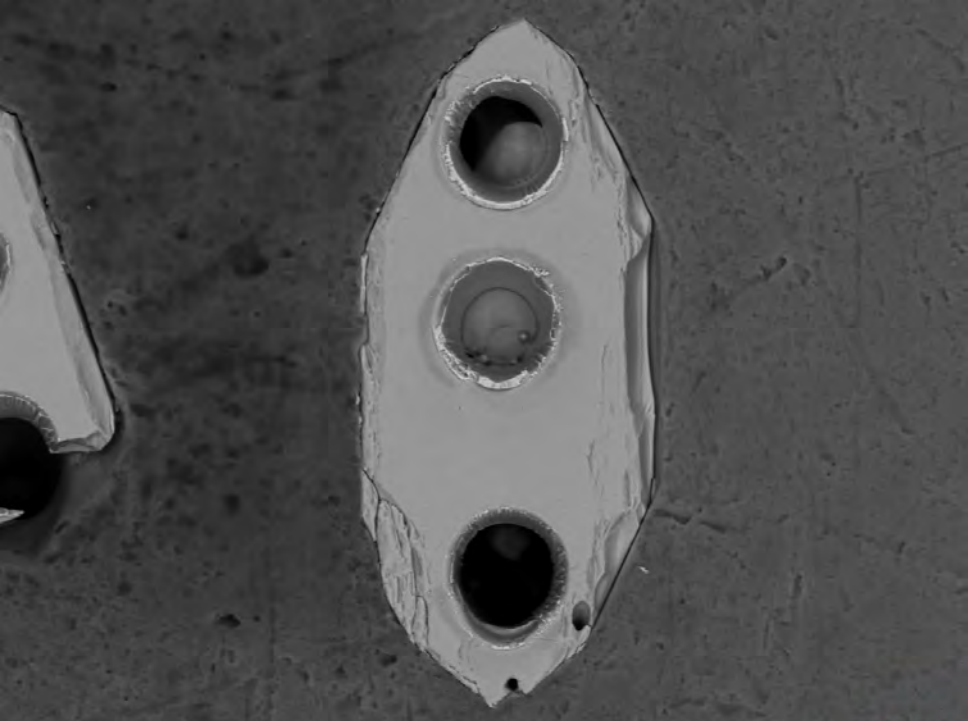


SED 20.0kV WD10.3mm Std.-P.C.60.0 HighVac. x430



50um
04 06 2017

EGI



BED-C 20.0kV WD10.3mm

Std.-P.C.60.0

HighVac.

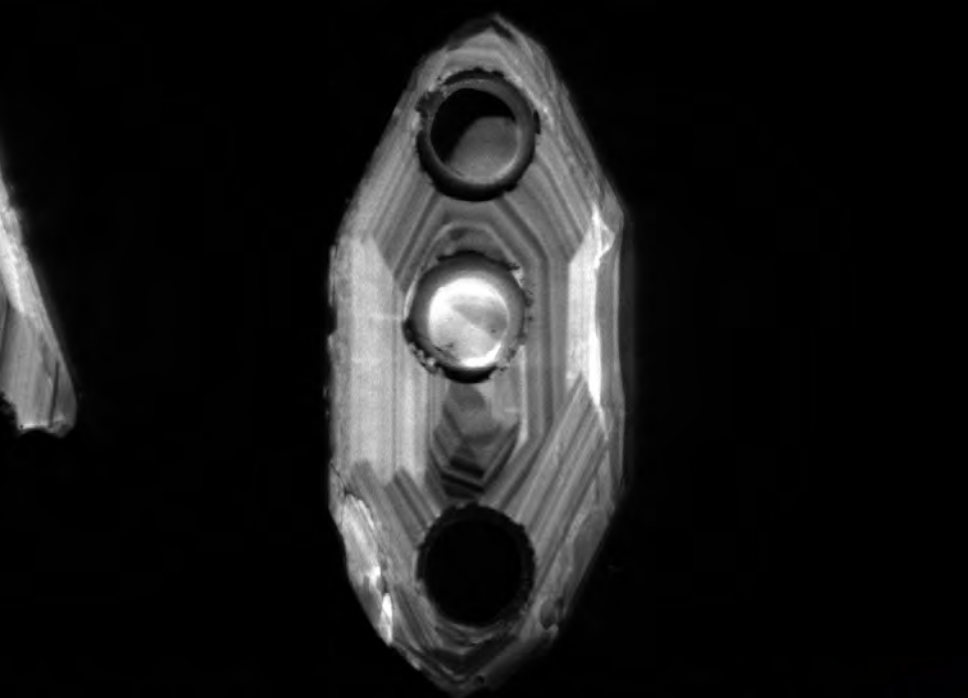
x370



50um

04 06 2017

EGI



AUX 20.0kV WD17.5mm Std.-P.C.60.0 HighVac. x370



50um
04 06 2017

EGI



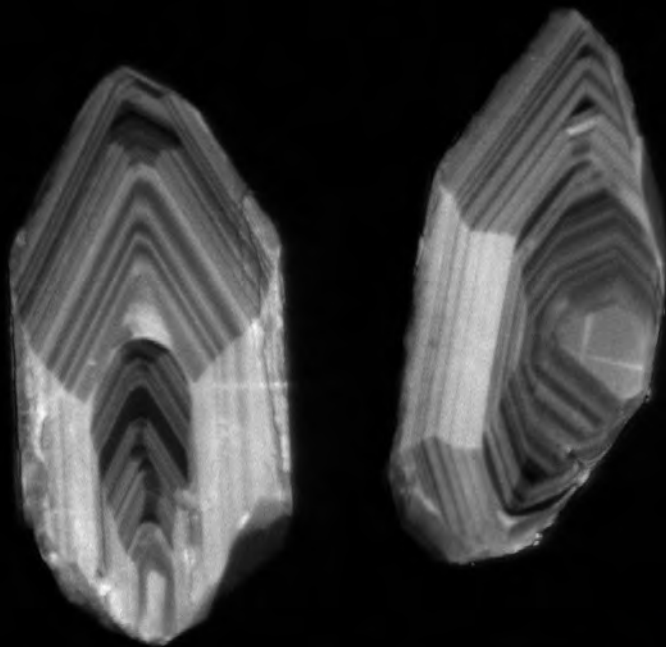
SED 20.0kV WD10.3mm Std.-P.C.60.0 HighVac. x370



50um

04 06 2017

EGI



AUX 20.0kV WD17.5mm Std.-P.C.60.0 HighVac.

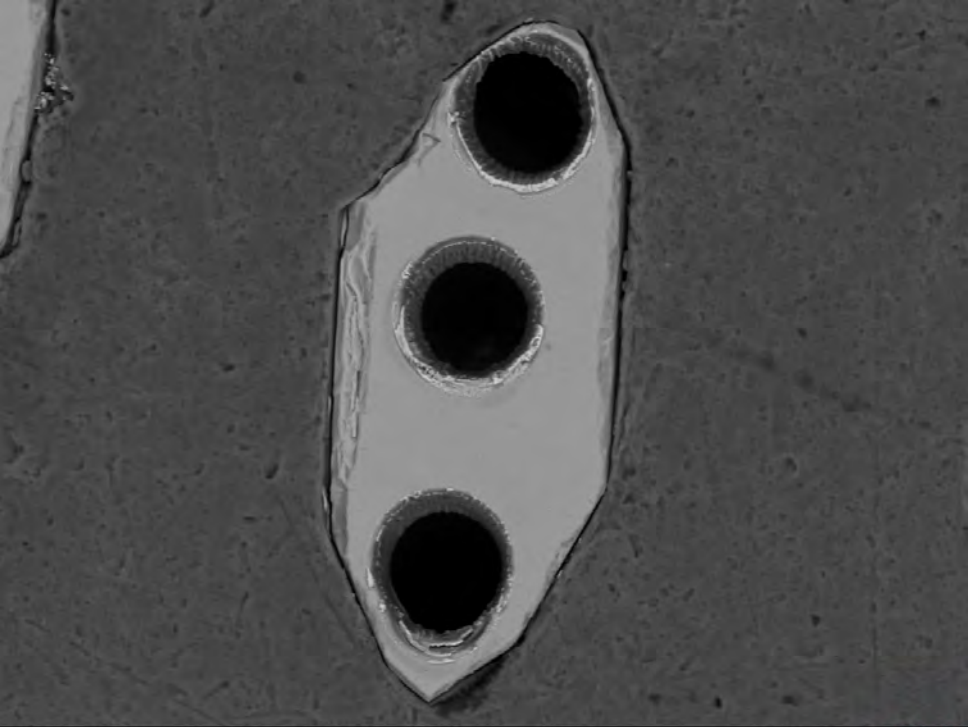
x450



50um

04 06 2017

EGI

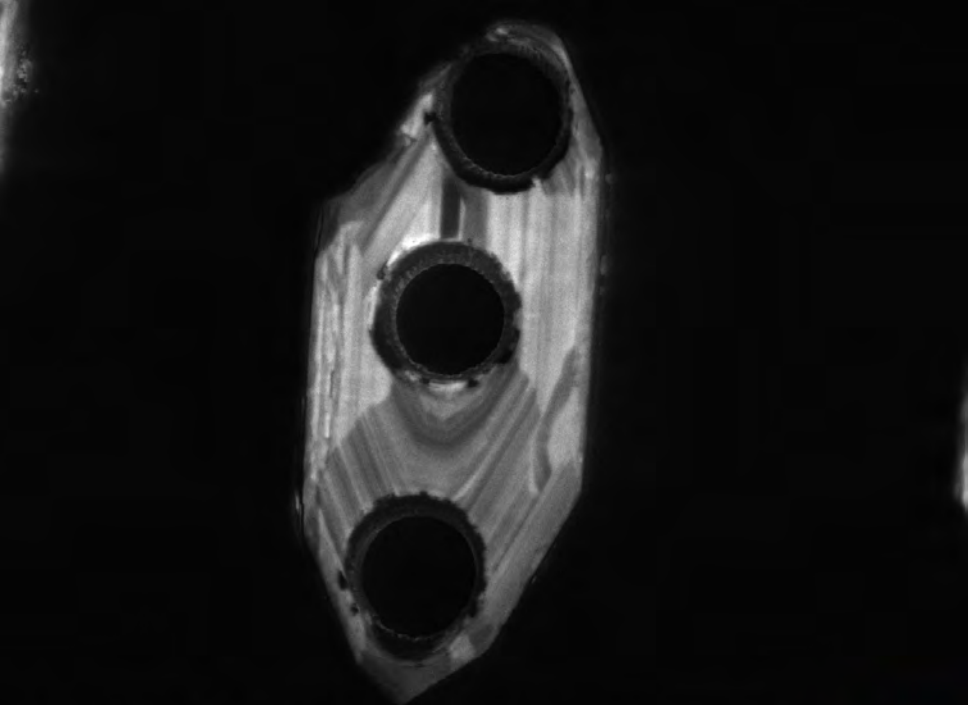


BED-C 20.0kV WD10.3mm Std.-P.C.60.0 HighVac. x450



50um
04 06 2017

EGI



AUX 20.0kV WD17.5mm Std.-P.C.60.0 HighVac. x450



50um
04 06 2017

EGI

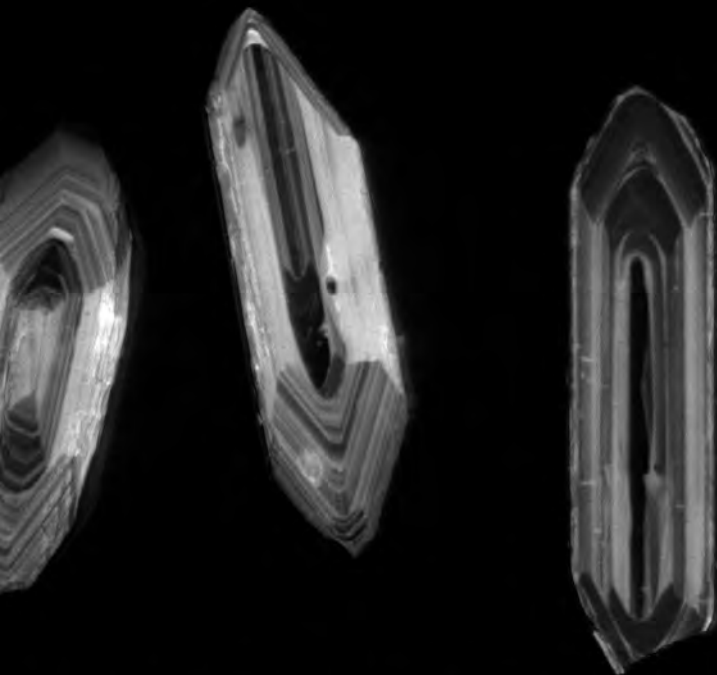


SED 20.0kV WD10.3mm Std.-P.C.60.0 HighVac. x450



50um
04 06 2017

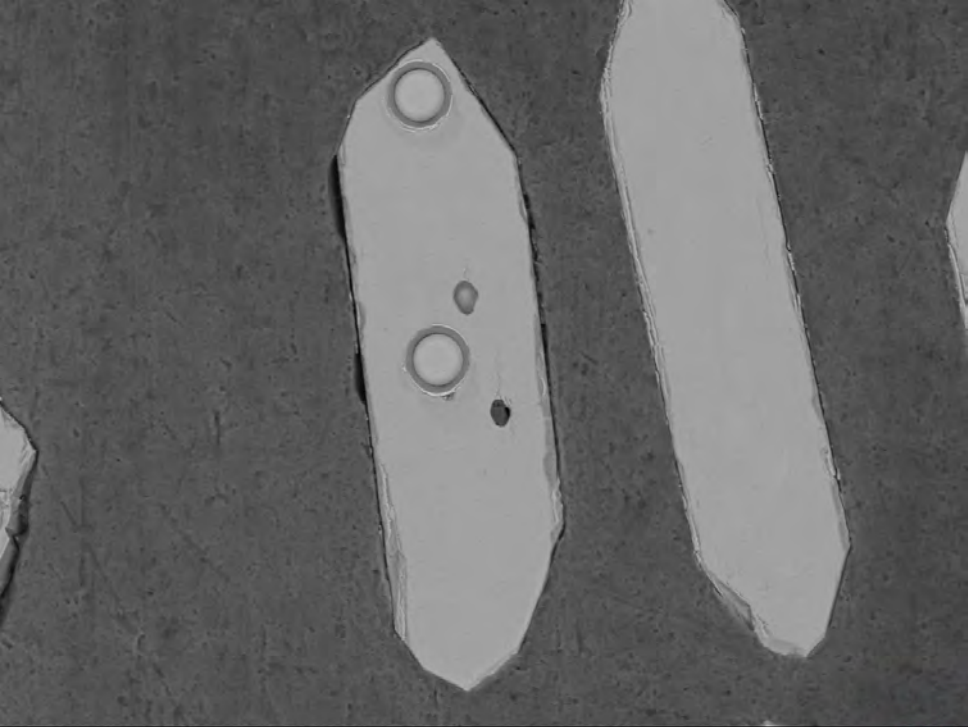
EGI



AUX 20.0kV WD17.5mm Std.-P.C.60.0 HighVac. x270  50um

04 06 2017

EGI



BED-C 20.0kV WD10.3mm

Std.-P.C.60.0

HighVac.

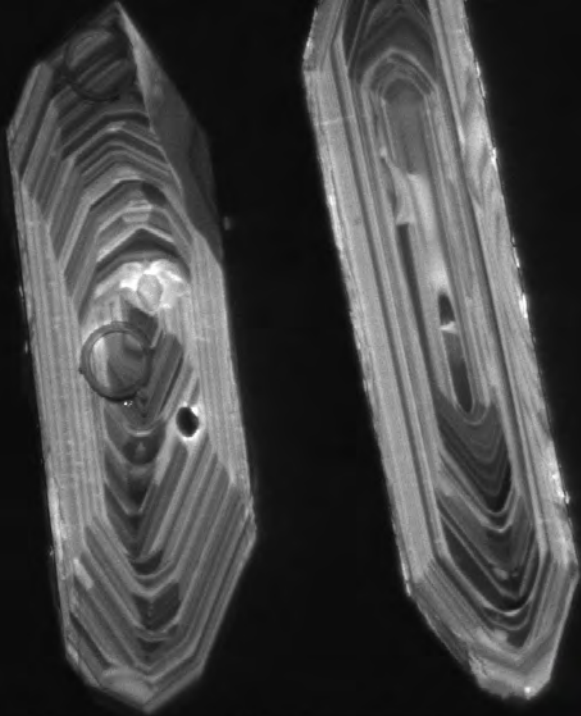
x270



50um

04 06 2017

EGI



AUX

20.0kV

WD17.5mm

Std.-P.C.60.0

HighVac.

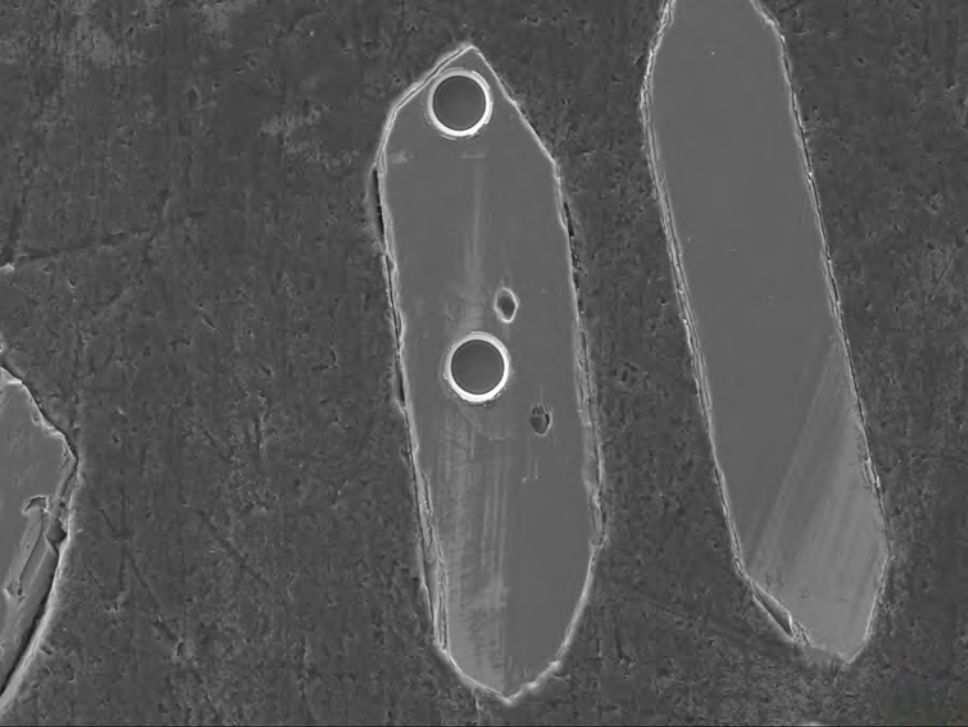
x300



50um

04 06 2017

EGI



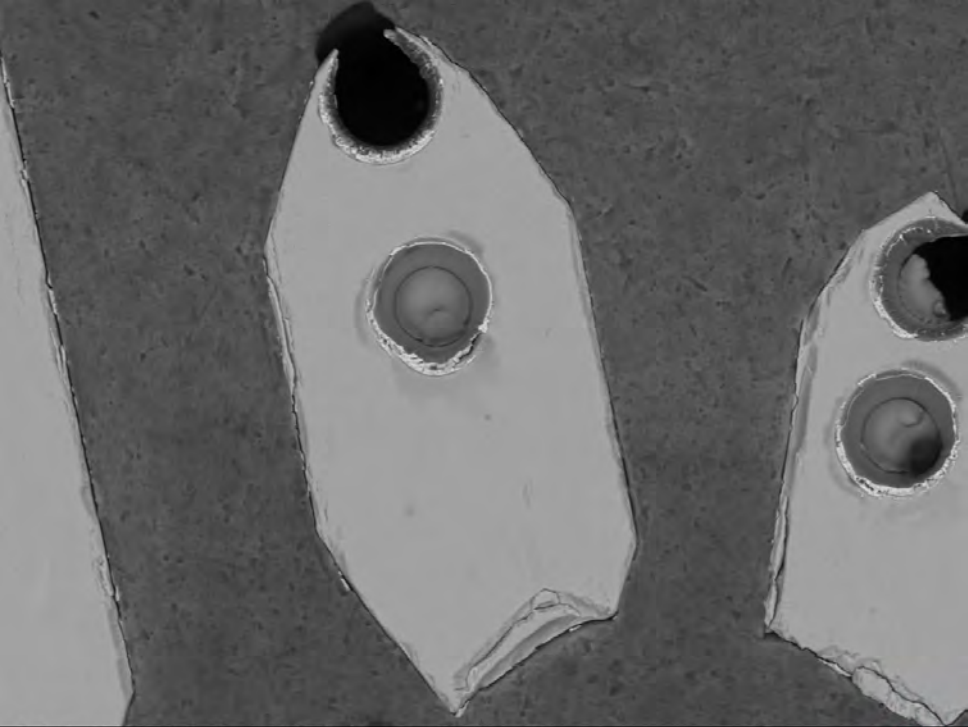
SED 20.0kV WD10.3mm Std.-P.C.60.0 HighVac. x270



50um

04 06 2017

EGI



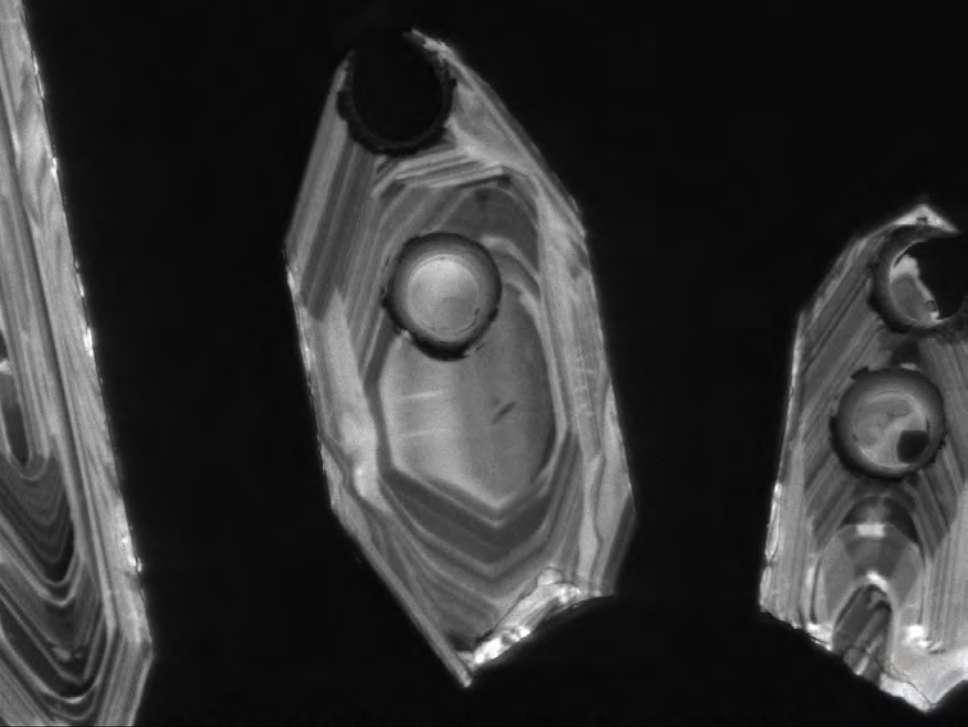
BED-C 20.0kV WD10.3mm Std.-P.C.60.0 HighVac. x370



50um

04 06 2017

EGI



AUX 20.0kV WD17.5mm Std.-P.C.60.0 HighVac.

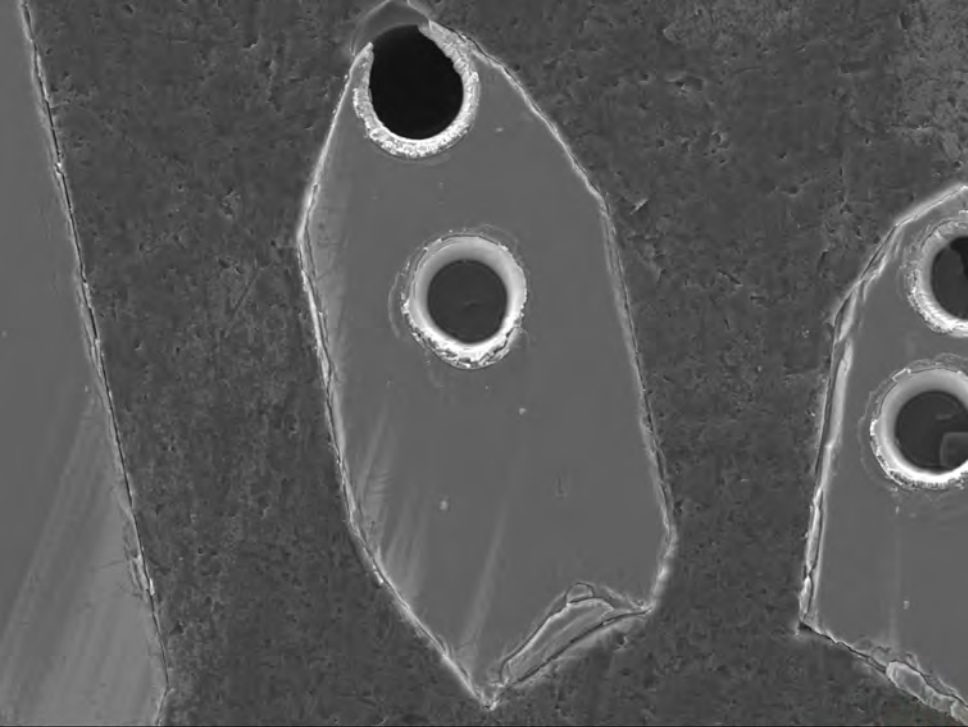
x350



50um

04 06 2017

EGI



SED 20.0kV WD10.3mm Std.-P.C.60.0 HighVac. x370



50um

04 06 2017

EGI

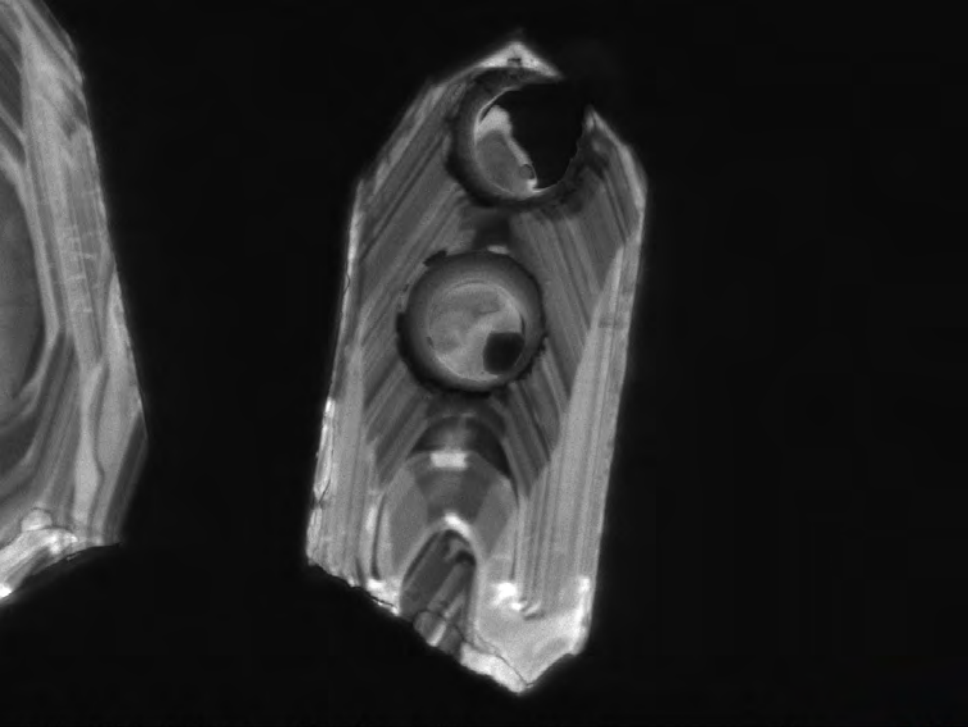


BED-C 20.0kV WD10.3mm Std.-P.C.60.0 HighVac. x450



50um
04 06 2017

EGI

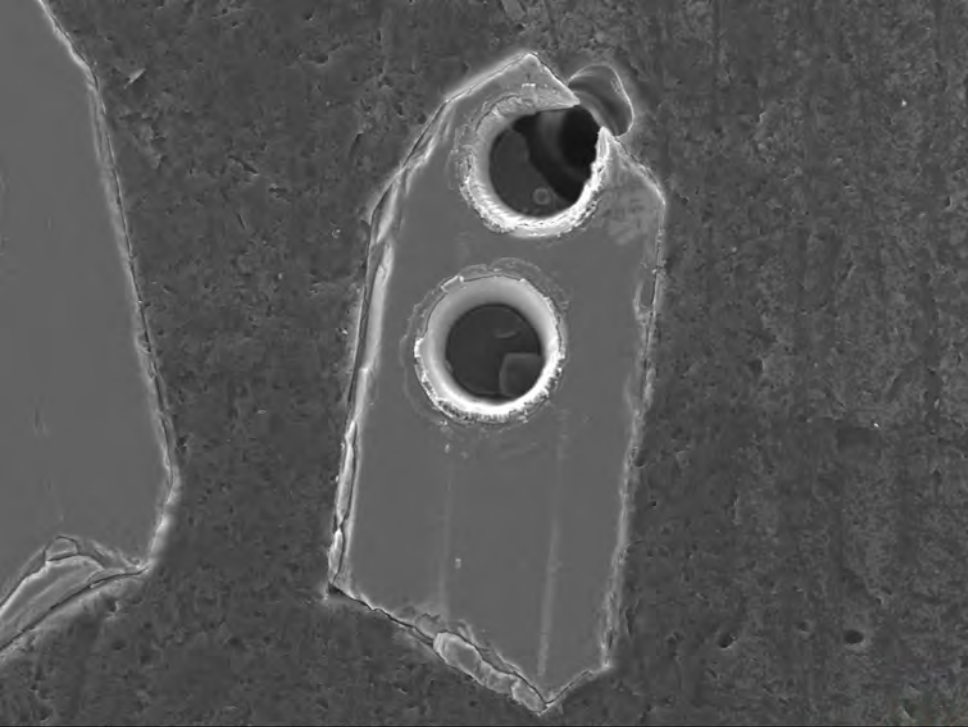


AUX 20.0kV WD17.5mm Std.-P.C.60.0 HighVac. x450



50um
04 06 2017

EGI

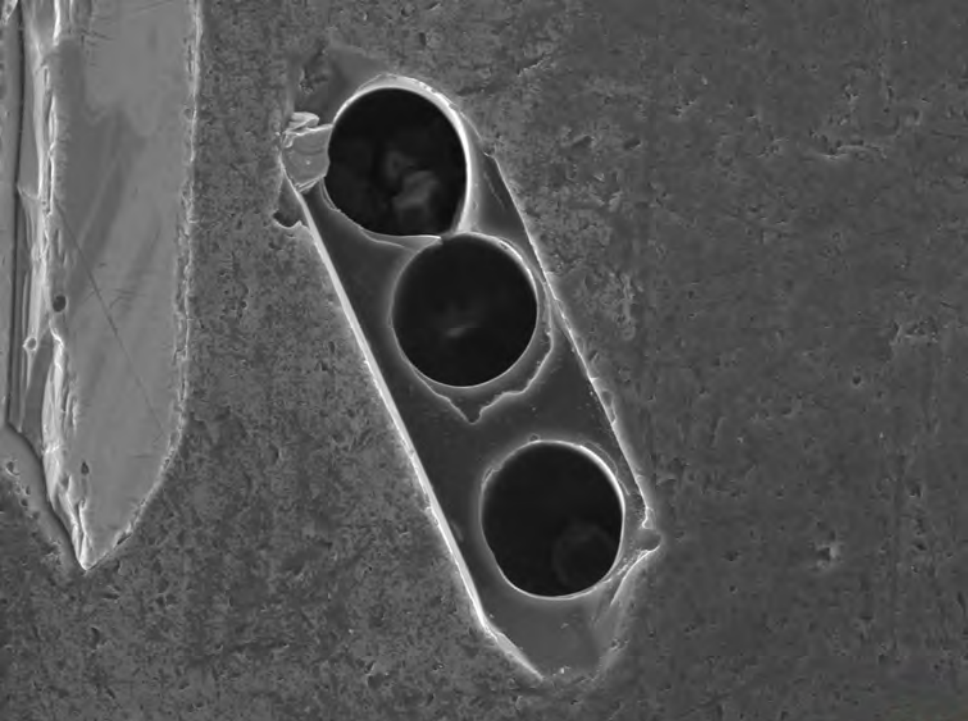


SED 20.0kV WD10.3mm Std.-P.C.60.0 HighVac. x450



50um
04 06 2017

EGI

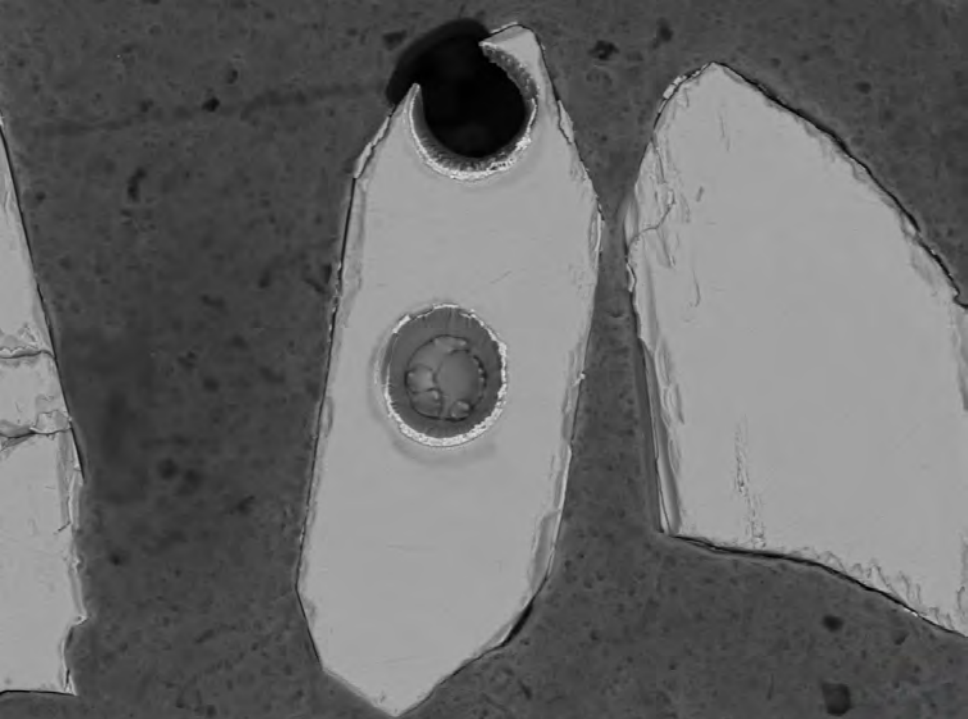


SED 20.0kV WD10.3mm Std.-P.C.60.0 HighVac. x430



50um
04 06 2017

EGI



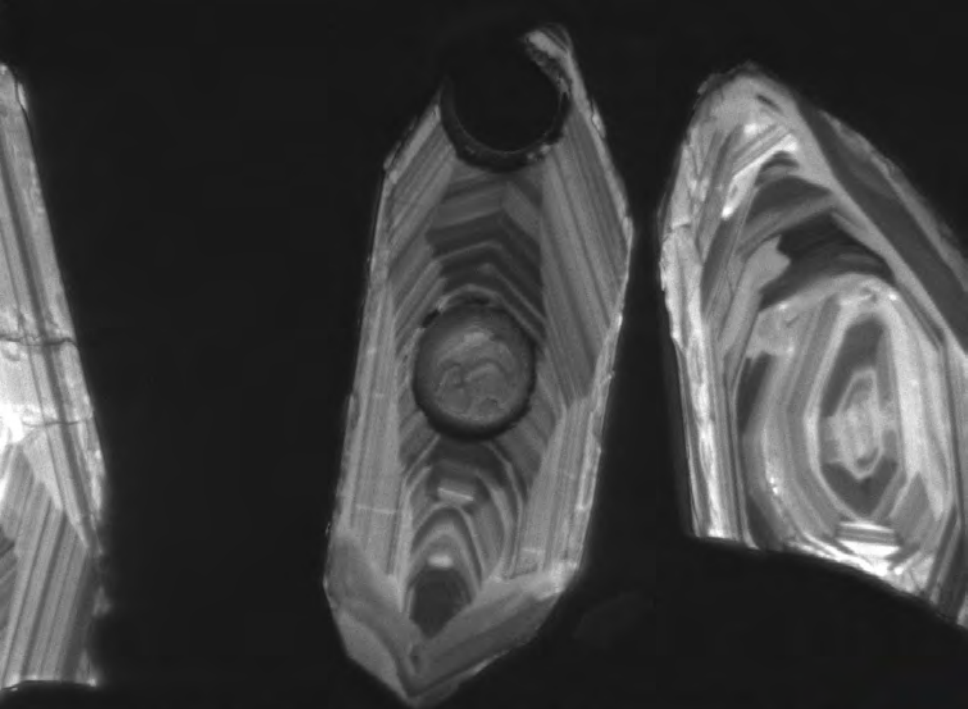
BED-C 20.0kV WD10.3mm Std.-P.C.60.0 HighVac. x400



50um

04 06 2017

EGI



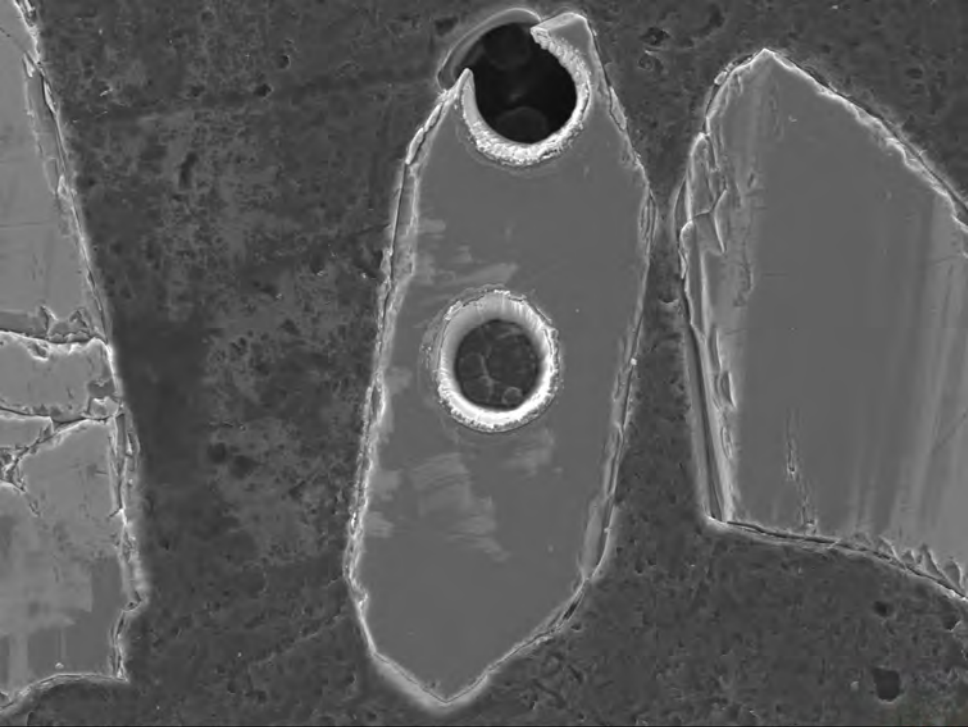
AUX 20.0kV WD17.5mm Std.-P.C.60.0 HighVac. x400



50um

04 06 2017

EGI



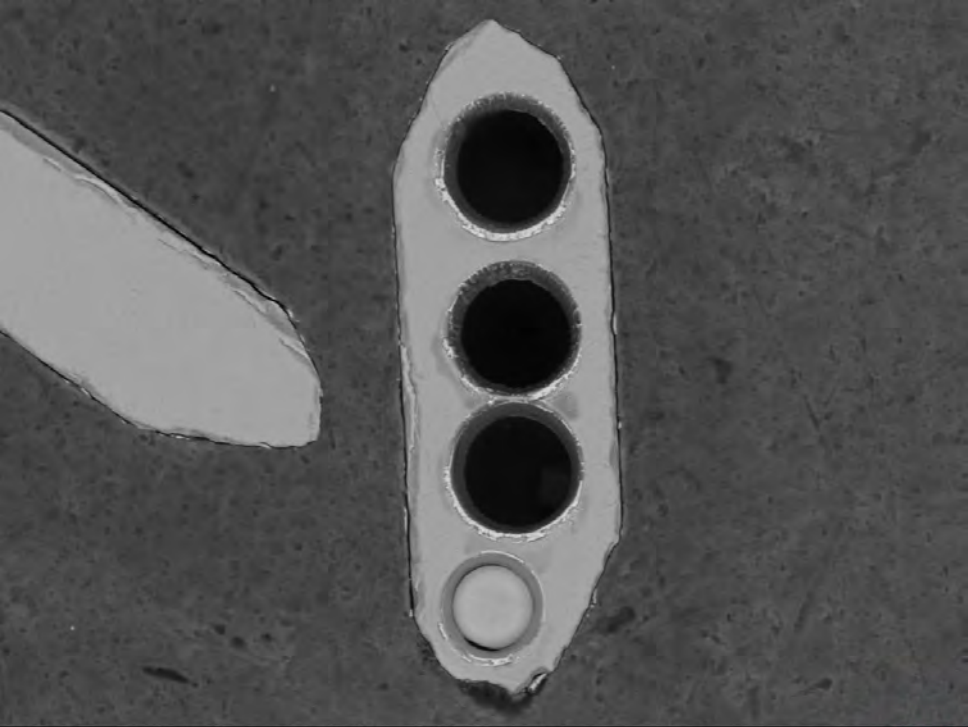
SED 20.0kV WD10.3mm Std.-P.C.60.0 HighVac. x400



50um

04 06 2017

EGI

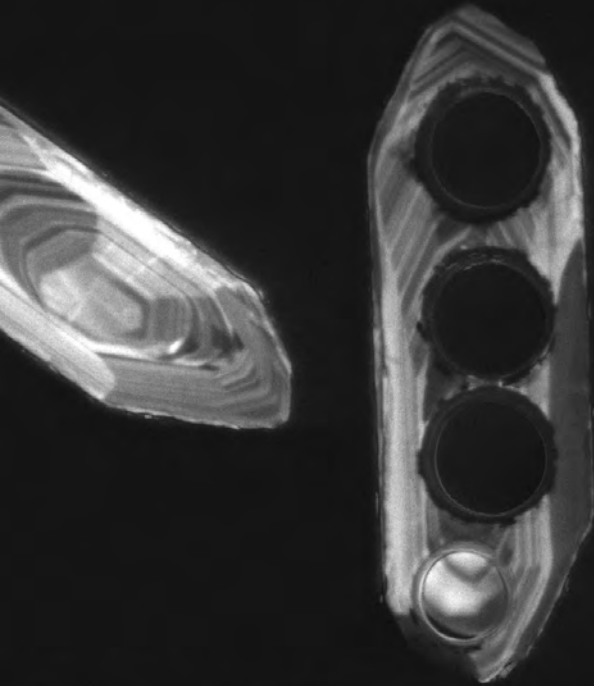


BED-C 20.0kV WD10.3mm Std.-P.C.60.0 HighVac. x430



50um
04 06 2017

EGI

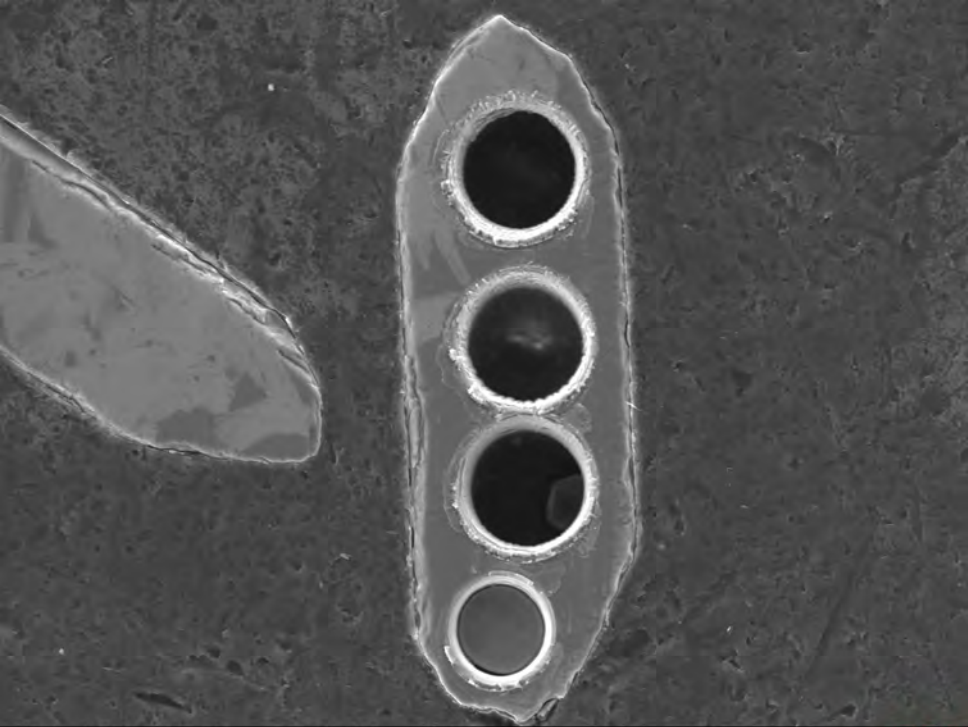


AUX 20.0kV WD17.5mm Std.-P.C.60.0 HighVac. x430



50um
04 06 2017

EGI

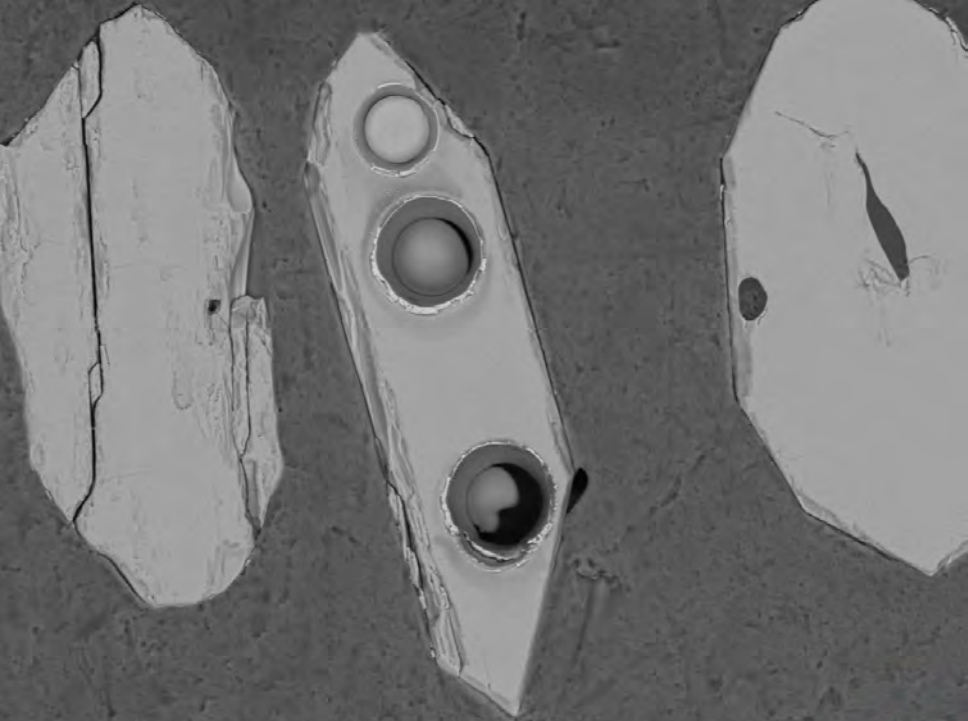


SED 20.0kV WD10.3mm Std.-P.C.60.0 HighVac. x450



50um
04 06 2017

EGI



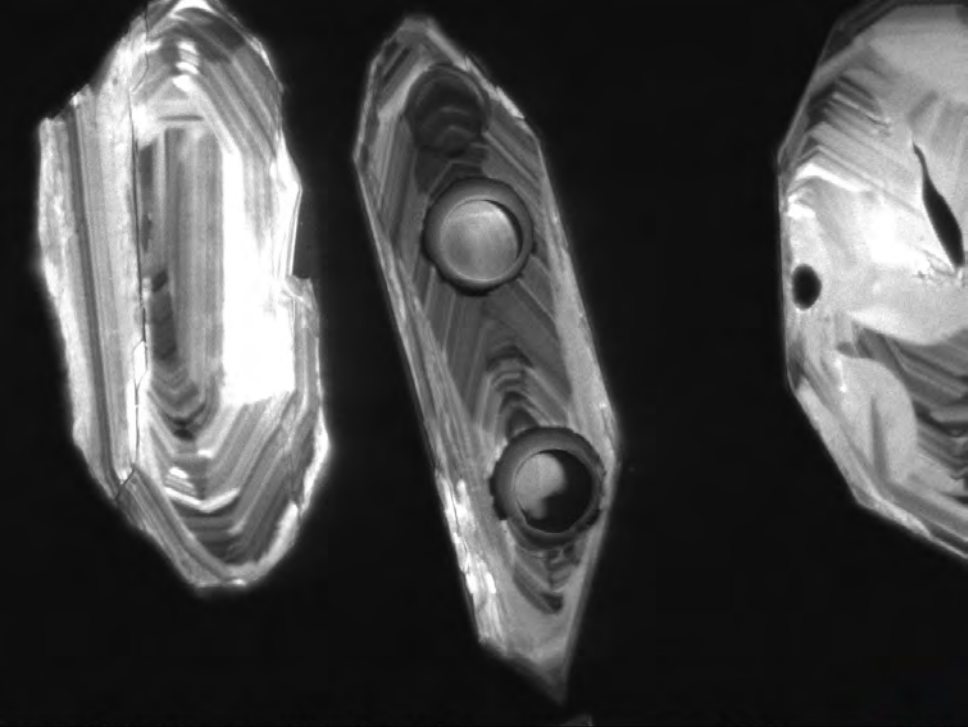
BED-C 20.0kV WD10.3mm Std.-P.C.60.0 HighVac. x350



50um

04 06 2017

EGI



AUX 20.0kV WD17.5mm Std.-P.C.60.0 HighVac.

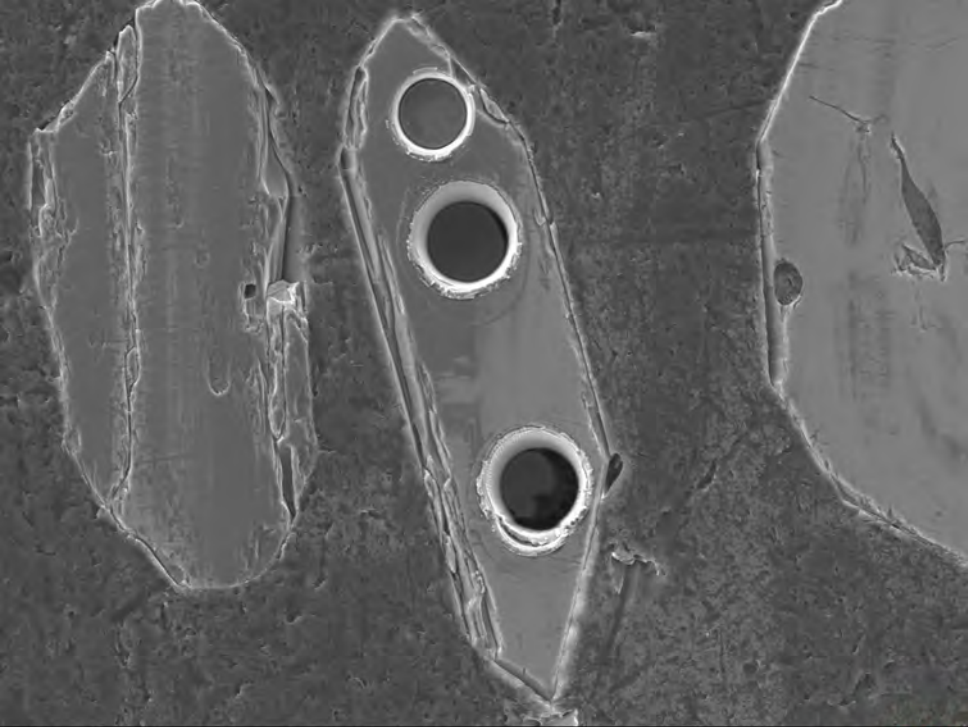
x350



50um

04 06 2017

EGI



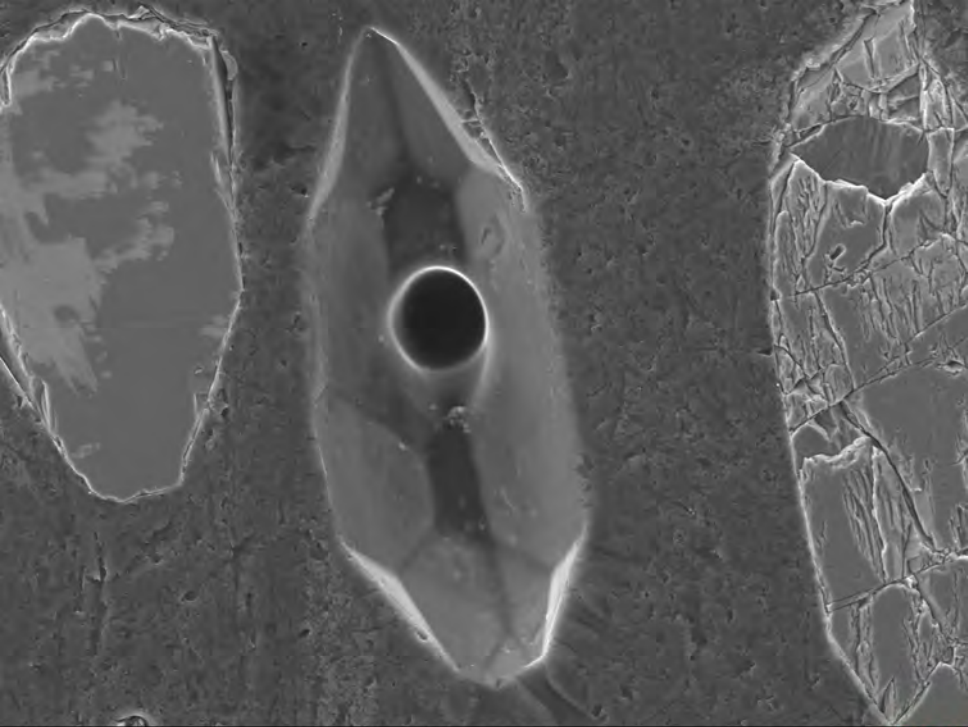
SED 20.0kV WD10.3mm Std.-P.C.60.0 HighVac. x350



50um

04 06 2017

EGI



SED 20.0kV WD10.3mm Std.-P.C.60.0 HighVac. x350



50um

04 06 2017

EGI



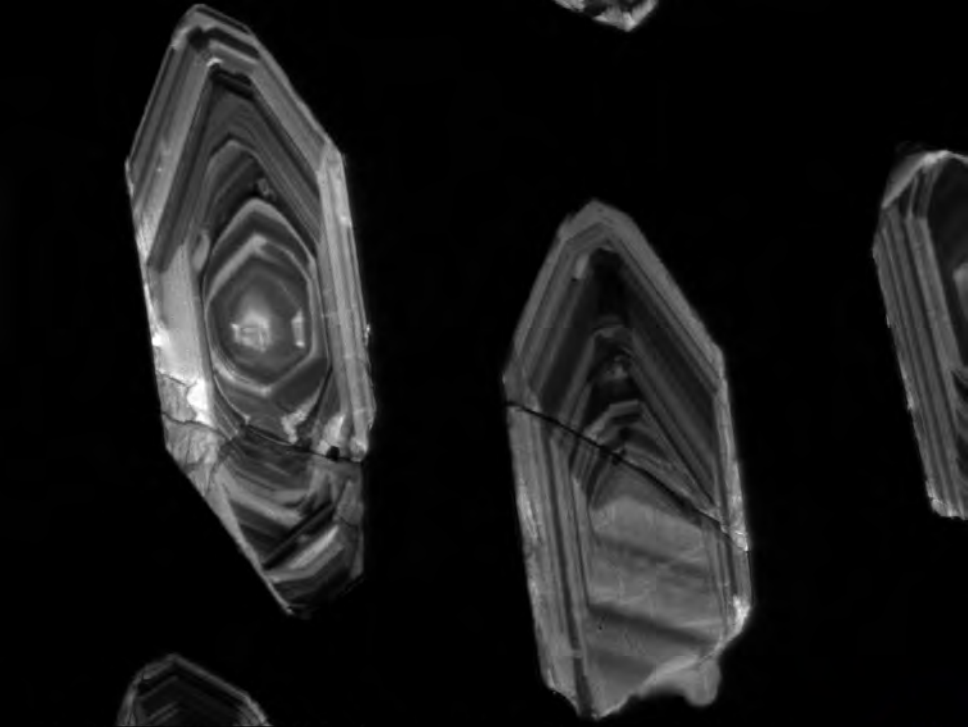
AUX 20.0kV WD17.5mm Std.-P.C.60.0 HighVac. x270



50um

04 06 2017

EGI



AUX

20.0kV

WD17.5mm

Std.-P.C.60.0

HighVac.

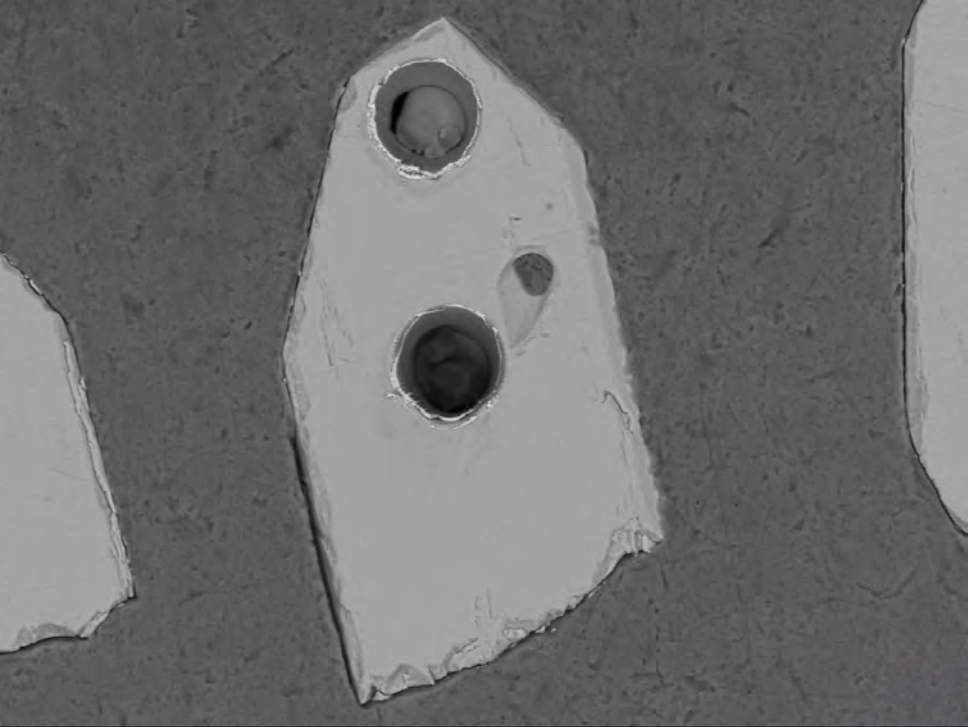
x300



50um

04 06 2017

EGI



BED-C 20.0kV WD10.3mm

Std.-P.C.60.0

HighVac.

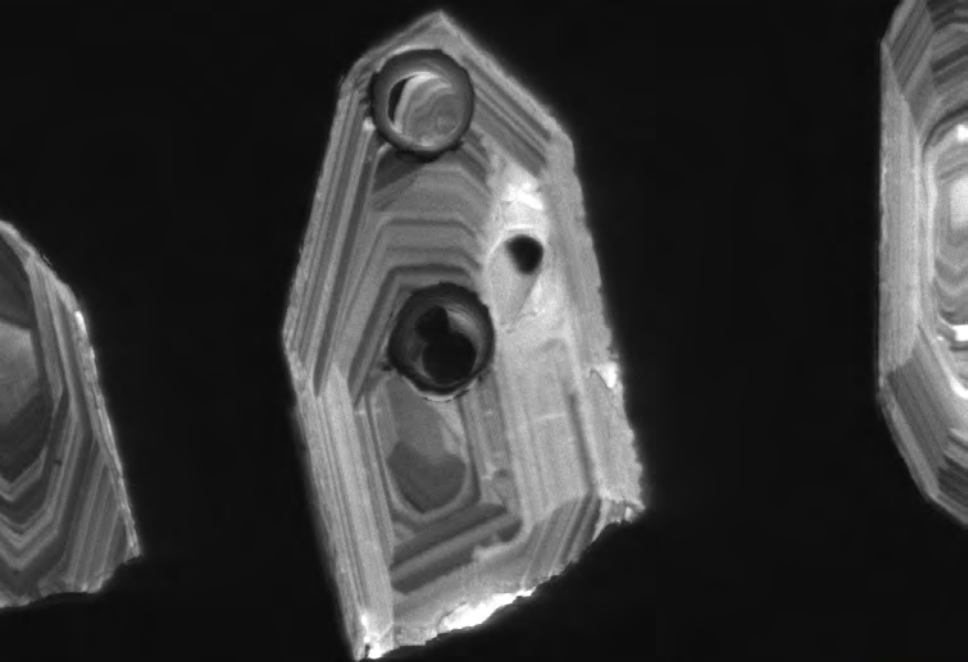
x350



50um

04 06 2017

EGI



AUX

20.0kV

WD17.5mm

Std.-P.C.60.0

HighVac.

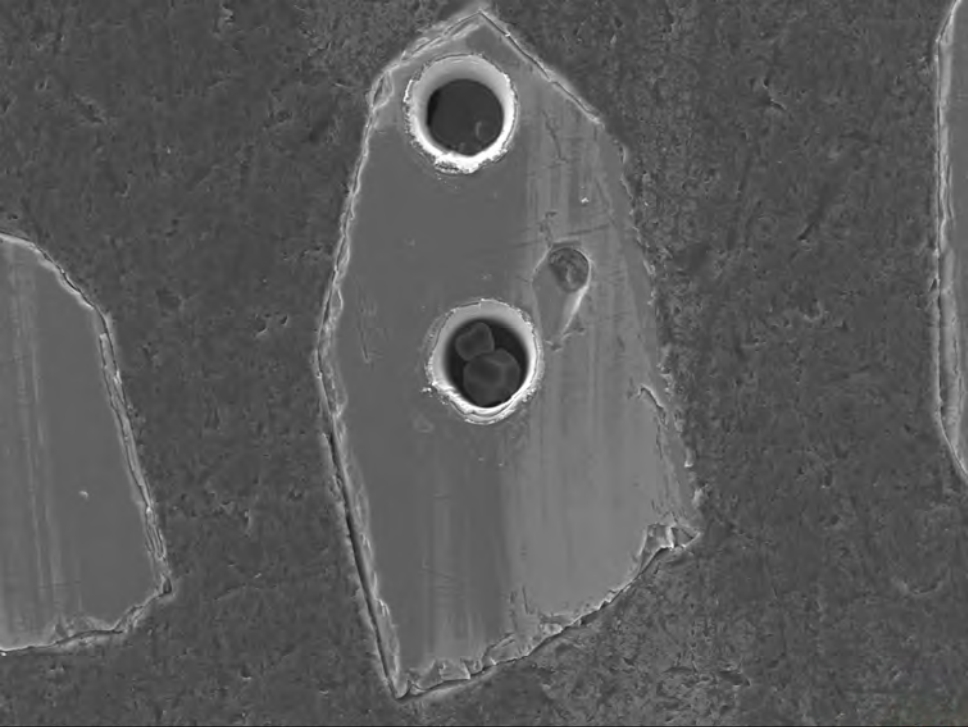
x330



50um

04 06 2017

EGI



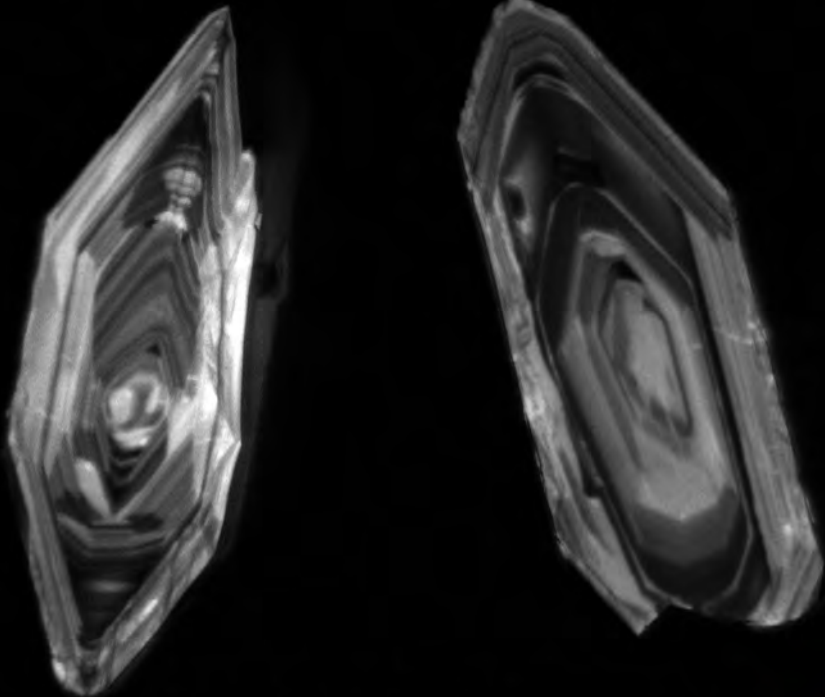
SED 20.0kV WD10.3mm Std.-P.C.60.0 HighVac. x350



50um

04 06 2017

EGI



AUX 20.0kV WD17.5mm Std.-P.C.60.0 HighVac.

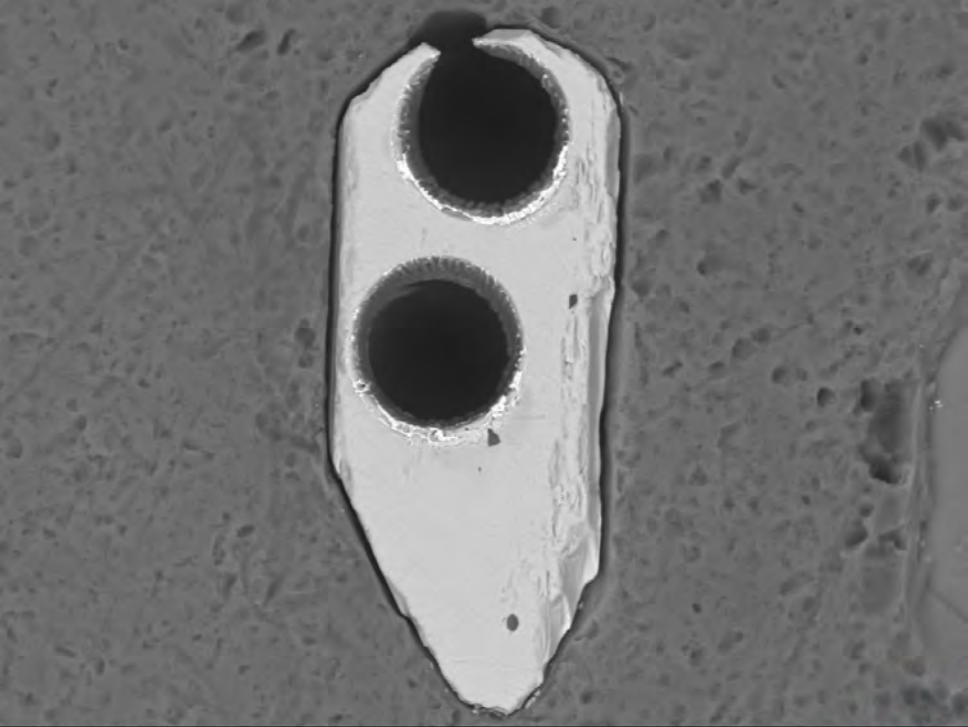
x430

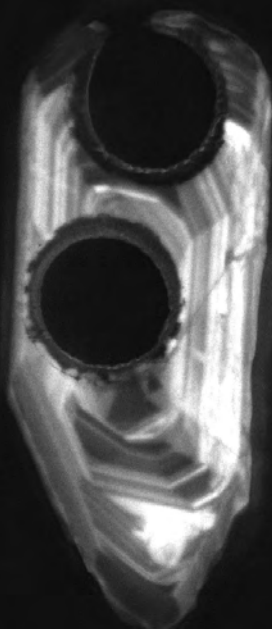


50um

04 06 2017

EGI





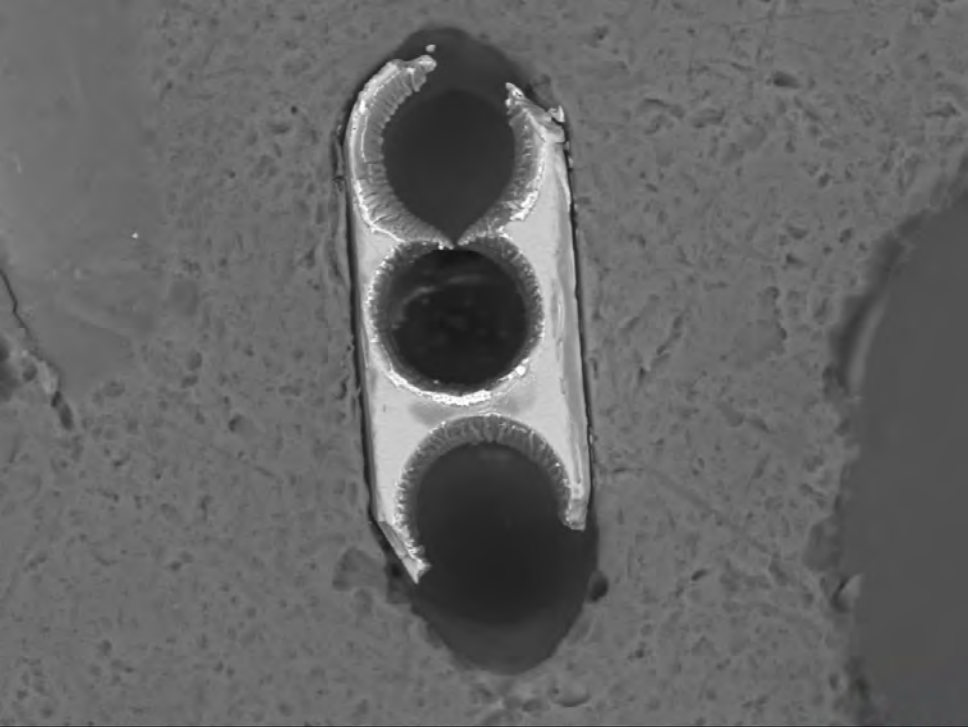
AUX 20.0kV WD17.4mm Std.-P.C.60.0 HighVac. x500



50um

04 06 2017

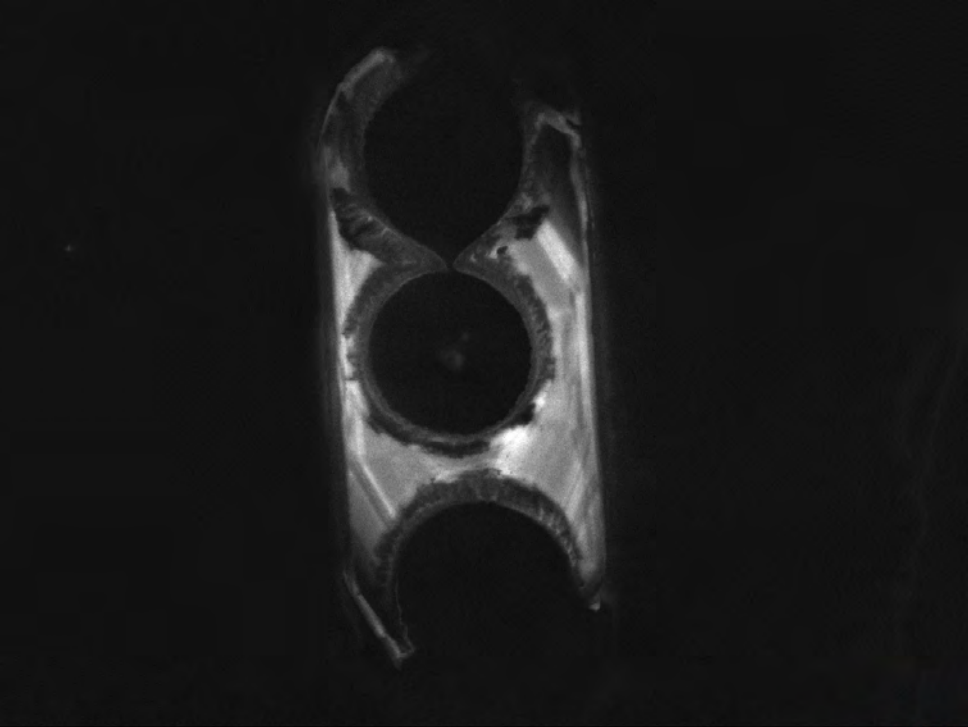




BED-C 20.0kV WD10.4mm Std.-P.C.60.0 HighVac. x550  20um

04 06 2017

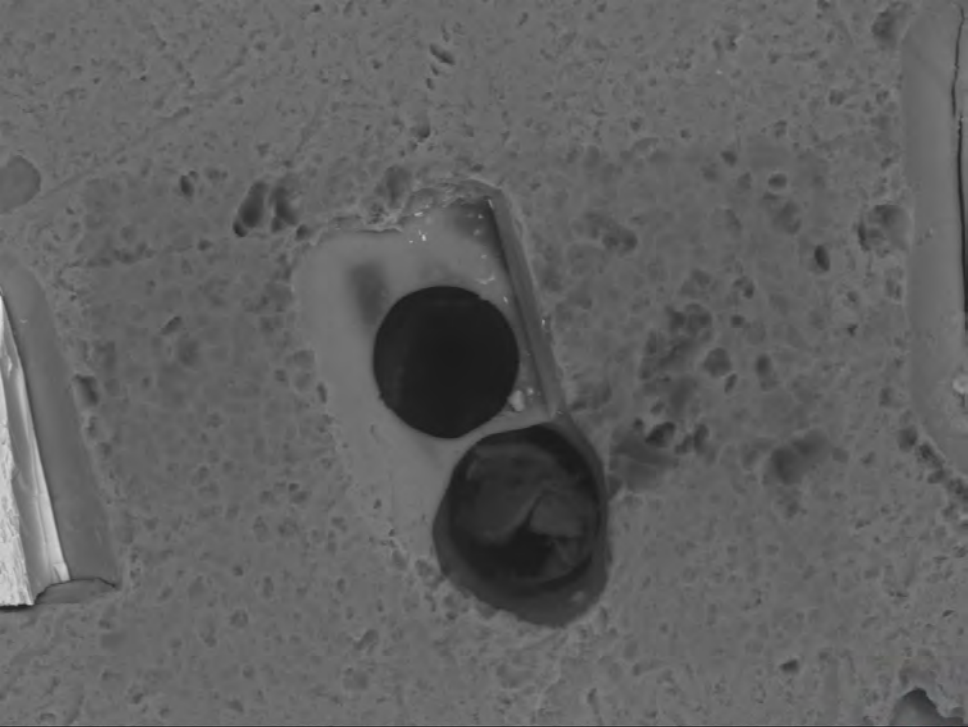
EGI



AUX 20.0kV WD17.4mm Std.-P.C.60.0 HighVac. x650  20um

04 06 2017

EGI

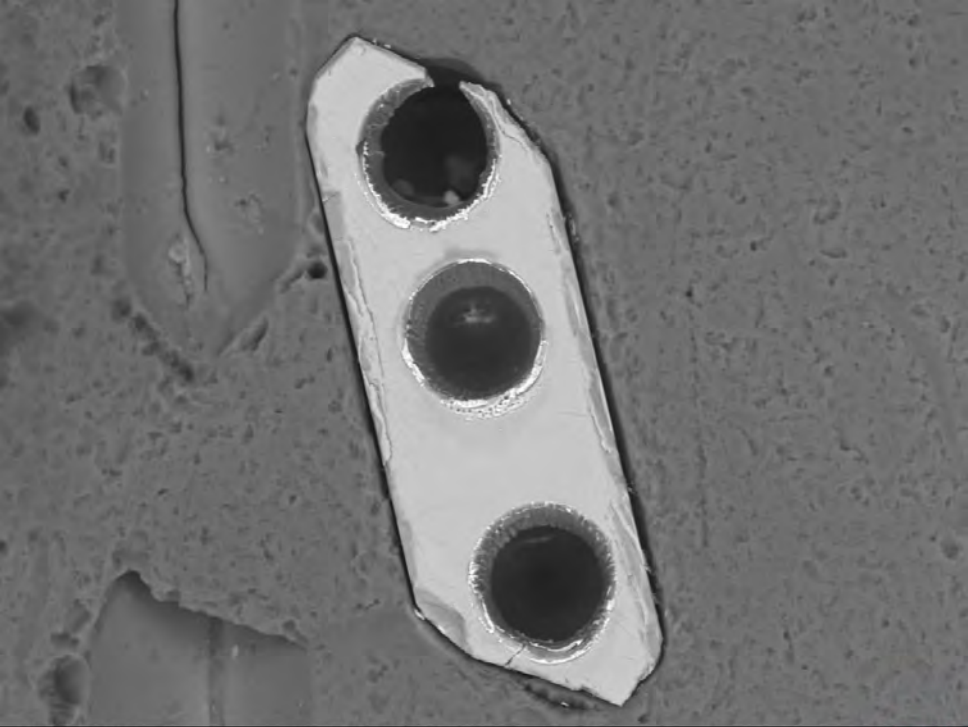


BED-C 20.0kV WD10.4mm Std.-P.C.60.0 HighVac. x430



50um
04 06 2017

EGI

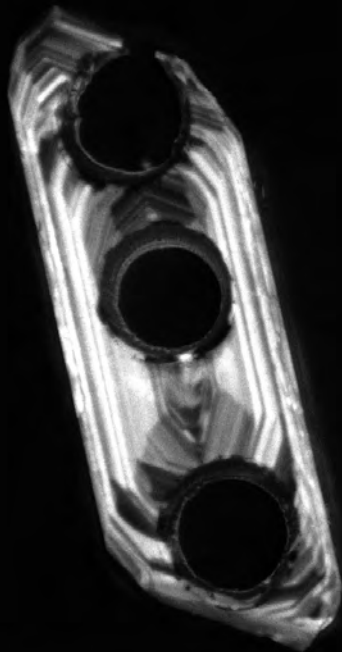


BED-C 20.0kV WD10.4mm Std.-P.C.60.0 HighVac. x450



50um
04 06 2017

EGI

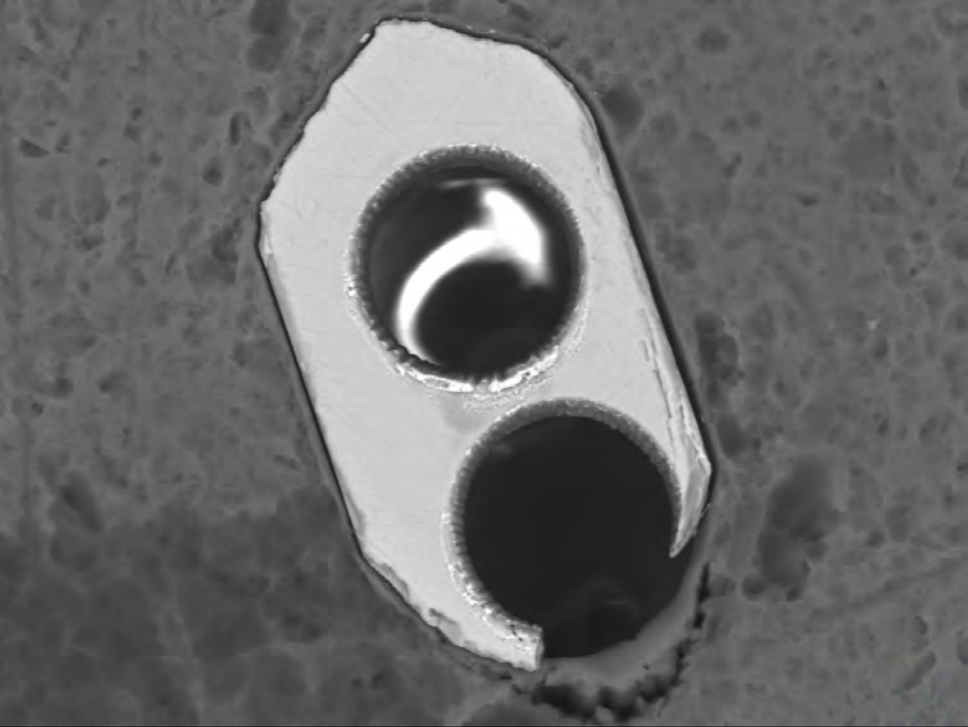


AUX 20.0kV WD17.4mm Std.-P.C.60.0 HighVac. x430



50um
04 06 2017

EGI



BED-C 20.0kV WD10.4mm

Std.-P.C.60.0

HighVac.

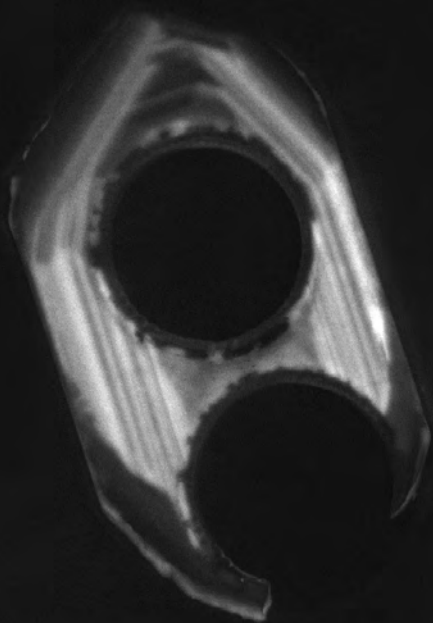
x750



20um

04 06 2017

EGI



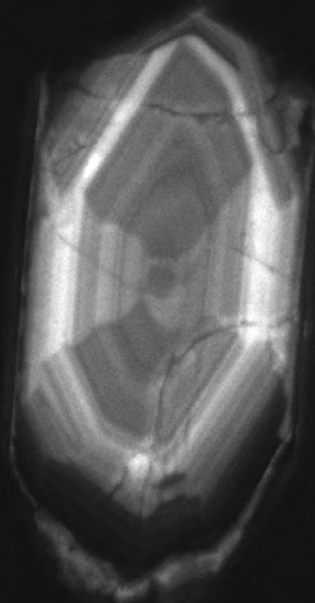
AUX 20.0kV WD17.4mm Std.-P.C.60.0 HighVac. x700



20um

04 06 2017

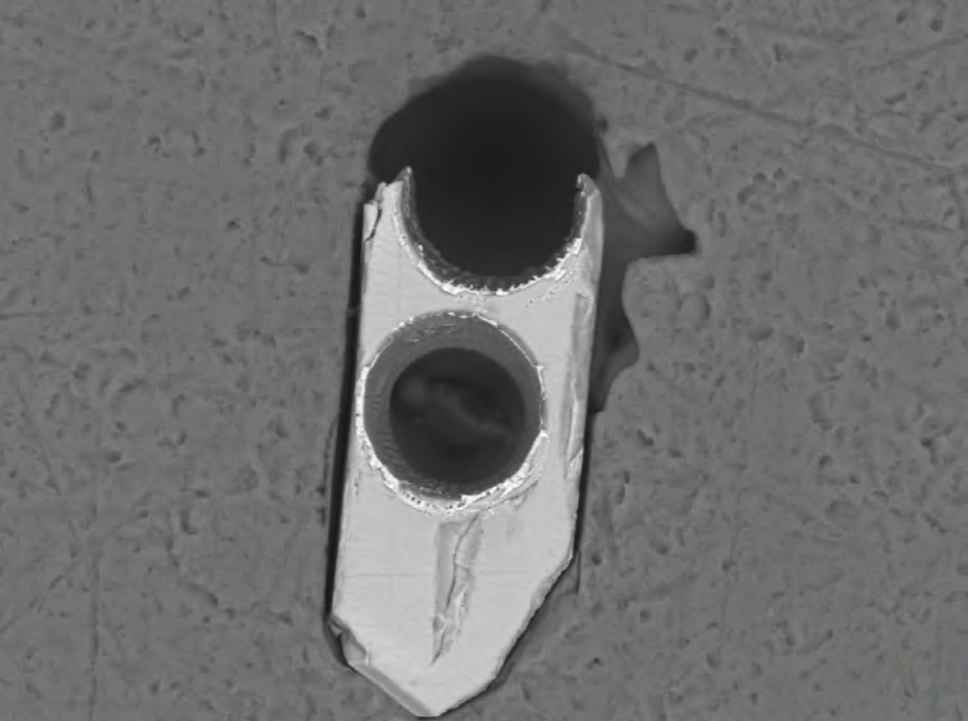
EGI



AUX 20.0kV WD17.4mm Std.-P.C.60.0 HighVac. x550  20um

04 06 2017

EGI



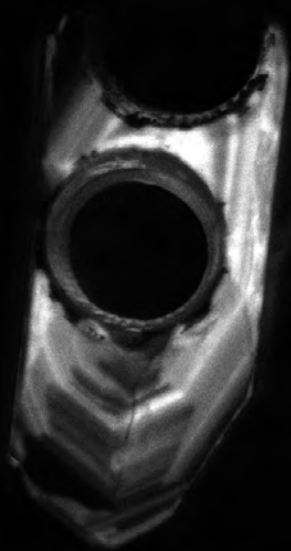
BED-C 20.0kV WD10.4mm Std.-P.C.60.0 HighVac. x600



20um

04 06 2017

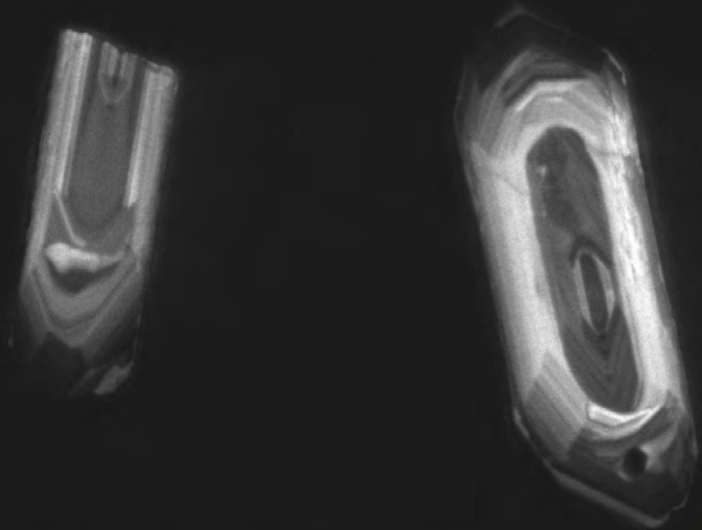
EGI



AUX 20.0kV WD17.4mm Std.-P.C.60.0 HighVac. x600  20um

04 06 2017

EGI



AUX

20.0kV

WD17.4mm

Std.-P.C.60.0

HighVac.

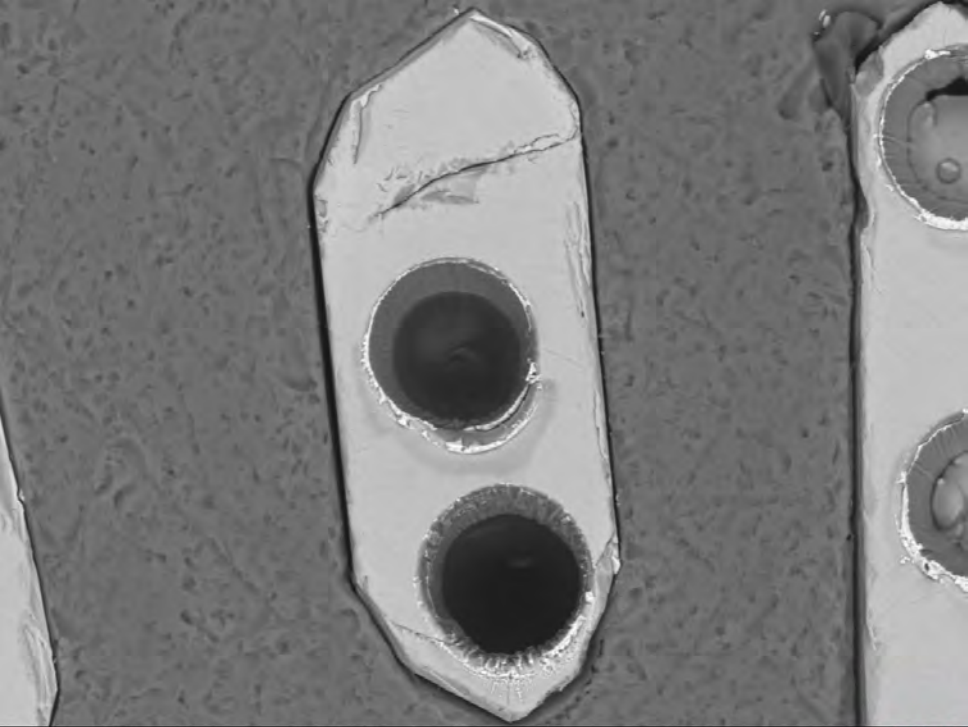
x400



50um

04 06 2017

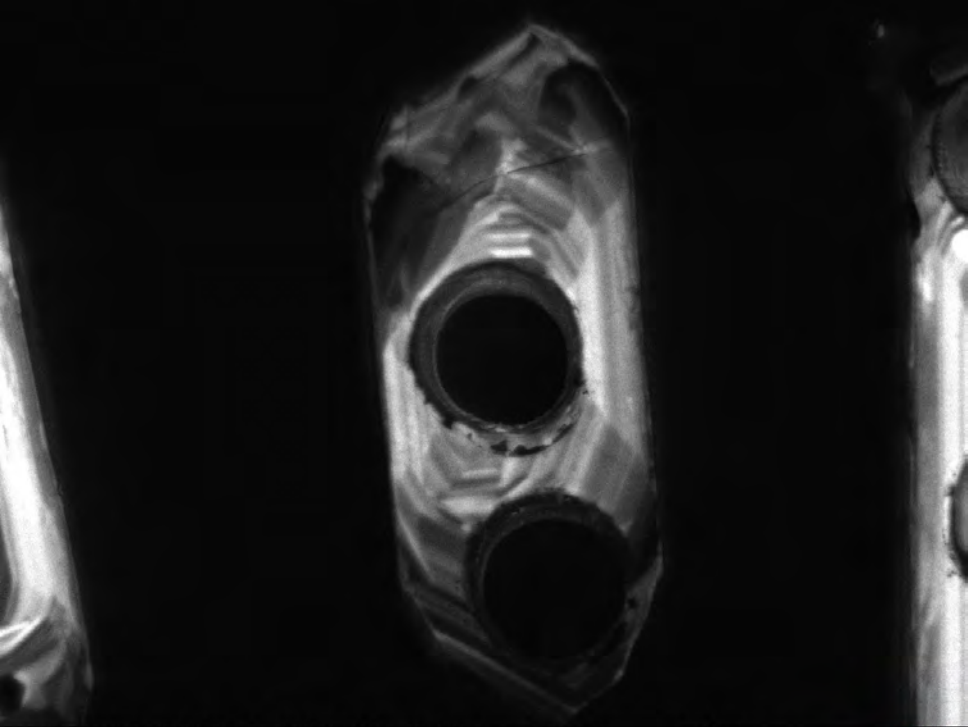
EGI



BED-C 20.0kV WD10.4mm Std.-P.C.60.0 HighVac. x550  20um

04 06 2017

EGI



AUX 20.0kV WD17.4mm Std.-P.C.60.0 HighVac. x550  20um

04 06 2017

EGI



BED-C 20.0kV WD10.4mm

Std.-P.C.60.0

HighVac.

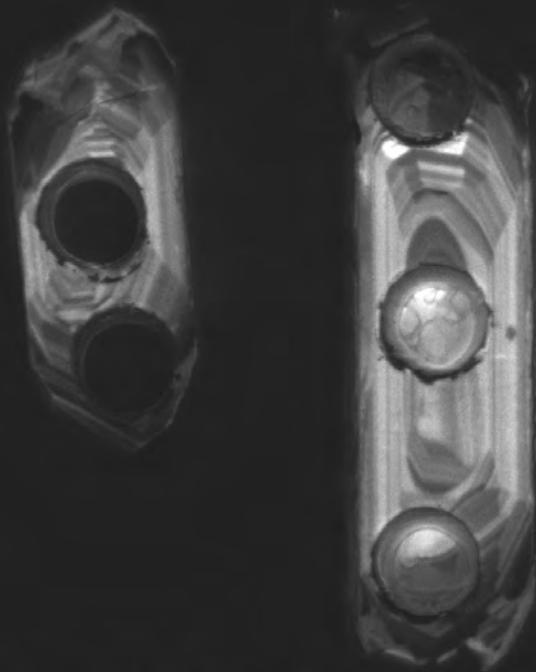
x370



50um

04 06 2017

EGI



AUX

20.0kV

WD17.4mm

Std.-P.C.60.0

HighVac.

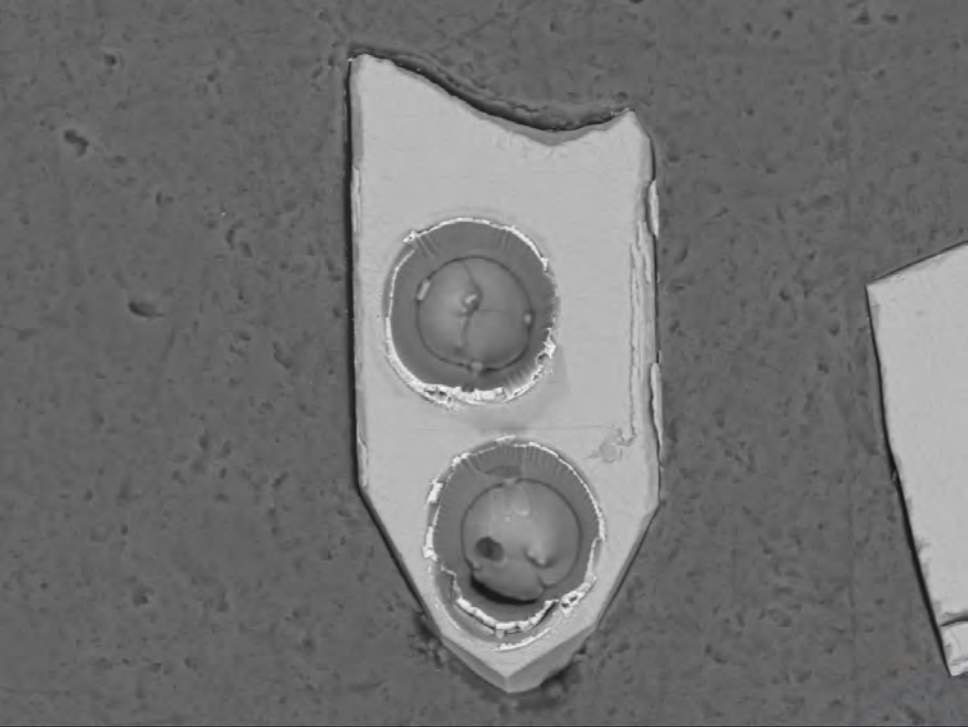
x350



50um

04 06 2017

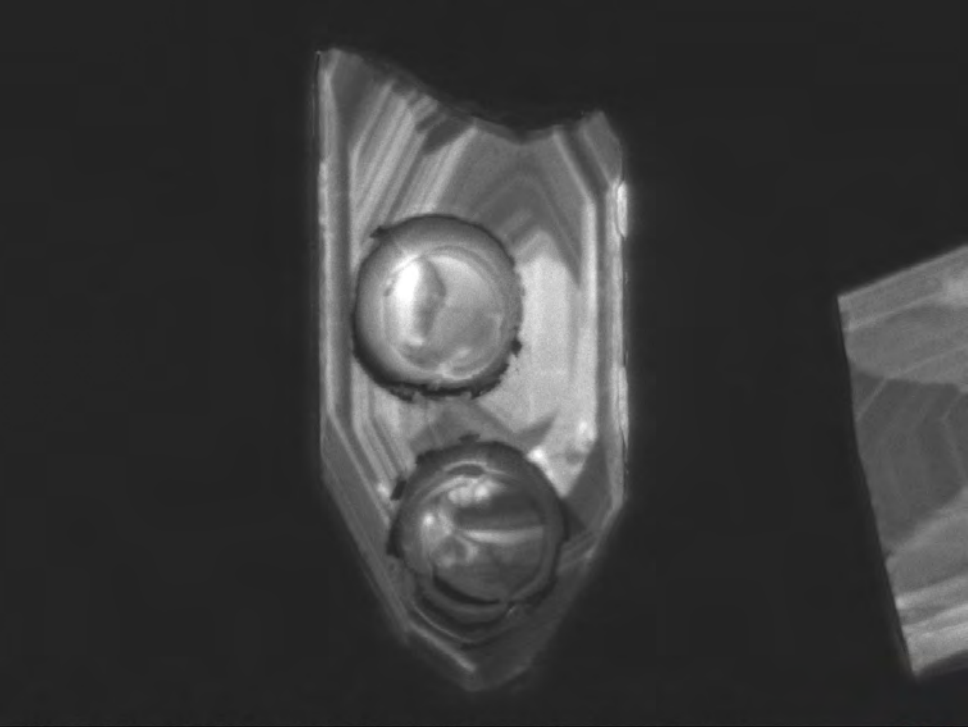
EGI



BED-C 20.0kV WD10.4mm Std.-P.C.60.0 HighVac. x550  20um

04 06 2017

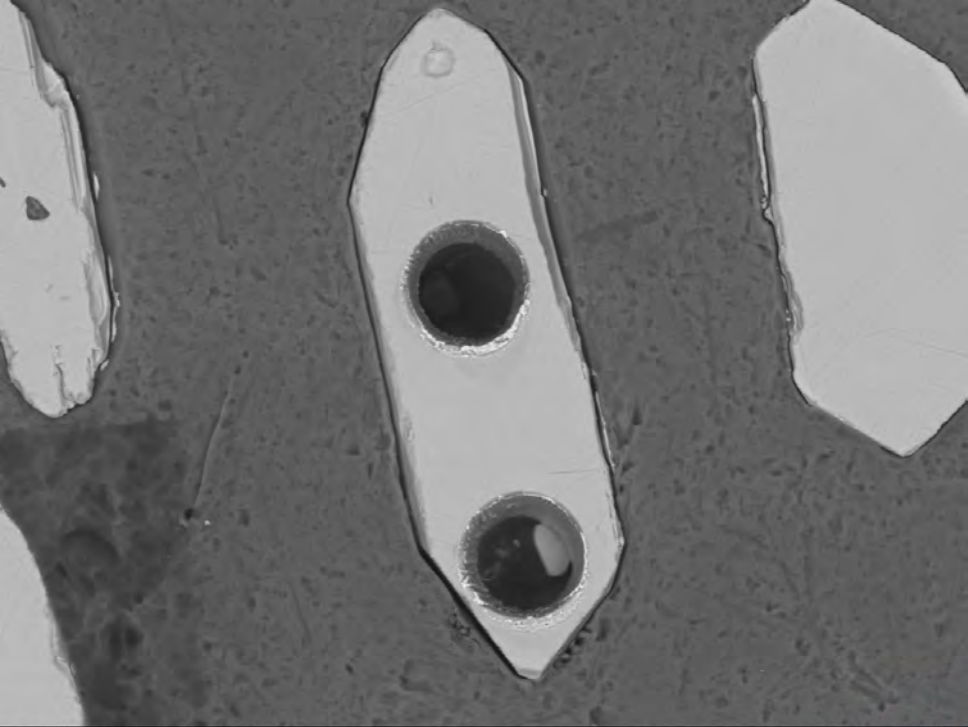
EGI



AUX 20.0kV WD17.4mm Std.-P.C.60.0 HighVac. x550  20um

04 06 2017

EGI



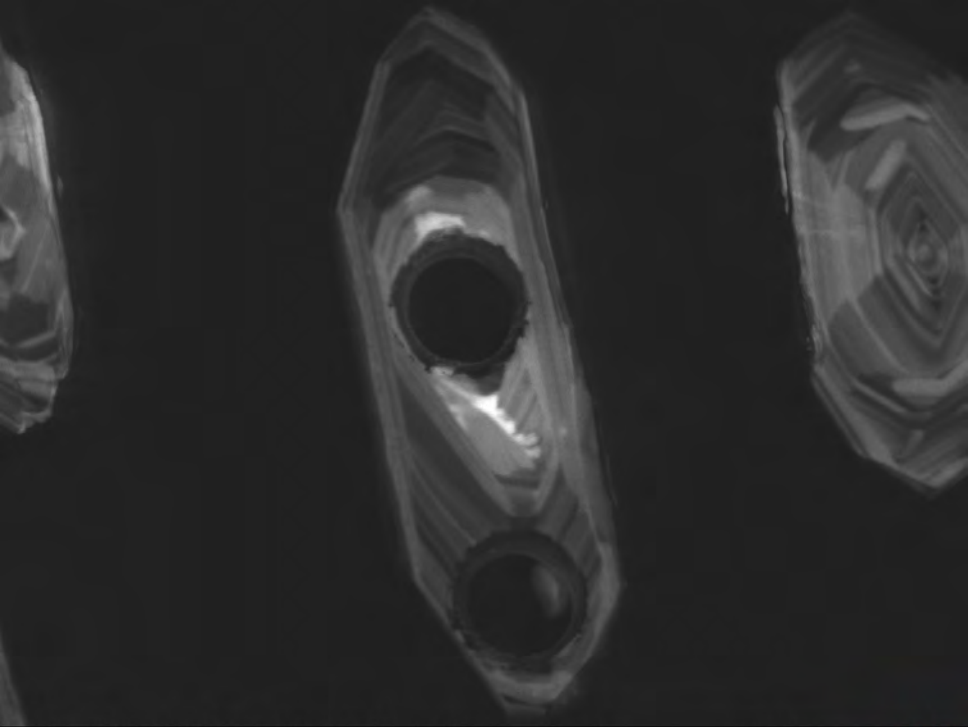
BED-C 20.0kV WD10.4mm Std.-P.C.60.0 HighVac. x400



50um

04 06 2017

EGI



AUX

20.0kV

WD17.4mm

Std.-P.C.60.0

HighVac.

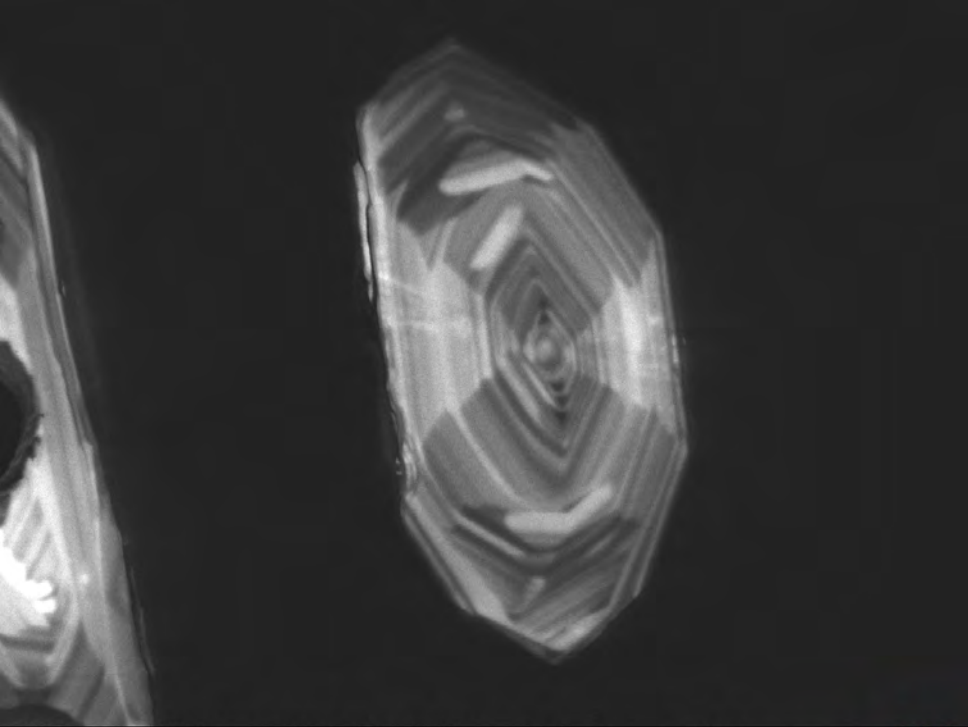
x430



50um

04 06 2017

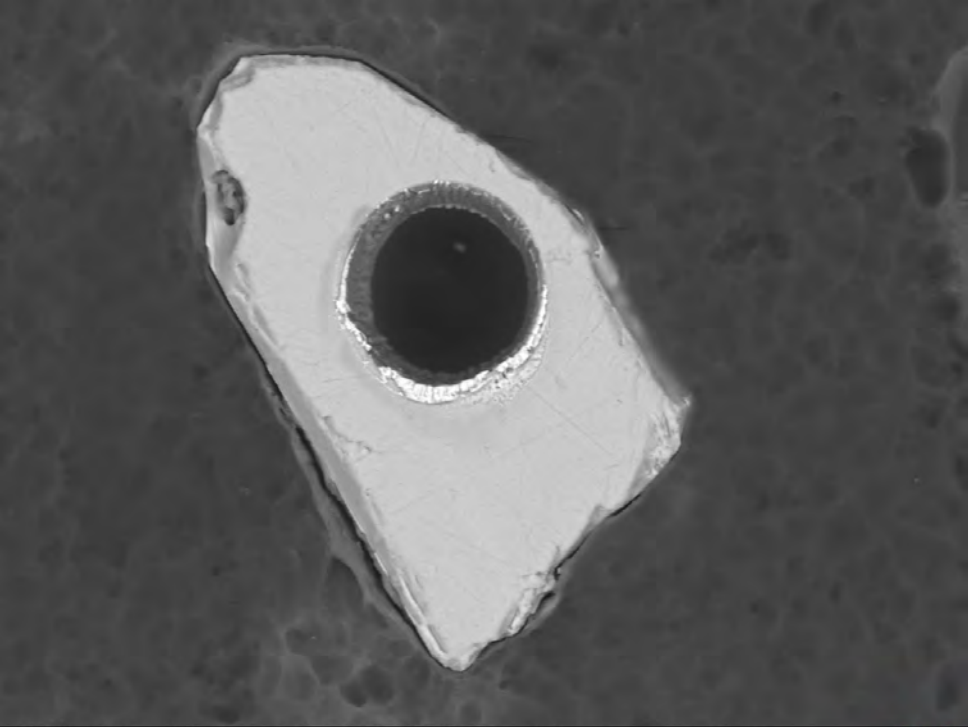
EGI



AUX 20.0kV WD17.4mm Std.-P.C.60.0 HighVac. x550  20um

04 06 2017

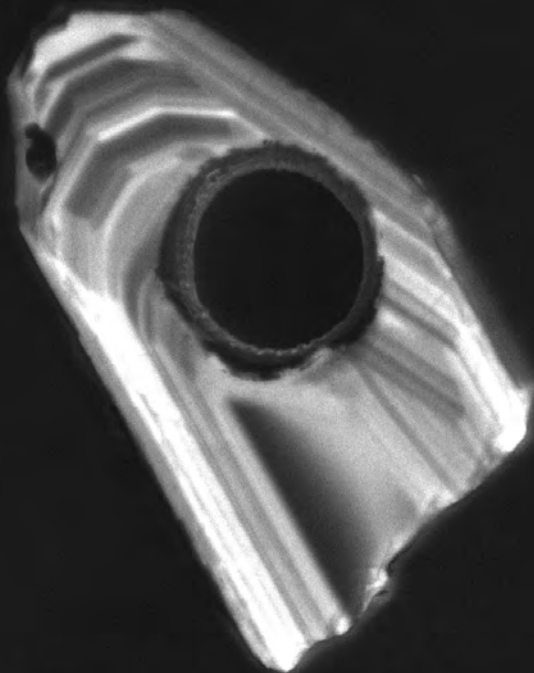
EGI



BED-C 20.0kV WD10.4mm Std.-P.C.60.0 HighVac. x650  20um

04 06 2017

EGI



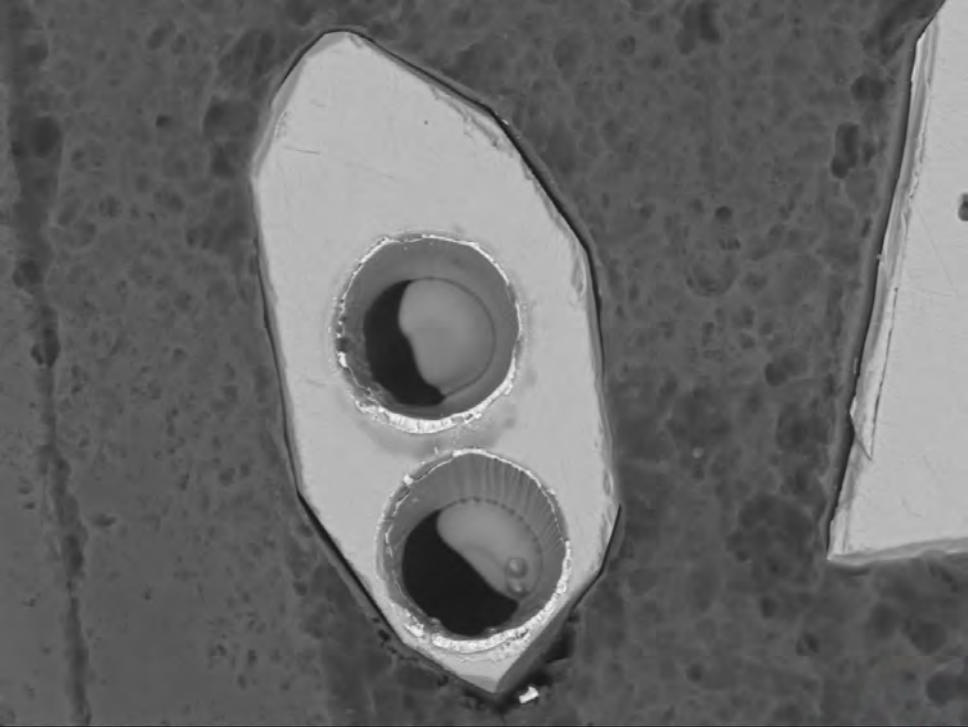
AUX 20.0kV WD17.4mm Std.-P.C.60.0 HighVac. x700



20um

04 06 2017

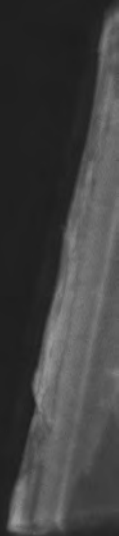
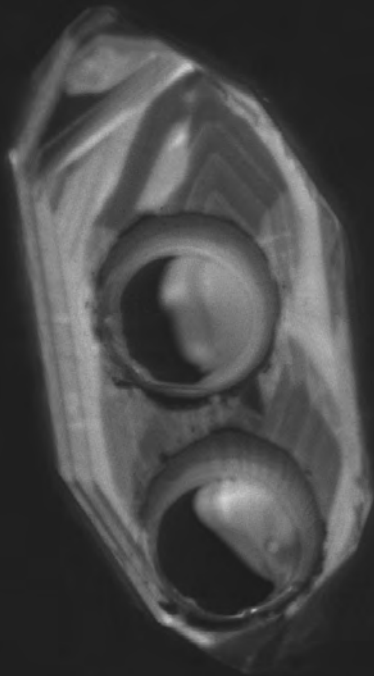
EGI



BED-C 20.0kV WD10.4mm Std.-P.C.60.0 HighVac. x600  20um

04 06 2017

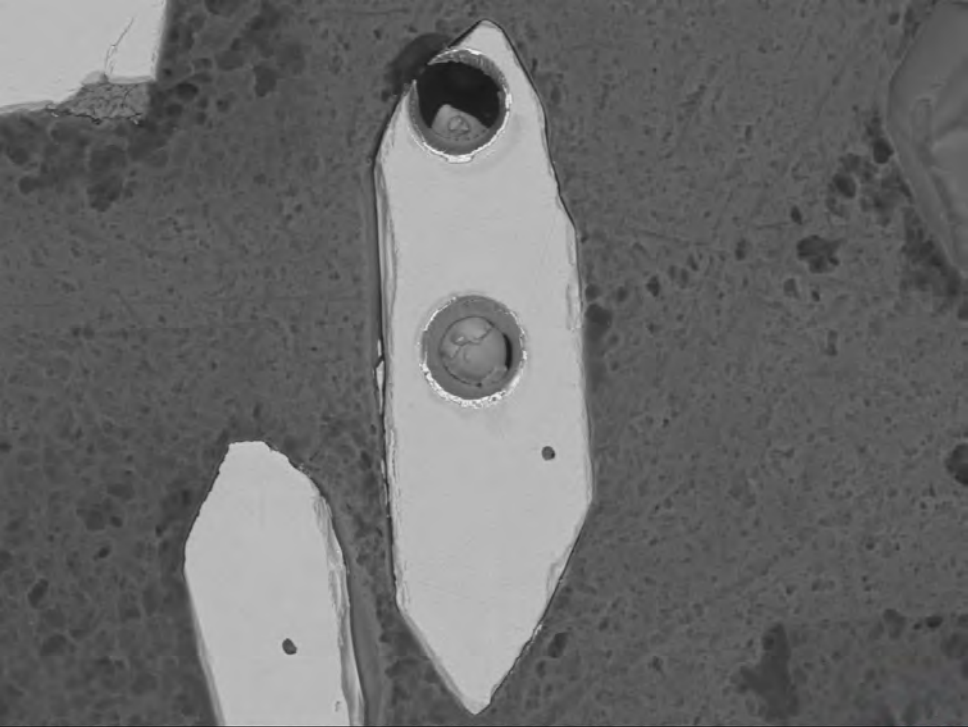
EGI



AUX 20.0kV WD17.4mm Std.-P.C.60.0 HighVac. x600  20um

04 06 2017

EGI



BED-C 20.0kV WD10.4mm

Std.-P.C.60.0

HighVac.

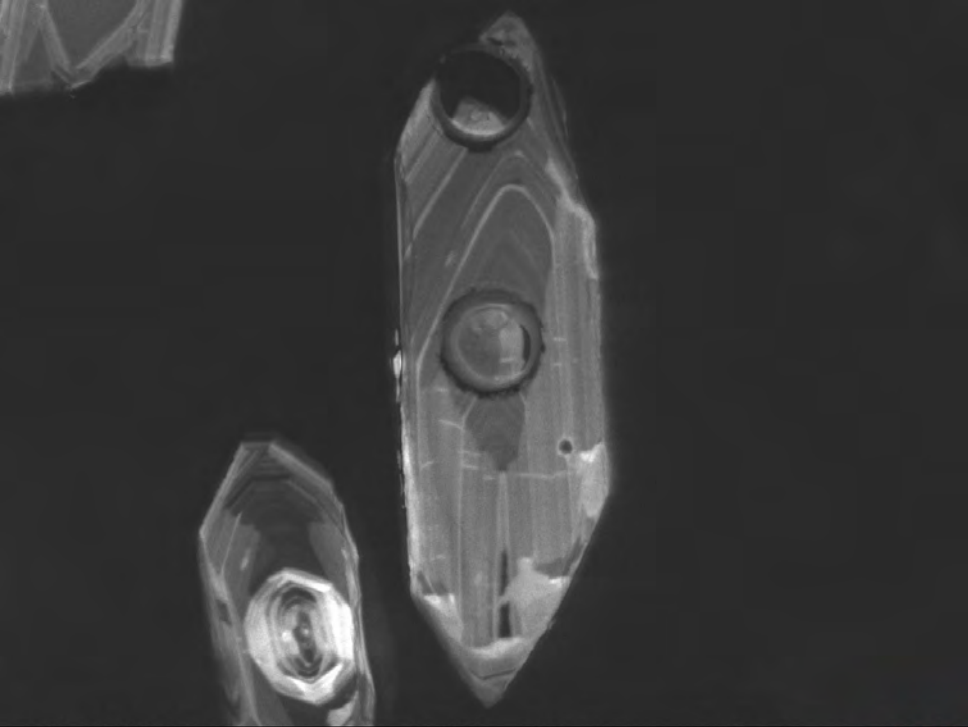
x330



50um

04 06 2017

EGI



AUX

20.0kV

WD17.4mm

Std.-P.C.60.0

HighVac.

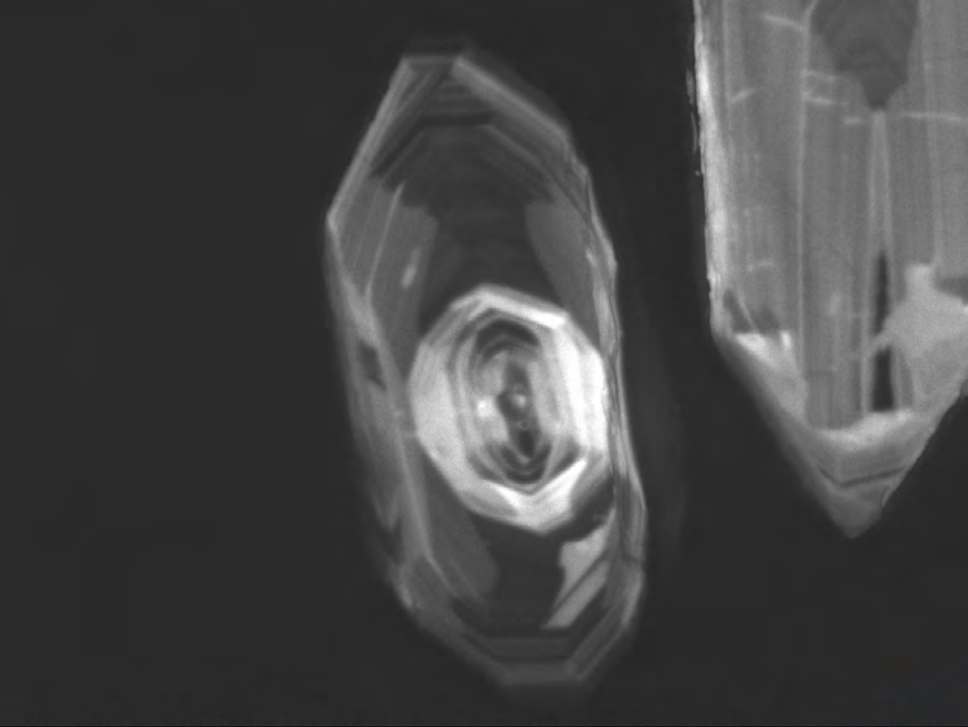
x330



50um

04 06 2017

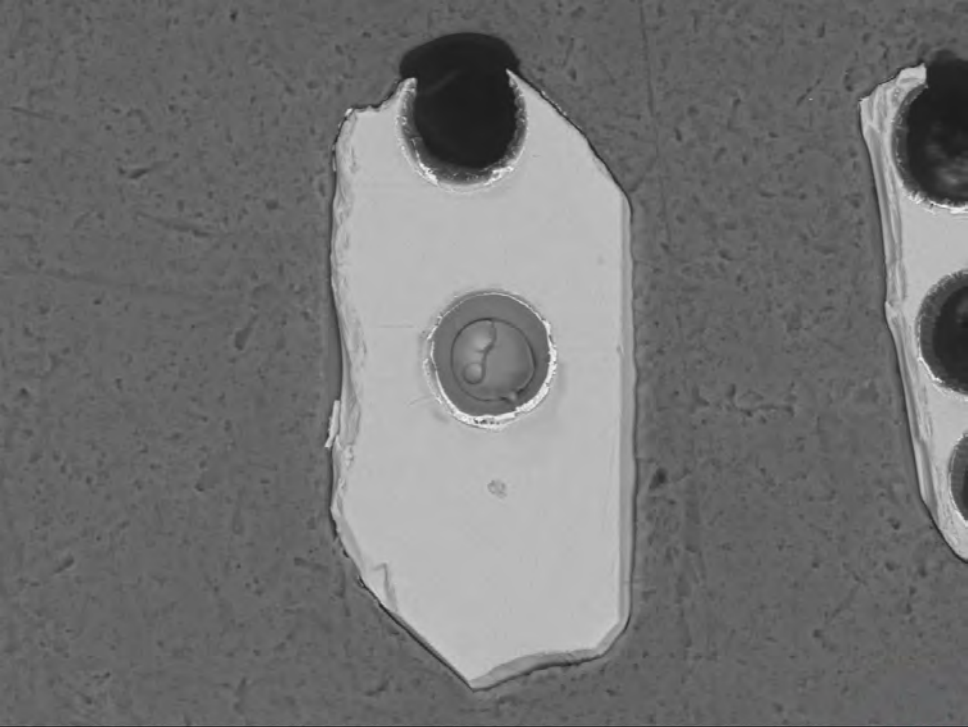
EGI



AUX 20.0kV WD17.4mm Std.-P.C.60.0 HighVac. x600  20um

04 06 2017

EGI



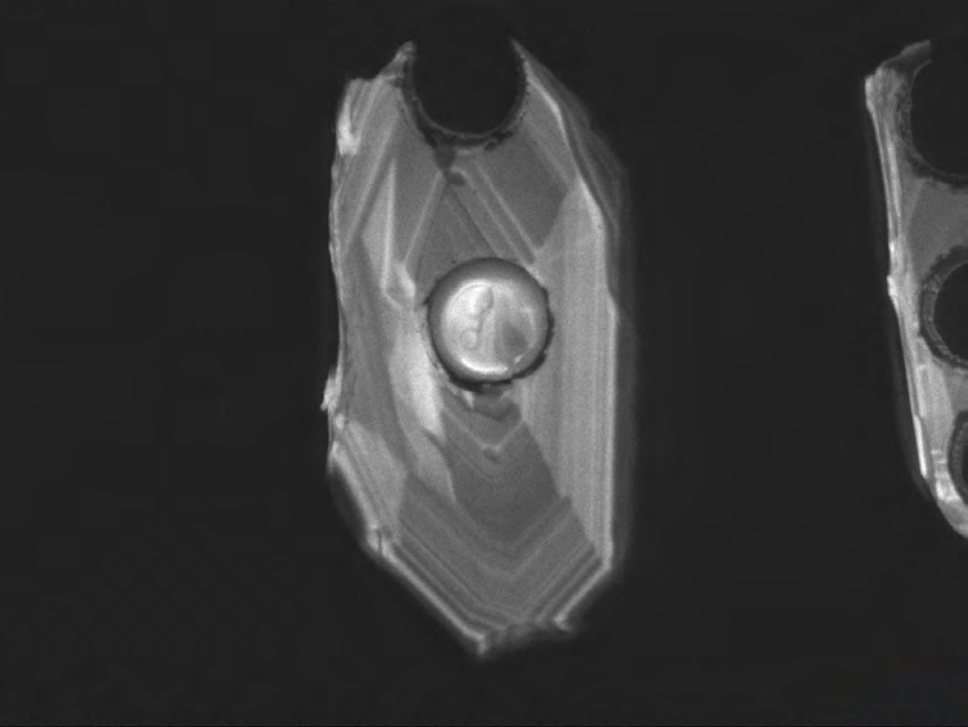
BED-C 20.0kV WD10.4mm Std.-P.C.60.0 HighVac. x400



50um

04 06 2017

EGI



AUX

20.0kV

WD17.4mm

Std.-P.C.60.0

HighVac.

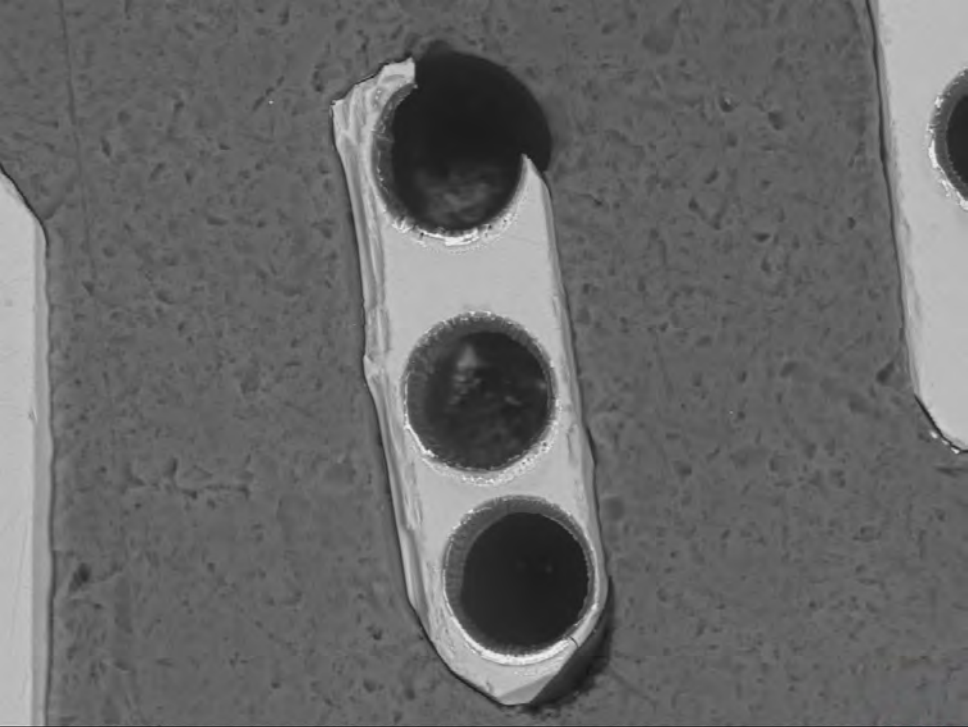
x400



50um

04 06 2017

EGI



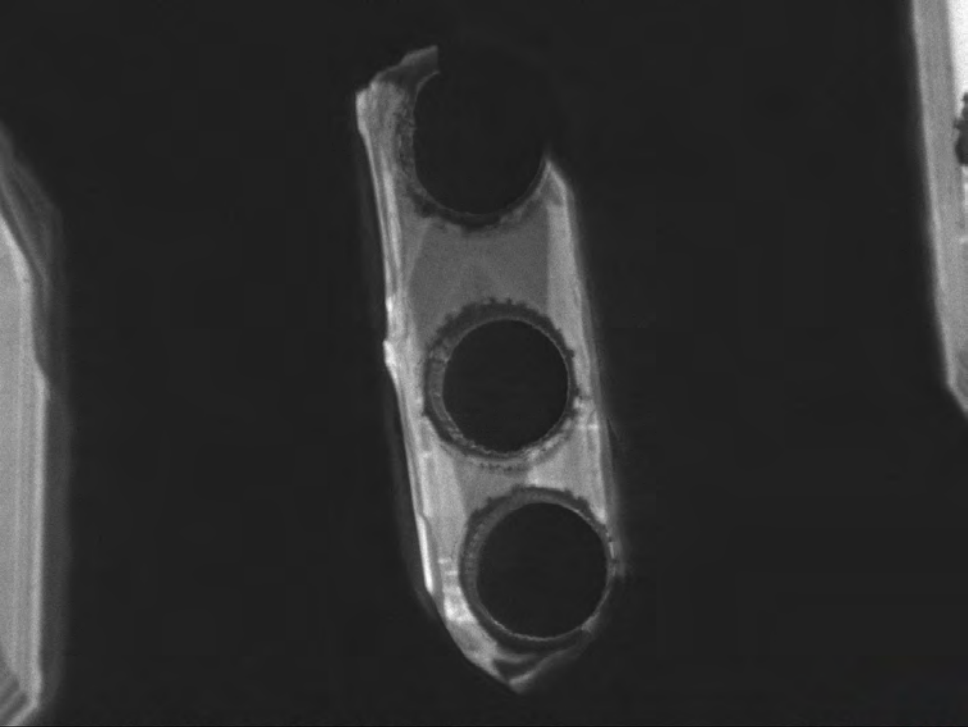
BED-C 20.0kV WD10.4mm Std.-P.C.60.0 HighVac. x500



50um

04 06 2017

EGI



AUX

20.0kV

WD17.4mm

Std.-P.C.60.0

HighVac.

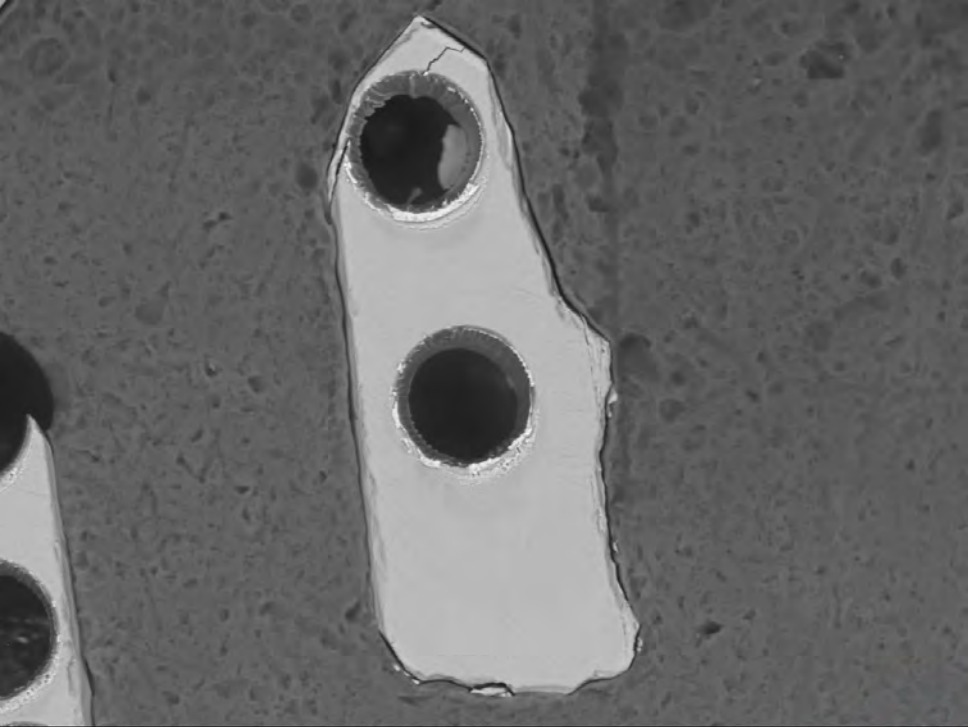
x500



50um

04 06 2017

EGI

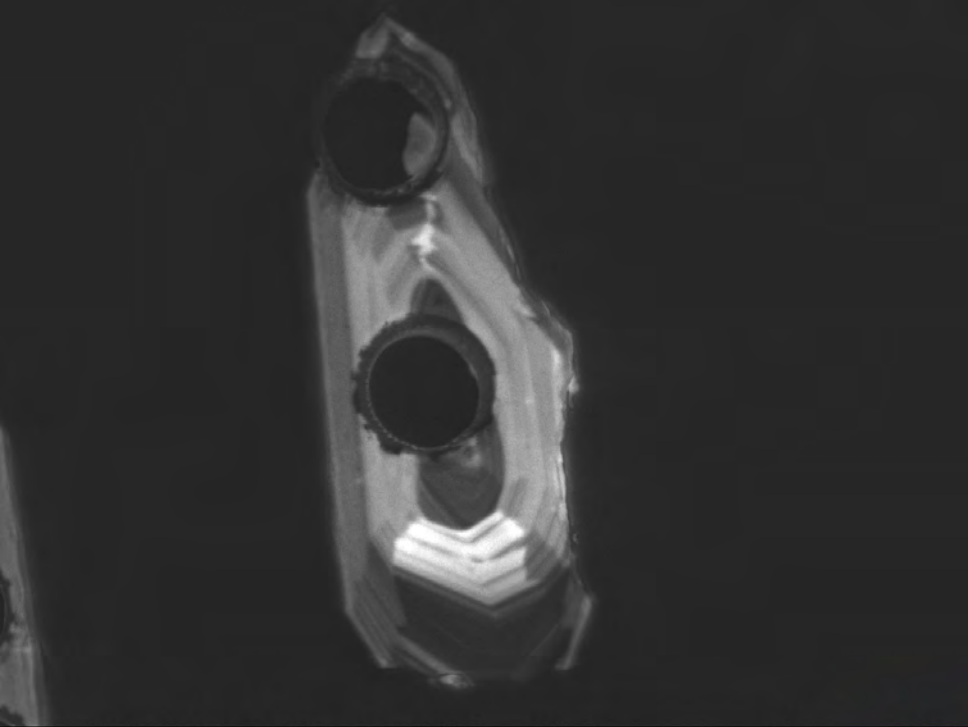


BED-C 20.0kV WD10.4mm Std.-P.C.60.0 HighVac. x450



50um
04 06 2017

EGI



AUX

20.0kV

WD17.4mm

Std.-P.C.60.0

HighVac.

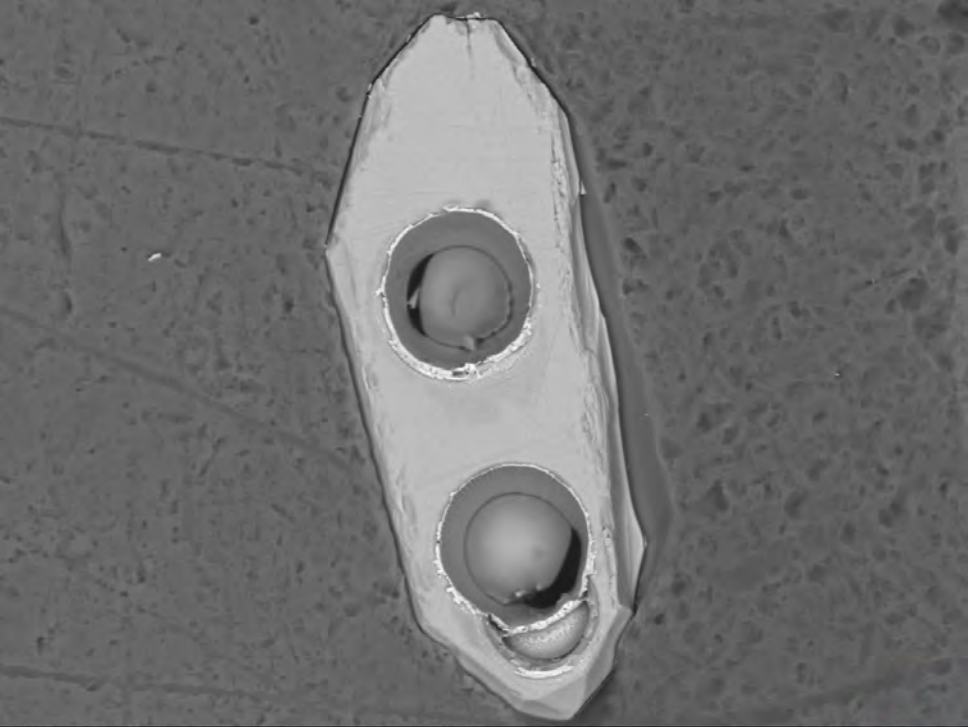
x450



50um

04 06 2017

EGI



BED-C 20.0kV WD10.4mm Std.-P.C.60.0 HighVac.

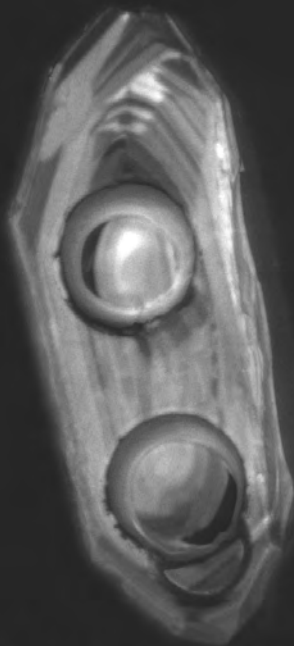
x500



50um

04 06 2017

EGI

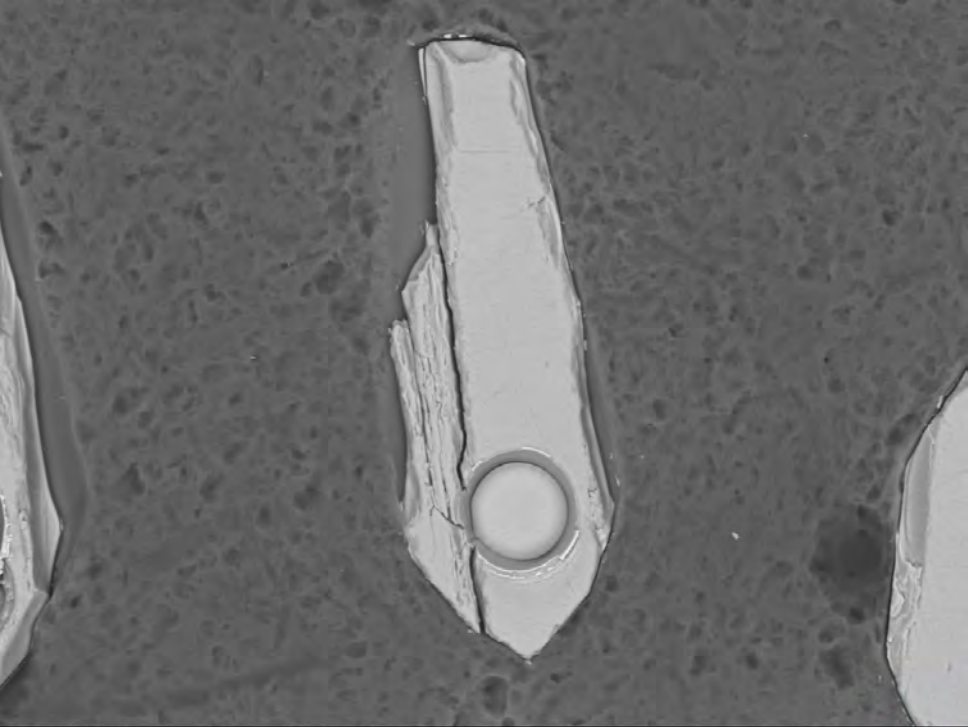


AUX 20.0kV WD17.4mm Std.-P.C.60.0 HighVac. x450



50um
04 06 2017

EGI



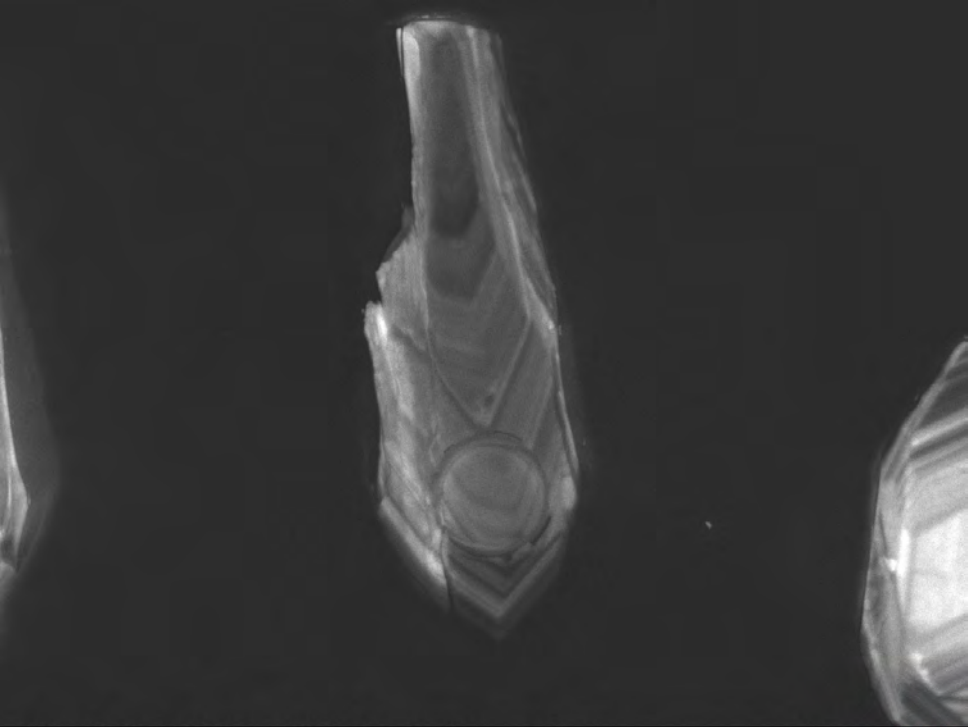
BED-C 20.0kV WD10.4mm Std.-P.C.60.0 HighVac. x500



50um

04 06 2017

EGI

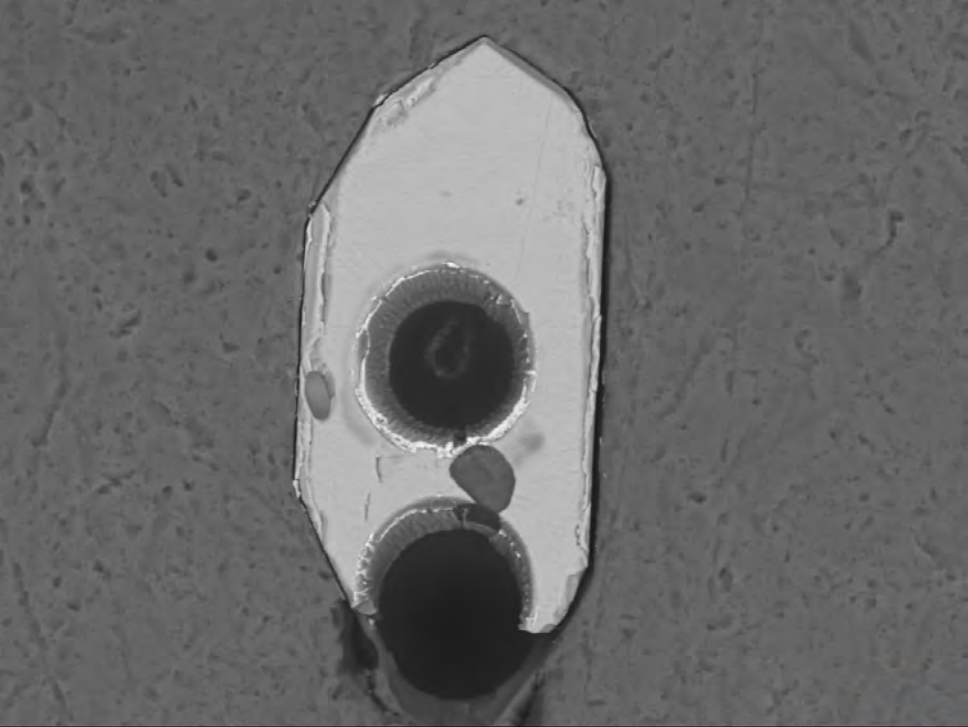


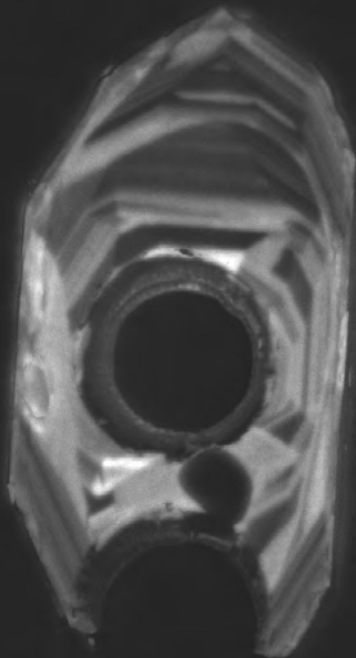
AUX 20.0kV WD17.4mm Std.-P.C.60.0 HighVac. x500

50um

04 06 2017

EGI

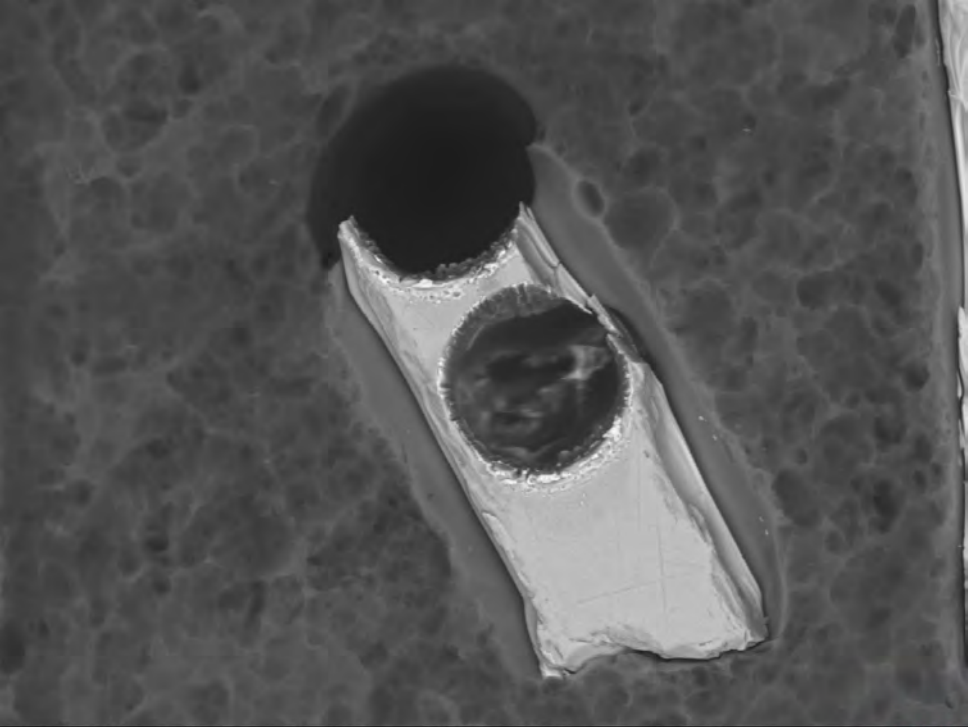




AUX 20.0kV WD17.4mm Std.-P.C.60.0 HighVac. x600  20um

04 06 2017

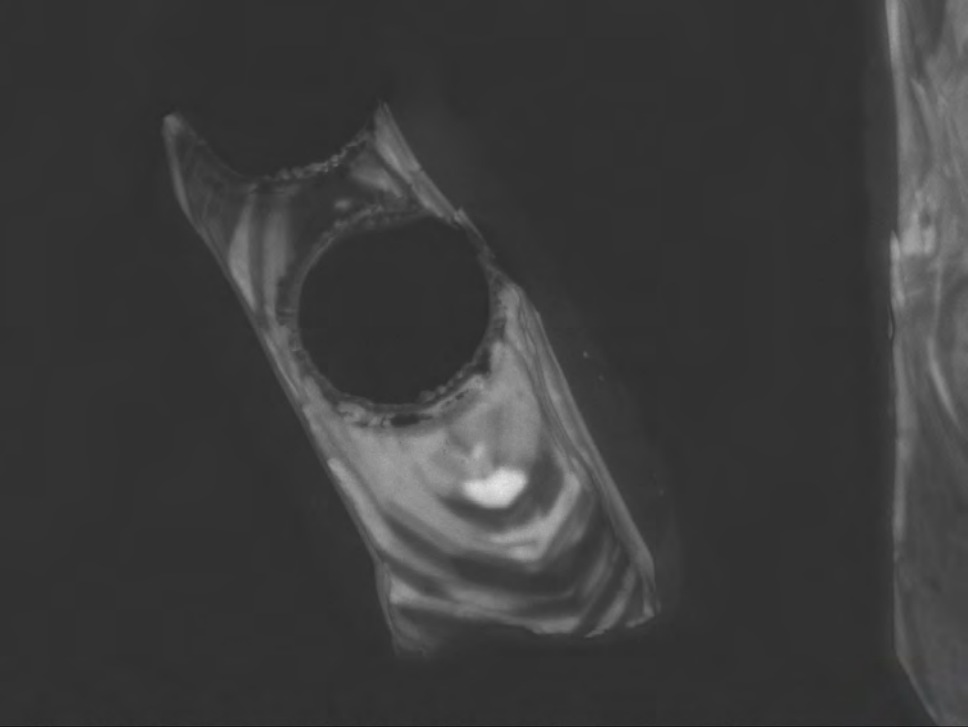
EGI



BED-C 20.0kV WD10.4mm Std.-P.C.60.0 HighVac. x600  20um

04 06 2017

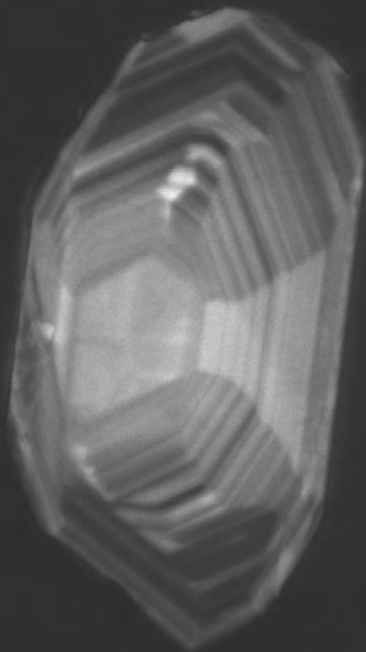
EGI



AUX 20.0kV WD17.4mm Std.-P.C.60.0 HighVac. x700  20um

04 06 2017

EGI



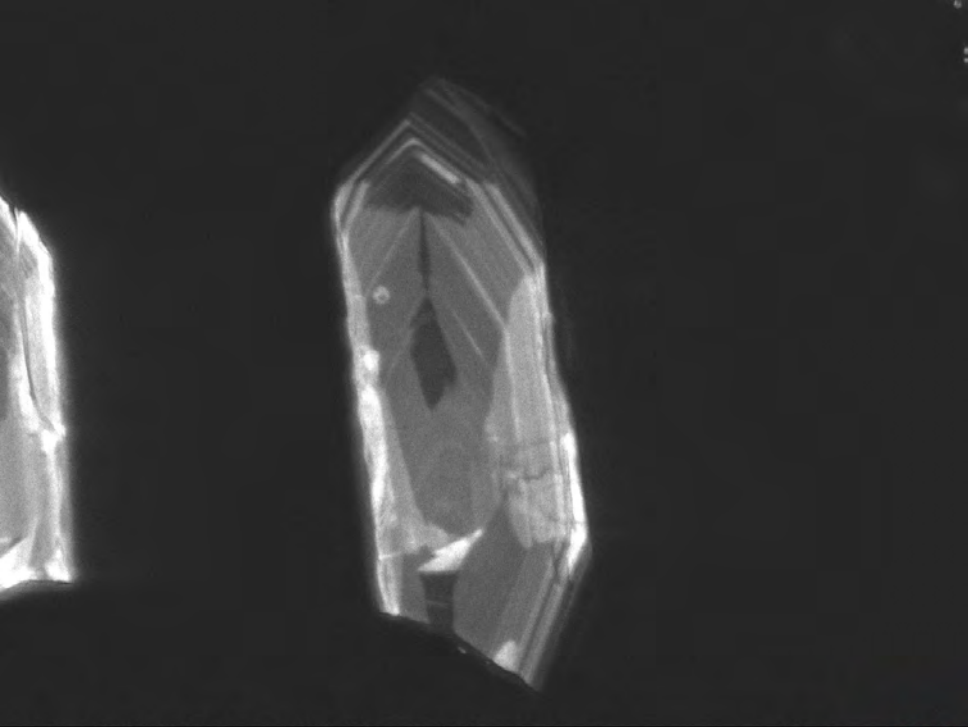
AUX 20.0kV WD17.4mm Std.-P.C.60.0 HighVac. x650



20um

04 06 2017

EGI

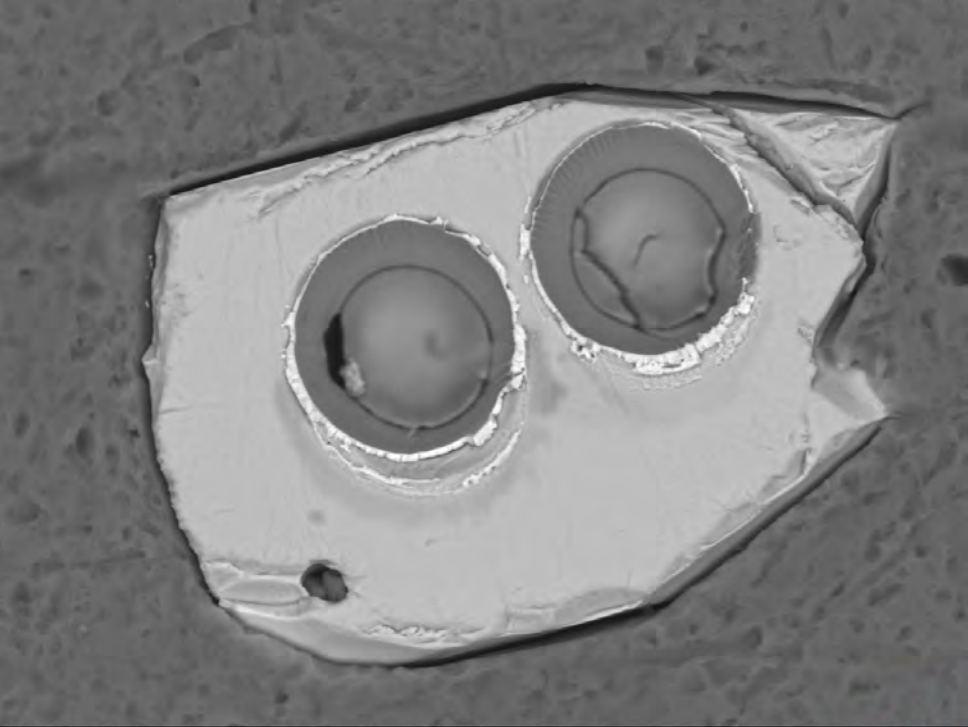


AUX 20.0kV WD17.4mm Std.-P.C.60.0 HighVac. x450



50um
04 06 2017

EGI



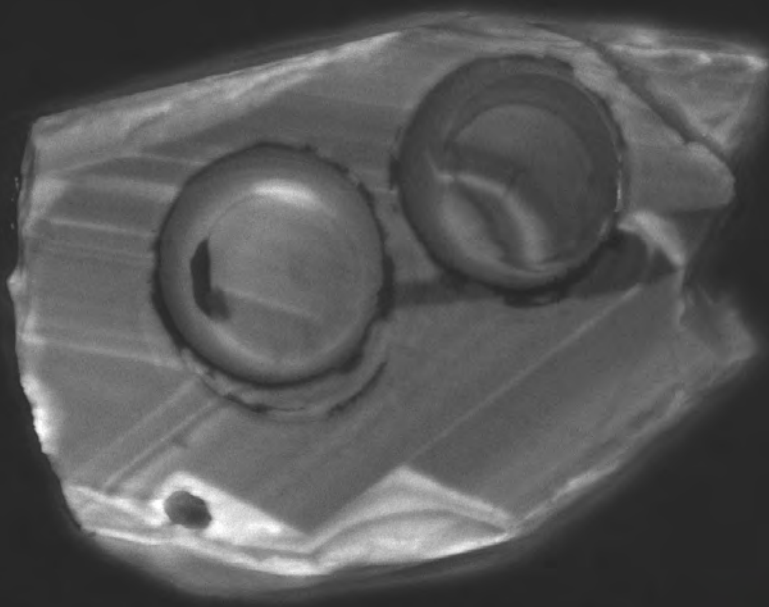
BED-C 20.0kV WD10.4mm Std.-P.C.60.0 HighVac. x750



20um

04 06 2017

EGI



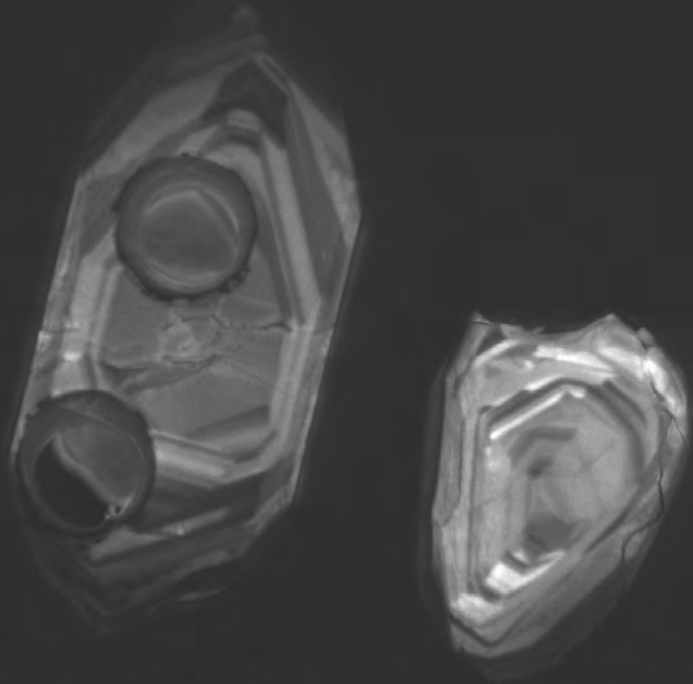
AUX 20.0kV WD17.4mm Std.-P.C.60.0 HighVac. x750



20um

04 06 2017

EGI



AUX 20.0kV WD17.4mm Std.-P.C.60.0 HighVac.

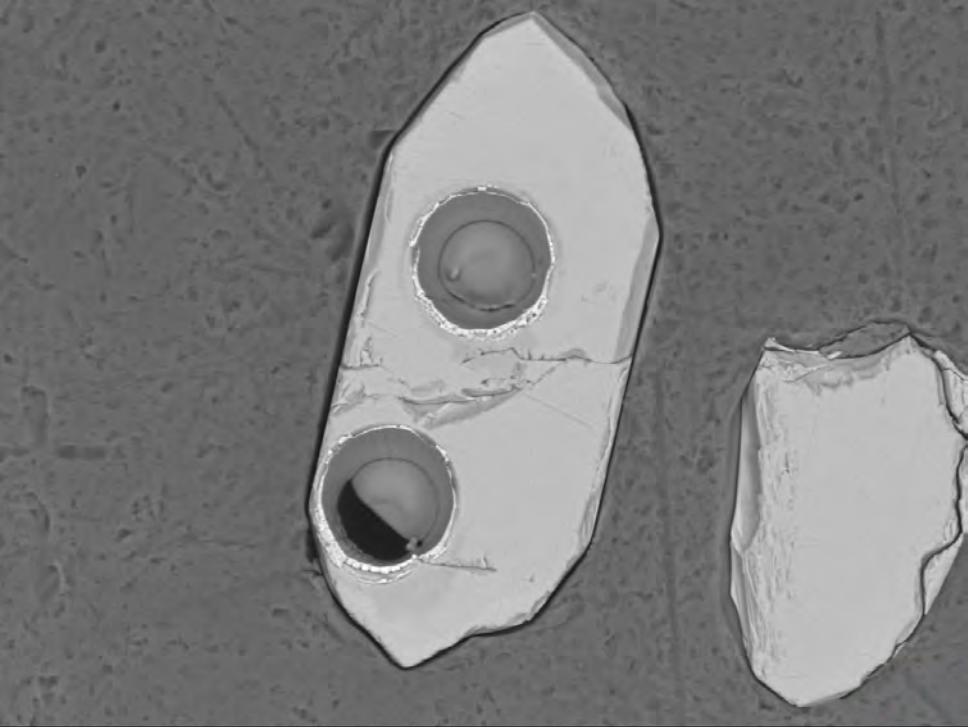
x450



50um

04 06 2017

EGI



BED-C 20.0kV WD10.4mm Std.-P.C.60.0 HighVac. x450



50um

04 06 2017



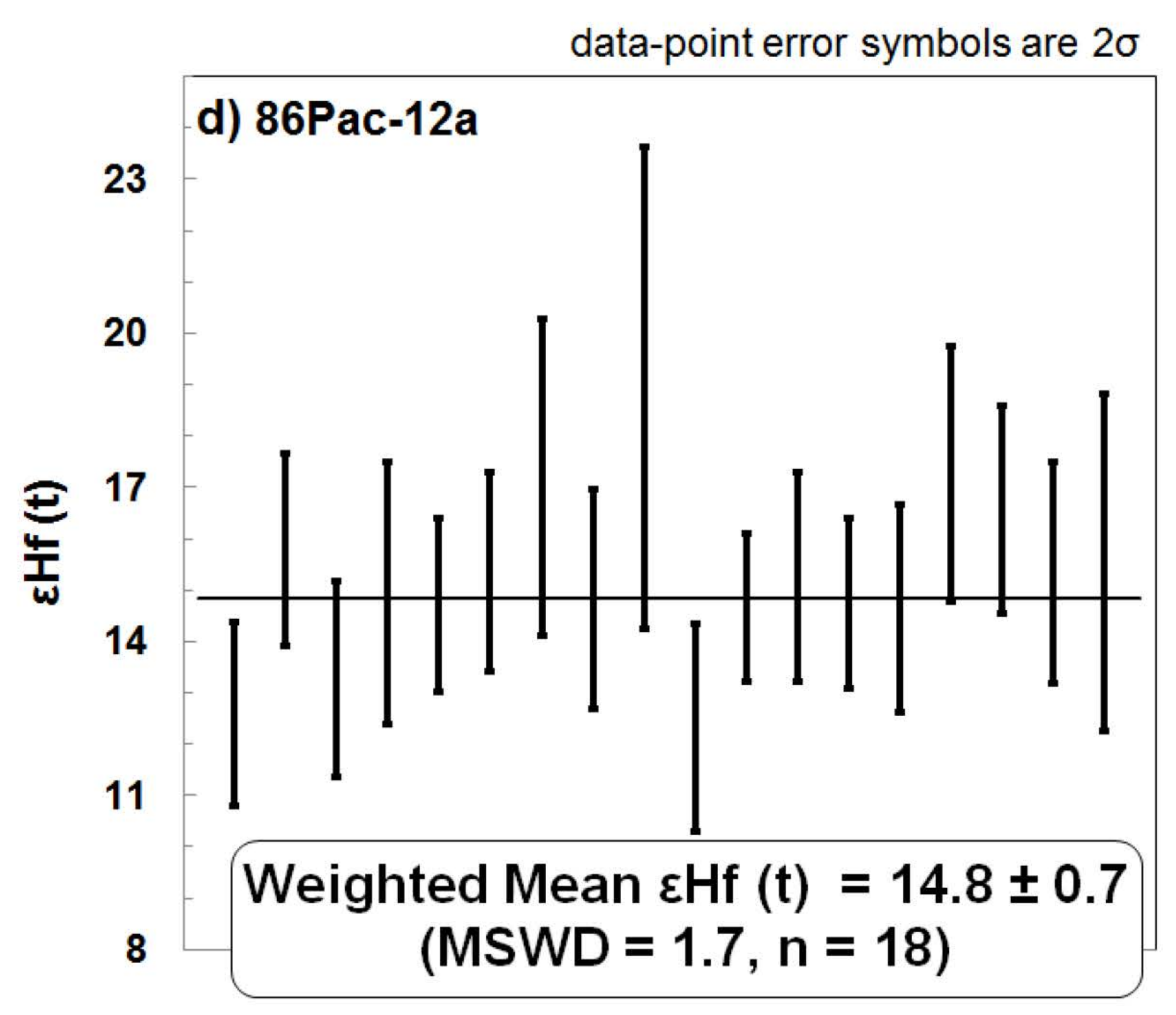
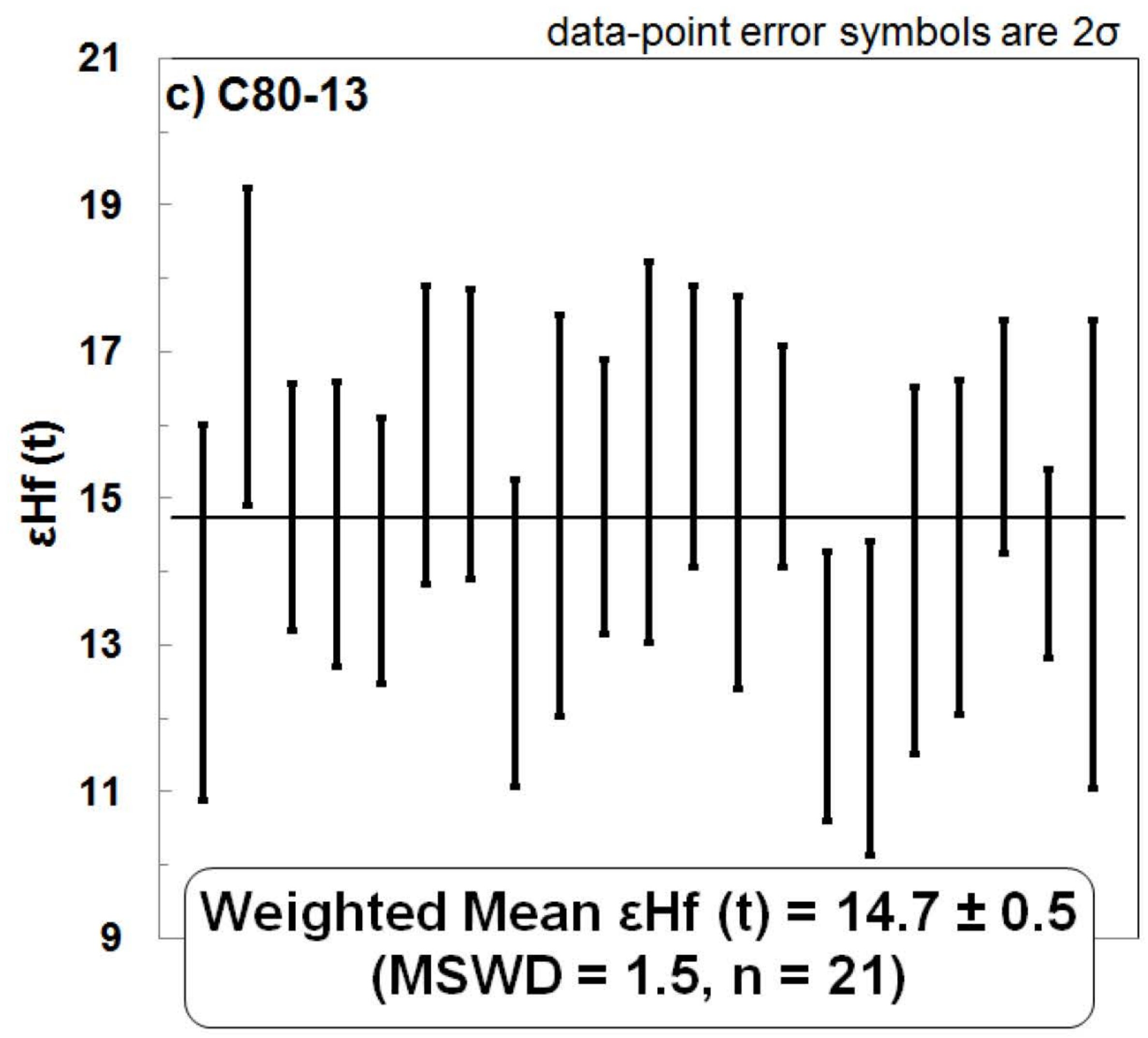
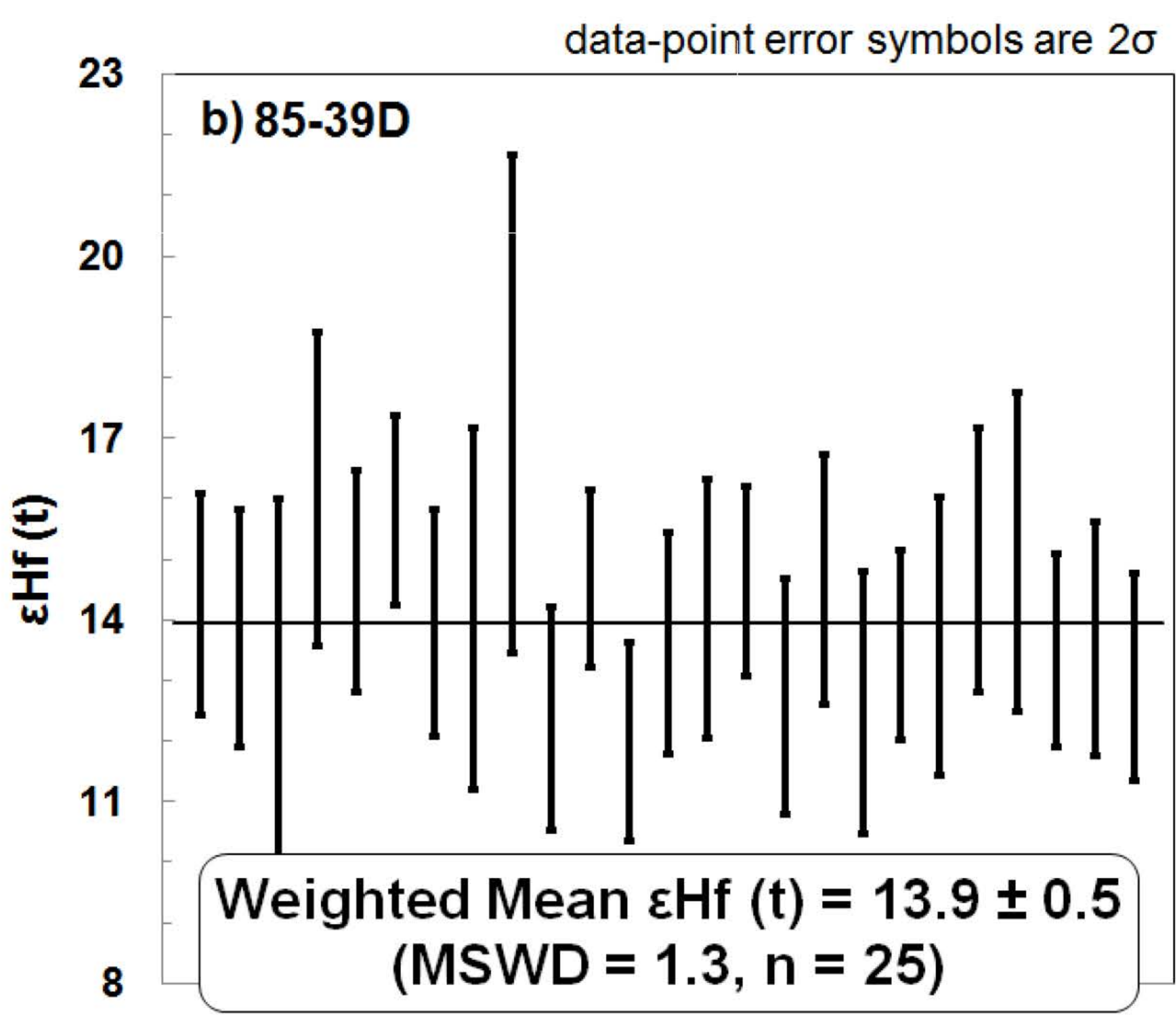
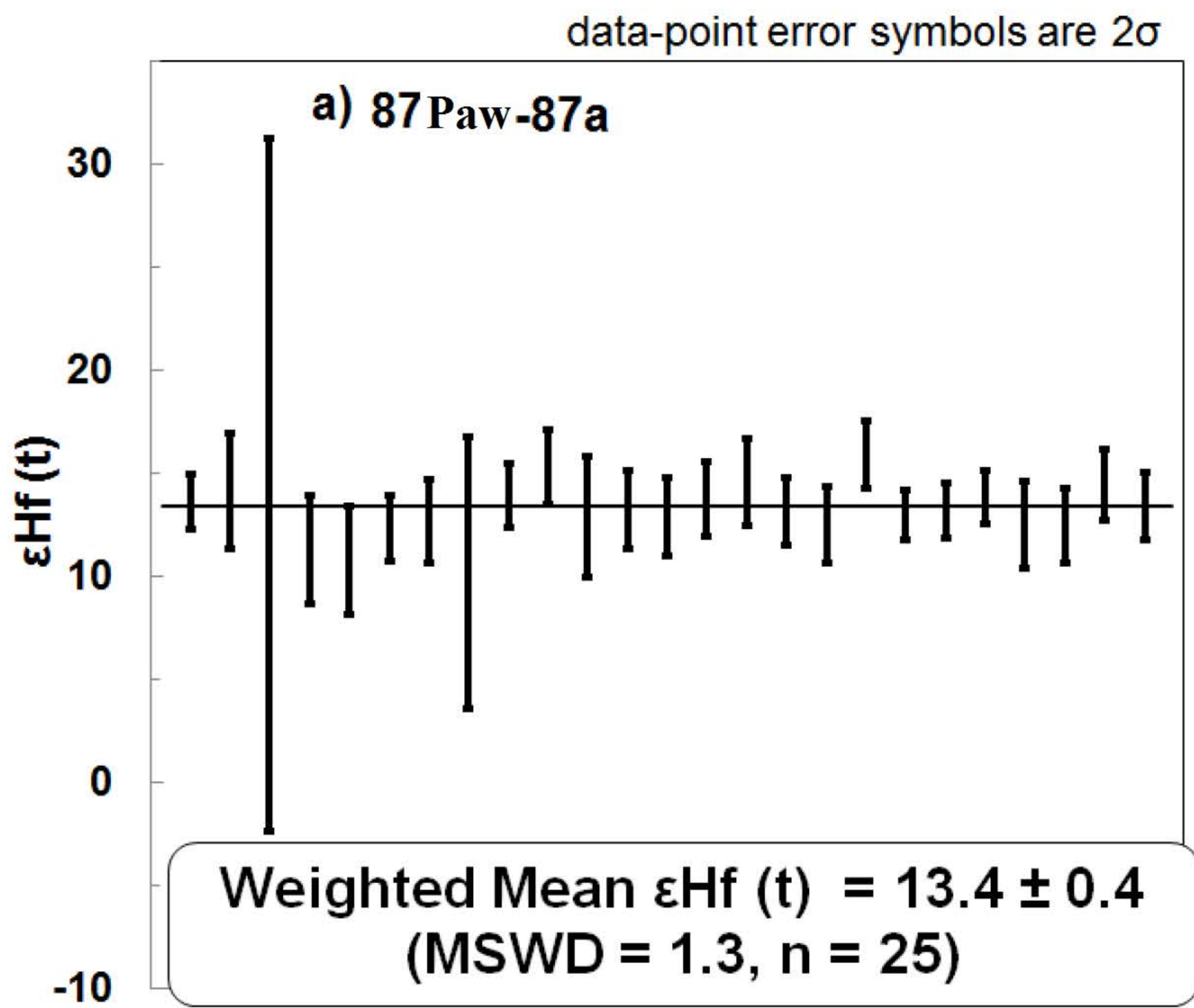


Figure S4: Weighted mean $\epsilon\text{Hf}(t)$ isotope composition of the studied plutons